Department for innovation in biological, agro-food and forest systems
PhD Course
Forest Ecology
XXIV cycle 2009 – 2011

GREENHOUSE GASES EXCHANGE OVER AND WITHIN A TROPICAL FOREST IN AFRICA

(AGR/05)

Course coordinator: Prof. **Paolo De Angelis**

_____

Tutor: Prof. **Riccardo Valentini**

_____

Co-tutor: Dr. **Gerardo Fratini**

_____

Co-tutor: Dr. **Paolo Stefani**

_____

PhD student: **Giacomo Nicolini**

_____

Greenhouse gases exchange over and within a tropical forest in Africa

Giacomo Nicolini

UNIVERSITÀ DEGLI STUDI DELLA Tuscia

DIBAF
Dipartimento per l'Innovazione nei sistemi Biologici, Agroalimentari e Forestali

Giacomo Nicolini
March 2012

CONTENTS

Abstract

Within the last years progress has been made in measuring trace gas fluxes at landscape scales thanks to development in technologies and their use in micrometeorological methods. However, there are still open questions. Two main factors contribute to limit the ability to precisely quantify annual or seasonal budgets of these gases. First, their net biosphere/atmosphere exchange rate is controlled by many biological, chemical and physical ecosystem parameters resulting in a very high temporal and spatial variability of fluxes. Second, such gases have a quite low atmospheric concentration, at least compared with CO_2, which, in combination with their small flux rates, makes the flux measurement a challenging technological achievement. As a consequence, exhaustive assessment requires high spatial resolution and continuous long-term monitoring. Eddy-based measurements can improve the accuracy of trace gas flux estimates, detect the short-term variability of fluxes, lead to estimates from site to landscape scales and provide a useful tool to parameterize and validate process-oriented models.
Measurement reliability can be optimized by an accurate field campaign and an appropriate data processing but assessing the source-sink mechanism in time and space, and the sources and magnitude of errors of estimates is still challenging.
Furthermore, some geographical areas like Africa still remain uncovered form such studies, while more information on trace gas exchange over these regions, especially within key ecosystems like forests, are becoming today urgent to properly understand the global cycles of trace gases.

In this thesis the fluxes of the two main greenhouse gases, CH_4 and CO_2, are measured by means of the eddy covariance technique in the rainforest of *Ankasa* in Ghana.
Since tropical rainforests play a prominent role in the global carbon and methane cycle, flux dynamics are investigated both over and within the forest canopy.
But while for CO_2 the measurement routine is more consolidated, here the potential of the EC techniques in measuring CH_4 flux in such complex ecosystem is also evaluated.

To achieve these results, the working plan was structured in several phases.
As EC methane flux measurements is a rather recently topic, a preliminary meta-analysis by which the state of the art in trace gas fluxes studies on global scale is reviewed to focus on needs and gaps on observations and to highlight strength and weakness of measurement techniques. This result is presented in chapter 2. In this analysis also nitrous oxide fluxes are included but filed works on this gas is not reported here as represent the aim of future works. The available data coming from different biomes it is synthetized grouping ecosystems in the broad categories (forest, managed land, wetlands and anthropic environments). Range of emissions across biomes according to different techniques are discussed along with flux detection limits and comparison with soil chamber measurements. Finally some considerations about future research directions and gaps on observation ore offered.

A challenging task like measure below canopy methane fluxes is reported in chapter 3. Beyond the high spatial and temporal variability of CH_4 sources, such kind of estimates is further complicated by the complex turbulence in the trunk space. In this chapter is reported the result of

two short measurement campaign, executed during the dry and wet season in a periodically swamped area near the main tower. The feasibility of the approach is evaluated with the aim of programming a longer sampling and comparing results with concurrent soil chamber measurements.

In chapter 4 is reported an investigation on CO_2 and CH_4 storage fluxes and how much they impact on above canopy fluxes. For CO_2 results are based on one year dataset of continuous profile measurements while for CH_4 24 hours samplings were performed over different seasons. The relation between the two storages and between storages and some controlling environmental variables are explored with the aim of either properly correct the above canopy flux, test the magnitude and the suitability of such corrections and eventually parameterize the storage flux trend.

In chapter 5, CH_4 and CO_2 fluxes measurement over the forest canopy is reported. This is the core of the thesis and a deeper analysis is performed. The sampling has regarded several months covering the shift from the wet to dry season. Prior to the reported measurement period, further campaigns have been conducted but instrument failures, energy cut-offs and other technical problems have been prevent reliable results. Anyway such effort was useful to individuate the weakness of the measurement system and assess the methane gas sensor performances. In fact, a newly developed open path sensor was used and application experiences are currently being evaluated.
Beyond the fluxes quantification here it is reported the seasonal trend analysis of fluxes, the footprint analysis to localize the source regions, the error assessment and the quantification of the minimum detectable flux. Then a carbon balance for the analysed period is computed.

Sommario

Negli ultimi anni sono stati compiuti numerosi progressi nella stima dei gas-traccia su scala ecosistemica grazie allo sviluppo di tecnologie innovative e al loro utilizzo tramite tecniche micrometeorologiche. Tuttavia, ci sono ancora aspetti che devono essere chiariti.
Due fattori principali contribuiscono a limitare la capacità di quantificare esattamente i bilanci stagionali o annuali di questi gas. In primo luogo, il loro tasso netto di scambio tra biosfera e atmosfera è regolato da molti parametri biologici, chimici e fisici e ciò determina un' alta variabilità spaziale e temporale dei flussi. Inoltre, questi gas hanno delle basse concentrazioni atmosferiche (rispetto a quella della anidride carbonica) che, assieme a basse intensità di flusso, rendono la loro misura una sfida tecnologica. Di conseguenza, una valutazione esauriente richiede misure in continuo e con un' ampia risoluzione spaziale.
Le misure basate sulla tecnica dell' *eddy covariance* (EC) possono migliorare l'accuratezza di queste stime integrando la variabilità a breve termine dei flussi, fornendo stime su ampia scala e dati necessari alla parametrizzazione e validazione di modelli process-oriented.
L'affidabilità delle stime può essere ottimizzata da una campagna di misura accurata e un attento processamento dei dati. Tuttavia la valutazione del meccanismo di assorbimento/emissione e degli errori di stima presentano ancora ampi margini di studio.
Inoltre alcune aree geografiche come l'Africa sono poco interessate da questi studi nonostante il ruolo fondamentale che i loro ecosistemi, in particolare le foreste, svolgono nel bilancio globale del ciclo del carbonio.
Questa tesi riguarda lo studio dei flussi di metano (CH_4) e anidride carbonica (CO_2) misurati nella foresta tropicale di *Ankasa* in Ghana tramite la tecnica dell'eddy covariance. Le misure sono state effettuate sia sotto che sopra lo strato delle chiome. Sono state inoltre valutate le potenzialità di questa tecnica nel misurare CH_4 su ecosistemi complessi.
Per raggiungere questi obiettivi, il lavoro è stato articolato in fasi diverse.

Le misure EC di CH_4 rappresentano un aspetto recente nello studio dei gas serra, quindi è stata effettuata una meta-analisi preliminare attraverso la quale è stato possibile conoscere lo stato dell'arte di queste misure su scala globale, individuare le aree che maggiormente necessitano di osservazioni ed infine evidenziare i pro e i contro della tecnica. Il risultato di questa analisi è riportato nel capitolo 2. Qui viene incluso anche un altro gas traccia, il protossido di azoto (N_2O), ma le misure di questo gas non vengono ulteriormente trattate in quanto sono l'oggetto di un lavoro in fase di sviluppo. I dati raccolti tramite ricerca bibliografica, sono stati raggruppati in 4 grandi categorie di ecosistemi (foreste, terreni agricoli, zone umide e ambienti antropizzati). Per ogni categoria viene discusso: il range delle emissioni, il minimo flusso misurabile rispetto alla tecnica micrometeorologica adottata e il confronto con i risultati ottenuti con la tecnica delle camerette di accumulo al suolo. Infine vengono proposte alcune considerazioni sullo sviluppo di ricerche future e sulla necessità di aumentare il numero delle osservazioni.

La misura dei flussi di CH_4 sotto chioma è riportata nel capitolo 3. Oltre che per l'alta variabilità spaziale e temporale delle emissioni, questo tipo di misure è ulteriormente complicato dalla complessa turbolenza che si sviluppa tra i fusti degli alberi. In questo capitolo sono riportati i risultati di due campagne di misura eseguite su un'area periodicamente inondata, situata nei

pressi della stazione principale. La prima è stata condotta durante la stagione secca, la seconda in quella umida durante un periodo di inondazione. Oltre a valutare l'entità dei flussi e l'applicabilità della tecnica, questo esperimento è stato eseguito con lo scopo di programmare un campionamento più lungo e confrontare i risultati con stime effettuate al suolo con le camerette.

Nel capitolo 4 è riportata un'analisi dello storage di CO_2 e CH_4 e di quanto esso contribuisca ai flussi misurati dalla torre al disopra delle chiome. Per la CO_2 i risultati sono basati su un anno di misurazioni in continuo del profilo verticale lungo la torre. Per il CH_4 sono stati effettuati campionamenti di 24 ore durante tre campagne di misura in stagioni differenti. E' stata esaminata la relazione tra i due storage e tra questi e alcune variabili ambientali con lo scopo di correggere adeguatamente i flussi sopra chioma, testare la portata e l'intensità di queste correzioni ed eventualmente parametrizzarne il trend.

Il capitolo 5 descrive la stima dei flussi di CH_4 e CO_2 effettuata al disopra dello strato delle chiome tramite la tecnica dell'eddy covariance. Il campionamento è stato eseguito per diversi mesi durante il passaggio dalla stagione umida a quella secca. Nel periodo precedente alle misurazioni si sono verificati problemi di natura tecnica che hanno reso il dataset inutilizzabile. Tuttavia questo ha permesso di individuare i punti deboli del sistema e ottimizzare le prestazioni del sensore di CH_4. Infatti lo strumento utilizzato per la misura delle concentrazioni di questo gas è stato commercializzato solo di recente e la sua applicazione in campo è attualmente in fase di valutazione.
Oltre alla quantificazione dei flussi e l'individuazione della loro area sorgente (footprint), è riportata un'analisi dei trend, una valutazione dell'errore di stima e del flusso minimo misurabile dal sistema. Infine è stato calcolato il bilancio netto del carbonio durante il periodo di misura.

1 Introduction

1.1 Background on greenhouse gases

Earth atmosphere (air) is a mixture of gases and particles constituted by three major components, nitrogen (N_2), oxygen (O_2) and argon (Ar), representing about the 99.9% of atmosphere volume; three secondary components, water vapour (H_2O), carbon dioxide (CO_2) and ozone (O_3); and trace components such as methane (CH_4), nitrous oxide (N_2O) and halocarbons (CFCs, HCFCs). Due to the great mobility of the atmosphere together with its internal mixing, the proportion of such gases is almost constant at any latitude and up to 100 Km of altitude. The big importance of the atmosphere, as well as its first kilometres (around 10) where meteorological phenomena take place, lie behind the absorption of the cosmic radiation (x, gamma and UVC) emitted by the sun. Without the 'atmospheric filter' such radiations could get down to the Earth surface destroying the biosphere.

Despite the big contribution in terms of volume, the principal atmospheric components are effectively transparent to solar radiations, both long-wave and short-wave (but they play a role on short-wave diffusion, see later). Secondary and trace gases, even if they represent around 1 ‰ of the atmosphere volume, control the absorption and re-emission of radiation energy. In particular, due to their tri-atomic molecular structure, they absorb radiation in certain wavelengths, mostly in the long-wave region. Each gas absorbs in a different spectral band and these bands do not overlap so, as they are mixed in the air, the absorption takes place within all the characteristic bands of radiation. Between these bands there are two main windows through which part of the radiation can pass without being absorbed. One is the short-wave window ($0.3 < \lambda < 1.5$ μm) crossed by the solar irradiation peak coming to the Earth, and the other is the long-wave or infrared window ($8 < \lambda < 14$ μm) permeable to the Earth radiative emission going back towards the atmosphere (Fig. 1.1).

This selective absorption mechanism is universally known as *green-house effect*: the atmosphere, allowing short-wave incoming radiation to pass and absorbing most of the long-wave outgoing radiation, keeps the Earth temperature warmer than surrounding air.

The energetic balance of the Earth–atmosphere system with the external space is hence performed through this air mass that envelops the terrestrial surface, which has the clouds top as external frontier. To see the importance of this air layer, and of the green-house effect, let's consider a simplified version of terrestrial energetic balance model:

$$T_E^4 = \frac{\Phi_0 (1-A)(1-B)}{4\sigma} + E_m T_P^4 \qquad [1.1]$$

where Φ_0 = $1.38 \cdot 10^3$ W m^{-2} is the energy flux density from the sun (solar constant), $A \approx 0.3$ is the planetary albedo contribution (mainly due to clouds reflectance), $B \approx 0.2$ is the atmospheric absorption contribution, σ = $5.67 \cdot 10^{-8}$ W m^{-2} K^{-4} is the terrestrial emittance, Em = 0.9 is the atmospheric emissivity and Tp = 255 K is the planetary temperature. Solving this

model we get a value of 291 K (18 °C), close to the measured mean terrestrial temperature of 288 K.

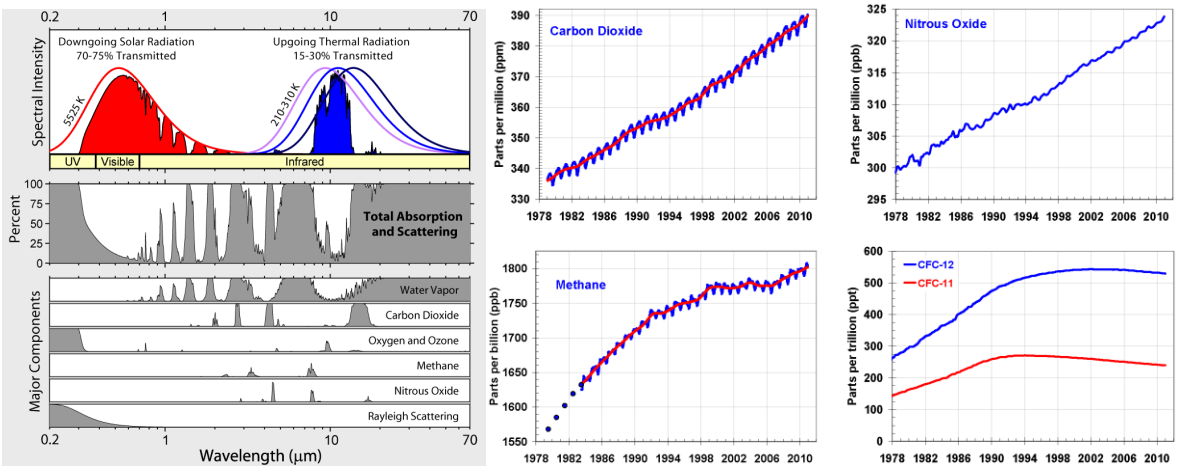

Figure 1.1. Left side: absorption bands in the Earth's atmosphere (middle panel), for major GHG (lower panel) and their impact on both solar radiation and up-going thermal radiation (top panel). The sun emissions peak is in the visible region (next to the short-wave window absorption band), emissions from the Earth vary with temperature, latitude and altitude peaking in the infrared (next to the long-wave window). Absorption bands are determined by the chemical properties of the gases, Rayleigh scattering represent the aerosol contribution. Right side: global average abundances of the major GHG. These gases account for about 96% of the direct radiative forcing by long-lived greenhouse gases since 1750. The remaining 4% is contributed by minor halogenated gases [http://www.esrl.noaa.gov/gmd/aggi/index.html].

If, for example, green-house gases (GHG) drastically diminish resulting in a lower atmospheric emissivity Em = 0.4 – 0.5, T_E would drop down to -5 – 0 °C, causing a freezing of the Earth crust. On the contrary, a GHG increase causing the atmosphere to become like a black body (Em = 1), would correspond to an Earth surface mean temperature rising up to 23 °C, dangerously compromising life of all vegetal and animal species.

The evolution and the current composition of the atmosphere is strictly linked not only to the origin of our planet and to its geology, but also to the life forms that are born and evolved on it. Hence it is natural believe that its characteristics can change in the future in relation to the evolution of the biosphere, and in particular of the human species.

Historical changes in the atmosphere composition are reconstructed by analysing air bubbles within cores extracted from ice, wetlands and lakes. The trend for the last 30 years is showed in figure 1.1. Up to mid 1700, CO_2 concentration was in the range 280 ± 20 ppm. During the industrial era it rose roughly exponentially to 367 ppm in 1999 and up to 379 ppm in recent years [Le Treut, et al., 2007]. Carbon dioxide has increased from fossil fuel use in transportation, manufacture, gas flaring and cements production. Deforestation releases CO_2 and reduces its uptake by plants. CO_2 is also released during land use changes, biomass burnings and natural biomass decomposition.

Direct atmospheric measurements since 1970 have also detected the increasing atmospheric abundances of methane and nitrous oxide. CH_4 abundance was constantly around 700 ppb until the 19th century, then a steady increase brought CH_4 abundances to 1745 ppb at the end of 20th century [IPCC, 2001] and near 1800 ppb in 2010, becoming the most abundant non-

CO_2 GHG in the atmosphere today [Montzka et al., 2011]. Methane has increased as a result of human activities related to agriculture, natural gas distribution and landfills. It is also released from microbial processes (methanogens) that occur in soil, sediments, wetlands and water bodies [Davidson and Shimel, 1995, Flechard et al., 2007]. At present N_2O abundance is 19% higher than pre-industrial levels and has increased at a mean rate of 0.7 ppb yr^{-1} during the past 30 years, passing from 314 ppb in 1998, 319 ppb in 2005 to 322 ppb at present [Le Treut, et al., 2007; Montzka et al., 2011]. Nitrous oxide is also emitted by human activities such as use of fertilizers in agriculture and fossil fuel burning. About 70% of the total amount of N_2O emitted from the biosphere derives from soils [Mosier et al., 1998]. Oceans also release N_2O.

Radiative forcing (RF) is used to assess and compare the anthropogenic and natural drivers of climate change and it has proven to be particularly applicable to the assessment of the climate impact of GHGs as it can be linearly related to the global mean surface temperature change [Ramaswamy et al., 2001]. RF is computed basing on GHG concentration rate of change relative to 1750's values and its efficiency in absorbing available infrared radiation. As reported by Montzka et al. [2011], by 2009 the increase in non-CO_2 GHGs contributed a direct radiative forcing of 1.0 W m^{-2}, 57% of that from CO_2, half of which (0.5 W m^{-2}) is due to CH_4. In figure 1.2 GHGs current RF and projection are reported.

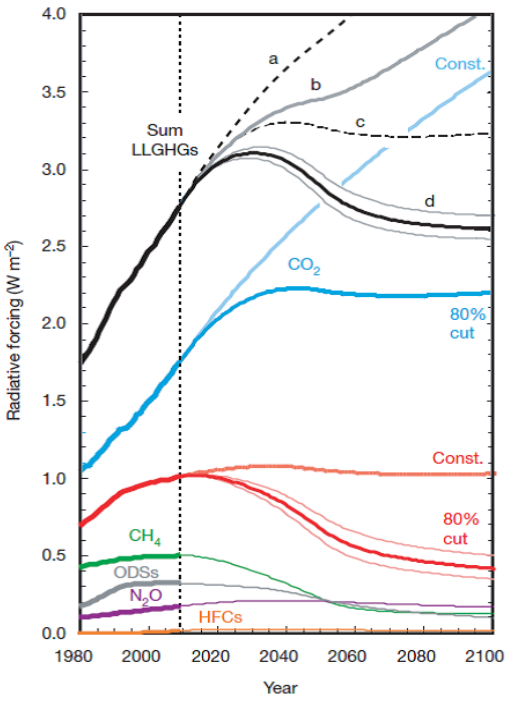

Table 1.1. GWPs of some GHGs.
Readapted from Forster et al., 2007

GHG	RF	GWP		
	$Wm^{-2}ppb^{-1}$	20-yr	100-yr	500-yr
CO_2	$1.4\ 10^{5}$	1	1	1
CH_4	$3.7\ 10^{4}$	72	25	8
N_2O	$3.03\ 10^{3}$	289	298	153
CCl_3F	0.25	6730	4750	1620
CCl_2F_2	0.32	11000	10900	5200
$CClF_3$	0.25	10800	14400	16400
$CBrF_3$	0.32	8480	7140	2760
CCl_4	0.13	2700	1400	435
CHF_3	0.19	12000	14800	12200
CH_2F_2	0.11	2330	675	205
SF_6	0.52	16300	22800	32600
NF_3	0.21	12300	17200	20700
CF_4	0.10	5210	7390	11200
C_2F_6	0.26	8630	12200	18200

Figure 1.2. Left side: radiative forcing derived from observed and projected abundances of long-lived gases (LLGHGs). Projections are made either assuming constant future emissions at 2008 levels and 80% cuts off. Future forcing from the sum (black lines) of changes in CO_2 (blue lines) and the sum of non-CO_2 LLGHGs (red lines). These sums is shown for different emission scenarios [see Montzka et al., 2011 for further detail].

To compare the impact of different GHGs on climate change, the global warming potential (GWP) index is used. It is based on the time-integrated global mean RF of a pulse emission of

1 kg of some compound relative to that of 1 kg of CO_2, taken as a reference [Forster et al., 2007]. Usually, non-CO_2 emissions are multiplied by 100-yr time horizon GWPs to give CO_2-eq emissions. Despite their minor abundance, the global warming potentials of CH_4 and N_2O are significantly higher than that of CO_2, 25 and 298 times respectively.
As a consequence, to properly managing future intervention on climate forcing and improve scientific knowledge, non-CO_2 gases must be given due consideration, as also reported by Montzka et al. [2011]. Non-CO_2 gases currently account for 1/3 of the total CO_2-eq emissions and 35–45% of total climate forcing from all GHGs, hence cuts in their emissions could substantially reduce future climate forcing. Act on shorter-lived non-CO_2 gases emissions, primarily on CH_4 as it accounts for half of their total climate impact, can cause a rapid decrease in the actual radiative forcing, otherwise impossible from cutting CO_2 emissions alone. On the other hand, such a quick response could not be achievable without concurrent substantial decreases in CO_2 emissions. The stabilization of climate forcing will be successfully achieved only with progresses in scientific research that enhance our understanding in the action-reaction mechanism of natural GHG fluxes on climate change and that improve our ability to properly quantify both natural and anthropogenic GHG fluxes.

1.2 Eddy covariance method

The eddy covariance (EC) technique is a micrometeorological method for measuring exchange of energy, momentum and mass (e.g. GHG) between a surface and the atmosphere. When this surface is horizontally uniform and flat the net exchange become mono-dimensional and the vertical flux density can be calculated as the covariance (see Sect. 1.2.1) between the turbulent fluctuation of vertical wind speed and the quantity of interest. This methods was originally proposed around the 1950 [Montgomery, 1948; Swinbank, 1950], the first measurement of a gas flux, CO_2, is dated back to early 1970s [Desjardins, 1974] and the first applications over forest were made after 1980s [Wesely et al., 1983; Fan et al., 1990; Valentini et al., 1991].
Mean flux across any plane implies correlation between the wind component normal to that plane and the entity in question, hence in their covariance there is a direct measure of the flux [Kaimal and Finnigan 1994]. Except for the first few millimetres of the atmosphere close to the earth surface, turbulent transport is the most important process in the exchange of energy and matter.
The turbulent motion of any variable ξ like e.g. the wind components (along a right-handed coordinate axes x, y and z respectively) u, v, w, the potential temperature θ, the mean specific humidity q or the gas concentration c, can be expressed as the sum of its mean component and the turbulent (fluctuation around the mean) component. Thus by the Reynolds decomposition we get

$$\xi(t) = \overline{\xi} + \xi'(t) \qquad [1.2]$$

where $\overline{\xi}$ represent the average of the time dependent variables and $\xi'(t)$ its fluctuating part. The mean part within the averaging period T, is computed as

$$\bar{\xi} = \frac{1}{T}\int_{t}^{t+T} \xi(t)dt \qquad [1.3]$$

Such decompositions (and the following derivations) requires some averaging rules (Reynolds postulates)

$$\begin{aligned}
&\bar{\xi}' = 0 && \text{I}\\
&\overline{\xi\zeta} = \bar{\xi}\bar{\zeta} + \overline{\xi'\zeta'} && \text{II}\\
&\overline{\bar{\xi}\zeta} = \bar{\xi}\bar{\zeta} && \text{III}\\
&\overline{a\xi} = a\bar{\xi} && \text{IV}\\
&\overline{\xi+\zeta} = \bar{\xi} + \bar{\zeta} && \text{V}
\end{aligned} \qquad [1.4]$$

These relations are theoretically obtained by ensemble averaging, i.e. averaging over many realizations under identical conditions [Kaimal and Finnigan, 1994]. Though in practice this is impossible given the natural variation of atmospheric conditions so the ensemble averages have to be approximated by averages over time, as the "ergodic" hypothesis asserts [Kaimal and Finnigan, 1994]. To satisfy this assumption, the fluctuations must be statistically stationary over the averaging period.

Turbulence in the atmosphere can be generated by mechanical production and buoyancy. The relative strength of both processes controls the vertical extent of turbulence.

The atmospheric boundary layer (ABL) is the part of the atmosphere that is directly influenced by the presence of the earth's surface and respond to surface's forcings with a timescale of about one hour or less [Stull, 1988]. This forcings include frictional drags, heat transfer, evaporation, transpiration, gas emissions and flow distortions induced by the terrain. The thickness of this layer is time and space dependent and varies from hundreds of meters to a few kilometres. The lowest 10% of the ABL is called surface (boundary) layer (SL). Fluxes in this layer can be considered approximately constant with height and the atmospheric turbulence is the primary way of transport. EC measurements are typically made at some height in the SL, which has a thickness of about 20-50 m in unstable atmospheric stratifications and 10-30 m under stable stratification [Stull 1988; Aubinet *et al.*, 2012], and can be considered representative of the underlying surface.

The turbulent structure of the SL can be evaluated by several parameters. Following the theory expressed by Monin and Obukhov [1954] the main characteristics of the turbulence are described by the buoyancy parameter $g/\bar{\theta}$ (with g being the acceleration of gravity), the friction velocity u_* and the length scale L (called Monin-Obukhov length).

The friction velocity is a generalized velocity dependent on surface nature and wind intensity representing the strength of wind stress. It may be usefully defined by [Foken 2008]

$$u_* = \left(-\overline{u'w'}\right)^{1/2} \qquad [1.5]$$

where u and w are expressed in m s^{-1}.
The Monin-Obukhov length is given in meters by

$$L = -\frac{\theta u_*^3}{\kappa g \overline{w'\theta'}} \qquad [1.6]$$

where κ is the von Karman constant often set to 0.4 [Kaimal and Finnigan 1994].
The non-dimensional ratio ζ of height z to the scaling length L is often used to discriminate between atmospheric stability conditions

$$\zeta = \frac{z}{L} = -\frac{\left(g/\bar{\theta}\right)\left(\overline{w'\theta'}\right)}{u_*^3/\kappa z} \qquad [1.7]$$

representing the relative importance of mechanical production (u_*) and buoyancy ($g/\bar{\theta}$). Generally ζ is negative in unstable atmosphere and positive when it is stable. Despite there are no fixed threshold values some classifications are proposed, one of which is reported in Table 1.2

Table 1.2. Surface layer stratification basing on the stability parameter $\zeta = z/L$. *M*odified from Foken [2008].

stratification	remark	ζ
unstable	independent from u_* free convection	$-1 > \zeta$
	dependent from u_* mainly mechanical turbulence	$-1 < \zeta < 0$
neutral	dependent from u_* purely mechanical turbulence	$\zeta \approx 0$
stable	dependent from u_* mechanical turbulence slightly damped by temperature stratification	$0 < \zeta < 0.5 - 2$
	independent from z mechanical turbulence strongly reduced by temperature stratification	$0.5 - 1 < \zeta$

1.2.1 Theory and equations

To derive the ecosystem exchange of a trace gas it is needed to base on the *conservation equation* of any atmospheric constituent, both scalar and vector, ξ:

$$\underbrace{\frac{\partial \rho_d \xi}{\partial t}}_{\text{I}} + \underbrace{\vec{\nabla}(\vec{u}\rho_d \xi)}_{\text{II}} + \underbrace{\mathrm{K}_\xi \Delta(\rho_d \xi)}_{\text{III}} = \underbrace{S_\xi}_{\text{IV}} \qquad [1.8]$$

where ρ_d is the dry air density, $\vec{\nabla}$ is the divergence $(\partial/\partial x, \partial/\partial y, \partial/\partial z)$, $\vec{u}$ is the 3D velocity field, Δ is the Laplacian operator $(\partial^2/\partial x^2, \partial^2/\partial y^2, \partial^2/\partial z^2)$, K is the ξ diffusivity and S is the ξ source/sink intensity [Aubinet et al. 2012; Gu et al., 2012]. By this model we can see that the sum of the rate of change of ξ (temporal variation, term I), its atmospheric transport (advection, term II) and molecular diffusion (flux divergence, term III), equals its production by a source or absorption by a sink (term IV). Considering ξ as a wind component (u, v, w) we get the conservation equation for the momentum, as a temperature ($cp\theta$), the conservation equation for the heat, while considering ξ as a trace gas mixing ratio (e. g. χ_{CO2}, χ_{H2O}, χ_{CH4}) we obtain the trace gas conservation equation.
Therefore, assuming that molecular diffusion can be neglected in comparison to turbulent mixing [Stull, 1988], the conservation equation of any gas s becomes

$$\frac{\partial \rho_d \chi_s}{\partial t} + \vec{\nabla}(\vec{u}\rho_d \chi_s) = S_s \qquad [1.9]$$

Considering the continuity equation as there is neither a source or sink of dry air in the atmosphere

$$\overline{\partial \rho_d} / \partial t + \vec{\nabla}(\vec{u}\overline{\rho_d}) = 0 \qquad [1.10]$$

and applying the Reynolds decomposition and the averaging postulates (Eq. from [1.2] to [1.4]) we get

$$\overline{\rho_d}\frac{\overline{\partial \chi_s}}{\partial t} + \overline{\rho_d}\overline{u}\frac{\overline{\partial \chi_s}}{\partial x} + \overline{\rho_d}\overline{v}\frac{\overline{\partial \chi_s}}{\partial y} + \overline{\rho_d}\overline{w}\frac{\overline{\partial \chi_s}}{\partial z} + \frac{\overline{\partial \overline{\rho_d}\,\overline{u'\chi'_s}}}{\partial x} + \frac{\overline{\partial \overline{\rho_d}\,\overline{v'\chi'_s}}}{\partial y} + \frac{\overline{\partial \overline{\rho_d}\,\overline{w'\chi'_s}}}{\partial z} = \overline{S_s} \qquad [1.11]$$

Under ideal conditions [Stull, 1988; Kaimal and Finnigan, 1994] $\bar{v}$ and $\bar{w}$ are 0 as the measurement system is aligned along the mean wind direction (no horizontal gradients); the gas concentration is steady with time (steady state condition) hence its time derivative nullifies; the underlying surface is homogeneous an flat so horizontal gradients (horizontal advection and flux divergences) equal zero. These assumptions simplify the gas conservation equation to a balance between the vertical gas flux divergence (gradient of eddy covariance) and its biological source/sink

$$\frac{\overline{\partial \overline{\rho_d}\,\overline{w'\chi'_s}}}{\partial z} = \overline{S_s} \qquad [1.12]$$

Defining a control volume over a flat homogeneous terrain with thickness z spanning from 0 to h (the measurement height in m), and considering the gas measurement made at height h as representative of the whole underlying volume, it is possible to integrate Eq. [1.11] just with

respect to height (hence not horizontally) obtaining the gas budget equation i.e. the EC method equation

$$\int_0^h \overline{\rho_d} \frac{\overline{\partial \chi_s}}{\partial t} dz + \int_0^h \overline{\rho_d} \overline{w} \frac{\overline{\partial \chi_s}}{\partial z} dz + \overline{\rho_d} \overline{w' \chi'_s} = F_s \qquad [1.13]$$

I II III IV

where term I is the gas *storage* in the underlying airspace (present when steady state condition is not met), term II is the *vertical advection* at the measuring point results from dry air density changes, term III ($\overline{w' \chi'_s}$) is the measured *turbulent flux* and F_s is the gas *net ecosystem exchange* (NEE) generally expressed in μmol m^{-2} s^{-1}.
Normally the vertical advection is negligible with respect to the other terms hence Eq. [1.13] is further simplified.
The storage change depends on the stability of the atmosphere. During unstable conditions (normal daytime condition), the gas concentrations are well mixed and the storage change is small, however, during stable conditions (typical at nigh), the gas concentrations accumulate due to suppressed vertical motion by buoyancy destruction and the storage change term can become significant. The storage flux (μmol m^{-2} s^{-1}) is calculated as [Aubinet et al., 2001]

$$Sc = \frac{P_a}{\Re T_a} \int_0^h \frac{\partial c(z)}{\partial t} dz \qquad [1.14]$$

where P_a is the atmospheric pressure, T_a is the air temperature, R is the molar gas constant, c is gas concentration measured along the vertical profile of height h over an averaging period.

The measured EC flux (term III of Eq. [1.13]) consists in a contribution of many eddies with different length scales, the turbulence spectrum [Stull et al., 1988]. The contribution of each eddy can be derived from the fast Fourier transform (FFT) analysis since each signals (wind velocity components, temperature or gas concentration) that contributes to the flux, can be seen as a linear combination of harmonic sine and cosine functions varying over a range of frequencies [Stull et al., 1988]. Assuming that signals are discrete time series consisting of N equally spaced data points (indexed by k = 0,..., N), then the available frequencies are n = 0, 1, ..., N-1 where n denotes the number of cycles within the averaging period. The contribution of each frequency to the variance of a quantity ξ is derived in two steps.
The signal $\xi(k\Delta t)$ is split in several sine and cosine terms by the Fourier transform

$$F_\xi(n) = \frac{1}{N} \sum_{k=o}^{N-1} \xi_k \cos(2\pi nk / N) - \frac{1}{N} \sum_{k=o}^{N-1} \xi_k \sin(2\pi nk / N) \qquad [1.15]$$

for n = 0,…, n_f, being n_f the Nyquist frequency which is equal to N/2, then the spectrum of the quantity ξ is given by

$$S_\xi(n) = \frac{1}{2}\left[A_\xi^2(n) + B_\xi^2(n)\right] \quad [1.16]$$

where

$$A_\xi(n) = 2F_{\mathrm{Re},\xi} \quad [1.17]$$

$$B_\xi(n) = -2F_{\mathrm{Im},\xi} \quad [1.18]$$

with $F_{Re,\,\xi}$ being the real part and $F_{Im,\,\xi}$ the imaginary part of $F_\xi(n)$.
The co-spectrum of ξ and another signal as w, is derived in a similar way and is given by

$$C_{w\xi}(n) = \frac{1}{2}\left[A_w(n)A_\xi(n) + B_w(n)B_\xi(n)\right] \quad [1.19]$$

The integral (or sum) over the whole frequency (f) range of the spectrum S_ξ (n) and co-spectrum $C_{w\xi}$ (n), represent the variance and covariance (flux) of the signal [Kaimal and Finnigan 1994]

$$\sigma_\xi^2 = \int_0^\infty S_\xi(f)df \cong \sum_1^{N/2} S_\xi(n) \quad [1.20]$$

$$\sigma_{w\xi} = \overline{w'\xi'} = \int_0^\infty C_{w\xi}(f)df \cong \sum_1^{N/2} C_{w\xi}(n) \quad [1.21]$$

Consequently, when the (co)spectra are plotted on linear axes, the area under the curve represents the (co)variance. Anyway the (co)spectra are usually plot on semi-log or log-log scale, maintaining the characteristic that the area under the curve represents the total (co)variance [Stull, 1988].

1.2.2 Eddy covariance raw data acquisition and processing

Data acquisition. The basic configuration of an EC system is a 3D sonic anemometer to measure the three components of the wind velocity u, v and w (m s^{-1}) and the sonic (then converted in ambient air) temperature (K or °C), a gas analyser measuring the trace gas and water vapour ambient concentration (mole fraction mol mol^{-1} or molar density mol m^{-3}) plus a set of sensors to collect ancillary meteorological variables necessary to further analyse flux data.
Gas analysers are generally based on infra-red spectroscopy and are divided into two main categories. The open-path and the closed-path sensors. The former quantify scalar concentrations *in situ*, close to the point where the wind speed is measured. The latter are situated at some distance from this point and quantify scalar concentrations of air sucked down through a tube from an intake close to the anemometer [Haslwanter *et al.*, 2009]. An

enclosed system aimed to maximize strength of both has been recently developed [Burba *et al.*, 2012].

Both the anemometer and the gas analyser must have a fast frequency response, i.e. sampling and collect data at rates up to 20 Hz (the anemometer sampling rate is normally twice). Such high frequencies are needed to ensure sample along all the frequency range of the turbulent spectrum. The gas sensor should have enough accuracy and precision to resolve gas concentration at ppb level (see Chap. 2). Such high frequency signals have to be averaged on a time period long enough to sample all the micro-turbulent spectrum time scale and at the same time ensure the steady state condition to be respected. Presently such integration period span from 15 to 60 minutes but is usually set to 30 min [Aubinet et al., 1999].

The meteo variables are directly acquired on a half-hourly scale and the usual set comprises global and net radiation (W m^{-2}), photosynthetic photon flux density (PPFD, µmol m^{-2} s^{-1}), air and soil temperature profile (K or °C), soil heat flux density (W m^{-2}), precipitation (mm), air pressure (kPa), relative humidity (%), soil humidity profile (%).

The wind speed and gas concentration must be measured at a height above the vegetation that depends on the characteristics of the site. Normally the higher the measuring level the lower the required sampling rate because the size of the eddies increases (therefore their frequency decrease) moving away from the surface. However, with the increase of quote also increases the area over which the measured flux is integrated (source area), running the risk of sampling different source areas in case of inhomogeneous landscape. The extension of this area is defined by the *footprint* function, from which it is possible to calculate the fraction of the total flux due to a unitary element of surface positioned downwind within the source (see later). Normally the fetch (distance between sensors and the next soil/vegetation inhomogeneity) should be

$$d_{fetch} = 100(z_m - d) \qquad [1.22]$$

where z_m is the measurement height and d is the displacement height approximately taken as $d = 0.75\ h_c$ (the stand height). Traditional recommendation for z_m is

$$d + 5z_0 < z_m < 100m \qquad [1.23]$$

where z_0 is the roughness length approximately taken as $z_0 = 0.1\ h_c$.

Once high frequency data have been collected and stored on half hour base, they need to be screened before flux computation occurs. Such operation necessitates of several computing steps and software routines are necessary.

Below is reported the processing steps that have been follow in this thesis and are implemented in EddyPro™ (LI-COR, Inc.), a free licence software for processing raw EC data to compute fluxes.

Despiking and statistical screening. Raw data despiking consists in detecting and eliminating short-term outranged values in the time series. Usually spikes are one ore few consecutive values hence if more consecutive values are found to exceed the plausibility

threshold, they might be a sign of a real trend and don't have to be eliminated. The statistical tests [Vickers and Mahrt, 1997] are amplitude resolution (insufficient sampling rate), drop-outs (short periods in which data are statistically different from the period average), absolute limits (values outside a plausible physical range), discontinuities (sharp series discontinuities that lead to semi-permanent changes), steadiness of horizontal wind (systematic reduction or increase in wind components series). Then, third (skewness) and forth (kurtosis) order moments are calculated on the whole time series and variables are flagged if their values exceed normal values.

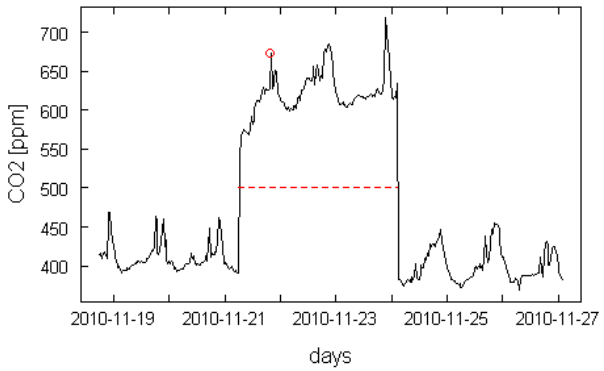

Figure 1.3. Example of spike (red circle) and drop-out (dotted red line) on CO_2 concentration time series.

Wind angle of attack and axis rotation (tilt correction). If the wind approaches the anemometer with a an angle that deviates significantly from horizontal, the structure of some sonic anemometer can distorts the flow, resulting in inaccurate measurements. If the angles of attack calculated throughout the current averaging period exceed a pre-fixed threshold, data have to be corrected [Nakai *et al.*, 2006].

As stated in the previous section, the reference coordinate system have to be aligned with the horizontal mean wind component (the *x*-axes parallel to *u* direction, the *z*-axes perpendicular to the mean stream flow and the *y*-axes perpendicular to the *xz*-plane) to respect the assumptions on the scalar conservation equation (Eq. [1.13]) i.e. negligible mean vertical wind component. Small errors in the alignment of the anemometer has big repercussion on fluxes estimate as the cross contamination of velocities that occurs with a nonaligned anemometer cause fluctuations in the longitudinal components of the wind appear as vertical velocity fluctuations and vice versa [Wilczak *et al.*, 2001]. There are three methods for addressing anemometer tilting: the double rotation, triple rotation, and the planar fit method.

In the double rotation method the first correction is the rotation around the *z*-axes to ensures that the coordinate system is oriented along the mean wind direction [Kaimal and Finnigan 1994]

$$\begin{aligned} u_1 &= u_m \cos\theta + v_m \sin\theta \\ v_1 &= -u_m \sin\theta + v_m \cos\theta \\ w_1 &= w_m \end{aligned} \qquad [1.24]$$

where u_m, v_m, w_m are the measured wind components and θ is the rotation angle defined as

$$\theta = \tan^{-1}\left(\frac{\overline{v_m}}{\overline{u_m}}\right) \qquad [1.25]$$

The second rotation is around the new y-axes until the mean vertical wind nullify

$$\begin{aligned} u_2 &= u_1 \cos\phi + v_1 \sin\phi \\ v_2 &= v_1 \\ w_2 &= -u_1 \sin\phi + w_1 \cos\phi \end{aligned} \qquad [1.26]$$

where u_2, v_2, w_2 are the rotated wind components and ϕ is the rotation angle defined as

$$\phi = \tan^{-1}\left(\frac{\overline{w_1}}{\overline{u_1}}\right) \qquad [1.27]$$

Now the rotated wind vector has zero $\bar{v}$ and $\overline{w}$ components, while $\bar{u}$ component holds the original value.

The third rotation (that imply the triple rotation method) tends to eliminates the covariance of the vertical and the horizontal wind components $\overline{w'v'}$ [Kaimal and Finnigan 1994]. Anyway such rotation does not significantly influence the fluxes while introduce some errors hence it is rarely applied [Aubinet et al., 2001].

The planar-fit method [Paw U et al., 2000; Wilczak et al., 2001] aims to assess the anemometer system with respect of the mean stream field basing on long period dataset. By this method a plane is fit to the average vertical wind component as a function of the horizontal components. If the anemometer is not properly mounted (or is placed over a sloping terrain), than its xy-plane is not aligned to mean stream and part of the horizontal wind vectors would contribute to the vertical component, that become

$$\overline{w_m} = b_0 + b_1\overline{u_m} + b_2\overline{v_m} \qquad [1.28]$$

Two rotation angles, α and β, are then defined by the fitting parameters (such relations are not reported here, see e.g. Wilczak et al., [2001]) and used to perform the first and second axis rotation to bring the z-axis perpendicular to the streamline plane. This is accomplished through

$$\overrightarrow{u_{pf}} = M_{pf}\overrightarrow{u_m} \qquad [1.29]$$

where $\overrightarrow{u_m}$ is the measured wind vector, $\overrightarrow{u_{pf}}$ the vector of the planar-fit rotated velocities and M_{pf} is the rotation matrix. Such operation leads to the following rotations

$$\begin{aligned} u_{pf1} &= u_m \cos\alpha - w_m \sin\alpha \\ v_{pf1} &= v_m \\ w_{pf1} &= -u_m \sin\alpha + w_m \cos\alpha \end{aligned} \qquad [1.30]$$

and

$$\begin{aligned} u_{pf2} &= u_{pf1} \\ v_{pf2} &= v_{pf1} \cos\beta + w_{pf1} \cos\beta \\ w_{pf2} &= -v_{pf1} \sin\beta + w_{pf1} \cos\beta \end{aligned} \qquad [1.31]$$

The planar-fit coordinate system fitted to the mean flow streamline is now characterized by $\overline{w} = 0$.

Detrending and fluctuations. Trends in time series should be removed to achieve stationarity of data. It imply removing the effect of fluctuations larger than the averaging period. The EC flux is derived from

$$F_{w\xi} = \frac{1}{n_s} \sum_{k=1}^{1} w'_k \, \xi'_k \qquad [1.32]$$

where n_s is the number of samples within the averaging time and where the subscript k refers to the k-th sample. The fluctuations w'_k and ξ'_k are computed as

$$\xi'_k = \xi_k - \overline{\xi_k} \qquad [1.33]$$

and can be determined on the basis of three main detrending methods: block averaging, running mean and linear detrending.
In case of a block average, the mean values are simply determined by

$$\overline{\xi} = \frac{1}{n_s} \sum_{k=1}^{1} \xi_k \qquad [1.34]$$

This is the only method that reduce the mean value of the fluctuations to zero as Reynolds hypothesis requests.
By running mean the average values comes from

$$\overline{\xi_k} = \left(1 - \frac{\Delta t}{\tau_f}\right)\overline{\xi}_{k-1} + \frac{\Delta t}{\tau_f}\xi_k \qquad [1.35]$$

where Δt is the interval between two samples in s and τ_f is a time constant (the running mean filter) in s.

In the linear detrending method $\overline{\xi_k}$ is computed by the least squares regression as [Aubinet et al., 1999]

$$\overline{\xi_k} = \overline{\xi} + b\left(t_k - \frac{1}{n_s}\sum_{k=1}^{n_s} t_k\right) \qquad [1.36]$$

where t_k is the k-th step time and b is the slope of the linear trend of the time series.

These methods acts as an high-pass filter on the time series: the smaller the time constant, the more low-frequency content is eliminated.

Gas concentration conversion. The amount of a scalar s in the atmosphere can be expressed in many units. *Density* ρ_s (kg m^{-3}) and *molar density* c_s (mol m^{-3}), *molar fraction* d_s, the ratio between moles of s and total moles of the (wet) air mixture (mol mol^{-1}), *mixing ratio* χ_s, the ratio between moles (or mass) of s and total moles (or mass) of dry air (mol mol^{-1} or kg kg^{-1}). Between these, only mixing ratio has conservative properties, i.e. does not change with changes in temperature, pressure and humidity [Aubinet et al. 2012]. Densities and molar fractions, the quantities that are normally measured in the field, are not conservatives, meanings that changes in environmental variables could results in variation of such quantities even if there is no production, consumption or transport of the concerning scalar. If is not possible using mixing ratio in the flux computation, corrections taking into account such effects need to be performed [Webb et al., 1980].

Time lag and covariance maximization. Sensors separation, the physical distance between the anemometer and the point where air is sampled, involves instantaneous gas concentrations measured with a certain delay with respect to their corresponding instantaneous wind measurement. Such time lag arises for different reasons in closed path and in open path sensors. In the former it is caused by the time air spends passing through the intake tube and depends mostly on the tube diameter and the sucking pump strength (flow rate). In the latter it is due to the distance between the two instruments (which are usually placed several centimetres apart to avoid mutual disturbances) as wind takes some time to travel from one to the other.

Actually the most suitable procedure to calculate time lags is the so called *covariance maximization* and consists in determining the time lag that maximizes the covariance between two variables, within a reasonable time window [Aubinet *et al.*, 1999; Fan *et al.*, 1990]

$$\overline{w'\xi'}_{MAX} = \overline{w'\xi'}(\tau) = \max\left(\sum_{k=1}^{n_s-j}\overline{w'_k\,\xi'}_{k+j}\right) \qquad [1.37]$$

where τ is the best time lag estimate, k is the current time step and j denotes the amount of increasing (or decreasing) time steps. Dividing the discrete value of τ by the acquisition frequency we get the time lag in seconds. Anyway, is not always possible detect a maximum, especially when fluxes (covariances) are small, and a fixed (pre-calculated) lag value might be used. Sensor separation involves signal frequency loss, typically in the high frequency range (low-pass filter), hence fluxes have to be corrected consequently with the proper transfer function. Below (Fig. 1.4) there is an example of covariance maximization procedure result.

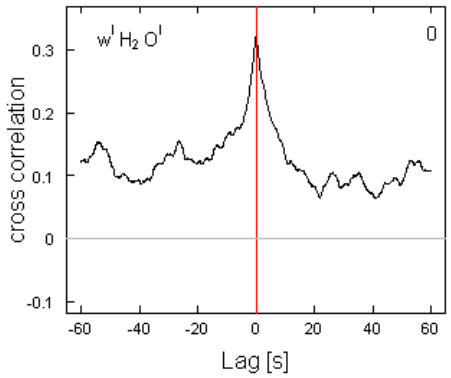

Figure 1.4. An example of the covariance maximization procedure. The time lag (in seconds) is individuated as the time at which the covariance between two variable has a peak.

Compensate density fluctuations. When measuring a trace gas turbulent flux, variations of the gas density due to the presence of heat and water vapour flux have to be taken into account as they cause expansion/contraction of air that strongly modulated density changes. If the measurement involves gas mixing ratio (relative to dry air) then no corrections are needed, while if molar fraction or molar density are available than fluxes have to be corrected accordingly to the so called Webb, Pearman and Leuning (WPL) theory [Webb et al., 1980]. The rationale is linked to the governing constraint of zero mean vertical flux of dry air. This corrections could be very important even up to 100% of the measured flux. Considering the actual density ρ of a gas c the WPL corrected flux become

$$F_s = \overline{w'\rho'_c} + \mu\frac{\overline{\rho_c}}{\overline{\rho_a}}\overline{w'\rho'_v} + (1+\mu\sigma)\frac{\overline{\rho_c}\,\overline{w'T'}}{\overline{T}} \qquad [1.38]$$

I II III

where subscripts a and v refers to air and vapour respectively, $\mu = m_a/m_v$ is the wet to dry air ratio being m_a the molecular mass of air, and m_v is the molecular mass of water vapour, $\sigma = \rho_v/\rho_a$ and T is the air temperature. On the RHS term I is the measured flux, term II is the water

vapour effect (dilution term) and term III is the temperature effect (thermal expansion and contraction term).

Frequency response losses. As stated in the previous section it is common to describe the frequency repartitions of the fluctuations by introducing the cospectral density and in the case of turbulent flux of a scalar ξ, the cospectral density is linked to the covariance [Stull, 1988; Kaimal and Finnigan 1994] by

$$\overline{w'\xi'} = \int_0^\infty C_{w\xi}(f)df \qquad [1.39]$$

where f is the cyclic frequency. In practice the cospectra integral range is limited at low frequencies by the averaging period and the high-pass filtering while at high frequencies by low-pass filtering [Aubinet et al., 1999]. Consequently the *measured* flux can be seen as an integration of the cospectral density over the frequency range multiplied by a *transfer function* (TF) describing the time delay between the output signal and the input signal (*phase shift*) and the damping of the amplitude [Foken 2008]:

$$\overline{w'\xi'}_m = \int_0^\infty C_{w\xi}(f)TF(f)df \qquad [1.40]$$

The measured fluxes have to be corrected to take these effect into account by means of a correction factor (CF) computed as the ratio of flux free from filtering and the measured flux

$$CF = \frac{\int_0^\infty C_{w\xi}(f)df}{\int_0^\infty C_{w\xi}(f)TF(f)df} = \frac{\int_0^\infty C_{w\xi}(f)df}{\int_0^\infty C_{w\xi}(f)TF_{HF}(f)TF_{LF}(f)df} \qquad [1.41]$$

where the total transfer function is partitioned into high frequency (TF_{HF}) and low frequency (TF_{HF}) components.

High-pass filtering determine flux spectral, hence covariance, losses in the low frequency range (passing the high frequency contribution), due to the finite averaging time and the detrending method, leading in general to a systematic underestimation of the fluxes [Moncrieff et al., 1997].

Low-pass filtering arise from the inability of the measurement system to resolve fluctuations associated with small eddies, and normally determines a flux underestimation. The damping of high frequency fluctuations may be due to the frequency response of the anemometer and/or the IRGA, the sensor response mismatch, the scalar path averaging, the sensor separation and the tube attenuation (for closed path sensor) [Moore 1986; Horst 1997].

Transfer functions can be estimated either theoretically and experimentally. Their derivation is not reported here, for a complete description refer to the cited papers.

Turbulence tests and quality control. After fluxes have been computed, their quality in terms of errors has to be assessed to validate results and discards methodology and site specific influence. Measurements errors may arise from technical (instruments failures) problems or violations of theoretical assumptions and can be systematic or random distributed [Foken and Wichura, 1995; Moncrieff et al., 1996]. Beyond the previously mentioned despiking and statistical tests performed on raw instantaneous data, there are other test aimed to ascertain if assumptions on developed turbulence are met. These tests are made on scalar fluxes and evaluate either the stationarity of the measuring process, the *steady state* (or stationarity) test, and the flux-variance similarity, the *integral* (or developed) *turbulence* test [Foken and Wichura, 1995].

The steady state test is based on Eq. [1.13] for the flux determination and consist in dividing the sampling interval (e.g. 30 minutes) into sub period of 5 min along which covariances are computed. If the difference (dispersion) between the covariances of the sub-sampled periods is less than 30% of the full period covariance, the measurement is considered to be stationary.

The integral turbulence test is based on the comparison of measured integral characteristics of the vertical wind (σ_w / u_*) and temperature (σ_T / T_*) with concerning models parameterised by Foken [1991]. If difference are kept down to 20-30 % flux-variance similarity is met.

Flux footprint. To know how much the measured fluxes are representative of the real ecosystem fluxes is necessary to locate the spatial distribution of sources and sinks. By the footprint analysis is possible to relate the one point measured flux to its turbulent diffusion from sources located upwind from the sampling point (the source region). The footprint represents the extent to which un upwind source contribute to the observed flux [Aubinet et al., 1999]. It can be computed by means of analytical models linked with measurement height, surface roughness, atmospheric stability, wind velocity and direction. Several footprint models are available [e.g., Kormann and Meixner, 2001; Kljun et al. 2004] differentiated in complexity. An example of an application of the footprint model by Kljun *et al.* [2004] over a forest canopy showing how measurement height can impact the sampling in the source region is showed in Fig. 1.5.

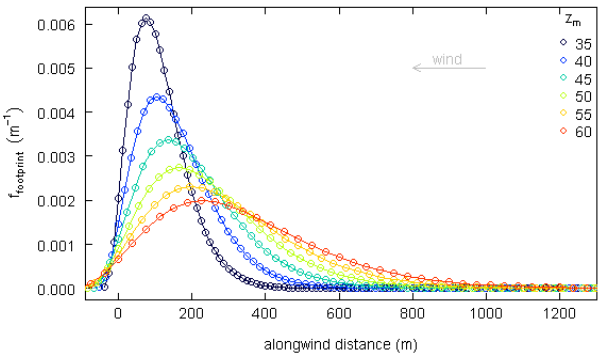

Figure 1.5. Example of crosswind-integrated flux footprint predictions considering six different measurement heights z_m over a forest surface. Footprint model by Kljun et al. [2004]. Scenario: PBL height = 1000 m, σ_w = 0.4 m s^{-1}, u_* = 0.4 m s^{-1}, roughness length z_0 = 3 m, tree height h = 30 m. For the model computation effective measurement height might be considered, i.e. z_m * d with d = 0.75 h being the displacement height.

In case of footprint estimations above forest surfaces, the height of sources plane is assumed to be $d + z_0$, that is close to the upper canopy mean level [Aubinet et al., 1999]. The source area of flux footprints estimated under a forest canopy is much contracted as compared to one evaluated above the canopy. In general, the understory footprint probability function peaks within 2-3 z_m (the sampling height) and its extent is restricted within 20-30 z_m [Baldocchi 1997].

1.3 Study site: Ankasa Forest Conservation Area, Ghana.

The Ankasa conservation area defines one of the oldest rainforest and the most biodiverse of Ghana. It is the only wet evergreen protected area in practically pristine state with almost 800 vascular plant species and many animal species. Ankasa is relatively uniform in its abiotic landscape features being a relatively undisturbed high forest climax community.
The area is located in southwest Ghana (Fig 1.6) on the border with the Ivory Coast. The protected area covers about 509 km^2 [Symonds 2000] and include the *Nini-Suhien National Park* and the adjoining *Ankasa Resource Reserve* (the measurement site). It lies within the administrative jurisdiction of *Jomoro District Assembly* and traditionally under the *Paramount Stool of Western Nzema* at *Beyin*. The Nini river is the northern boundary of the National Park.

Figure 1.6. Aerial images of the Ankasa forest reserve. The red square indicate the EC measurement tower. The dark green areas are the forest patches. (Images from *Google Earth*).

The climate is characterised by a distinctive bi-modal rainfall pattern occurring from April to July and September to November. The average annual rainfall is 1700 to 2000 mm. Mean monthly temperatures are typical of tropical lowland forest and range from 24 to 28 °C. Relative humidity is generally high throughout the year, being about 90% during the night falling to 75% in early afternoon.
The soil surface is characterised by rugged, deeply divided terrain in the north and west with flatter swampy ground associated with the *Suhien* watershed in the east. Its maximum elevation is 150 m at *Brasso Hill* in the National Park, though most lies below 90 m a.s.l..
The underlying geology consists of three major geological formations. The northern section is based on granites intrusions. The area is at the intermediate erosion stage of maximum slope

and is well dissected by an extensive and regular dendritic drainage system. At the south of the granites area there is the area of sediment of clay, hardened and foliated by heat and pressure. The southern most areas are relatively recent deposits.

In general the soils are classified as *Forest Oxysols*. They are deeply weathered, highly acidic (pH 3.5 to 4.0), disposed to the wind blowing off the Sahara from north, that deposits large quantities of fine soil particles. This annual deposit of clay minerals is likely to play an important role in maintaining forest fertility. The stock of carbon in the mineral soil to a depth of 1 m was measured to be 151 ± 20 Mg C ha^{-1}, a similar value in magnitude to the one of the aboveground biomass being 138-170 Mg C ha^{-1} including live and dead wood. Surface litter C is roughly 10% (15 ± 9 Mg C ha^{-1}) of the C in the biomass and soil [Chiti et al., 2010].

Recent studies report an average density of 950 plants ha^{-1}, leading to an aboveground biomass of about 270 t ha^{-1}. The LAI (leaf area index) is estimated to be 6 ± 1.01. The distribution of forest-types is largely determined by interacting environmental factors of which climate, geology and soils are the most important. Some of the main species are *Cynometra ananta, Heritiera utilis, Gluema ivorensis, Parkia bicolor, Lophira alata, Strephonema pseudocola, Uapaca guiinensis* [Marchesini et al, 2011].

An EC station for the monitoring of GHG and energy fluxes (Fig. 1.6) is operative as part of the CarboAfrica eddy covariance network. The facility, located in the Ankasa Conservation Area includes a 65 m tall steel tower equipped with a system enabling the measurements of fluxes at the top of the structure, air temperature and humidity along a vertical profile and of relevant physical parameters of the forest ecosystem.

A preliminary analysis made in August 2008 indicated a daily uptake of 1.33 ± 0.73 g C m^{-2} d^{-1} with the CO_2 flux measured above the canopies ranging from a night efflux of 2.3 to a day-time uptake of -14.8 µmol m^{-2} s^{-1}. The build-up of the CO_2 concentration in the closed canopy space at night (i.e. CO_2 storage) determines an underestimation of the ecosystem respiration on average by a factor 2 - 2.5 and by a maximum of 4 [Marchesini et al, 2011] demonstrating the importance of storage correction in such environment.

2 State of the art in micrometeorological trace gas flux measurements

The main sources and drivers of CH_4 and N_2O fluxes are well identified in most ecosystems, yet there is still large uncertainty in their relative strength. Two main factors contribute to limit the ability to precisely quantify annual or seasonal budgets of these two gases. First, their net biosphere/atmosphere exchange rate is controlled by many biological, chemical and physical ecosystem parameters [Ganzeveld et al., 2004; Matson et al., 2009; van Hulzen et al., 1999; Snyder et al., 2009] resulting in a very high temporal and spatial variability of fluxes [Cao et al., 1998; Iqbal et al., 2009]. Second, both gases have a quite low atmospheric concentration, at least compared with CO_2, which, in combination with their small flux rates, makes the flux measurement a challenging technological achievement. As a consequence, exhaustive assessment requires high spatial resolution and continuous long-term monitoring.

Among the approaches explored to quantify CH_4 and N_2O fluxes, micrometeorological techniques are thought to be the most appropriate for landscape estimations. They are able to integrate spatial scales of the order of hundreds meters to kilometers and this is particular important for distributed sources of emissions. Furthermore they can provide continuous flux measurements in order to capture pulse emissions, as it often occur i.e. for agricultural crops after fertilizer application [Moncrieff et al., 1997b; Denmead, 2008].

Direct methods like Eddy Covariance (EC), Eddy Accumulation (EA) or its modification Relaxed Eddy Accumulation (EA), are based on the principle of "frozen turbulence" [Taylor et al., 1938]. This is accomplished by sampling the air as it passes through a sampling point to measure its speed and scalar concentration, assuming that eddies time and spatial averaging at the observation point are equivalent. Fluxes are then estimated by the covariance of the scalar concentration with the vertical component of the wind speed.

Indirect methods, such as the Flux Gradient (FG) and Bowen Ratio (BR), attempt to quantify the rate of diffusion along a concentration gradient [Moncrieff et al., 1997b; Moncrieff et al., 2000] by using particular assumptions on the turbulent transport, through similarity theory and/or semi-empirical coefficients.

Direct and indirect methods have been compared in the last decades, and strength and weakness of both have been extensively discussed [Fowler et al., 1995; Moncrieff et al., 2000; Denmead, 2008]. Except for EC, the technique used in this work, other micrometeorological techniques are not further detailed here, in-depth descriptions can be found in more specific literature [see e.g. Fowler et al., 1995, Moncrieff et al., 1997a, b; Denmead, 2008 and references thereby]. However most of the methodological work, validation and uncertainty analysis of micrometeorological techniques have been carried out for carbon, water and energy fluxes. Such big effort is documented by a growing literature which was stimulated by the early establishment of the flux network FLUXNET in 1999 [Baldocchi et al., 2001]. The application of micrometeorological methods to non-CO_2 trace gases in different biomes and with continuous operations lagged behind with a certain preferences for enclosure techniques despite some known limits. However, the commercial development of reliable and fast response instrumentation in the last years increased the diffusion of micrometeorological

stations for N_2O and CH_4 flux observations, leading to an increasing number of experiments and relative published results.

2.1 Literature review of micrometeorological CH_4 and N_2O flux measurements

The review of past data is based on articles reporting results of micrometeorological determinations of CH_4 and N_2O exchanges, mostly published from early 1990s to now. A large degree of heterogeneity characterizes the collection, as experiments differ significantly with respect to a number of aspects, including: *i*) the observed ecosystem *ii*) the technique employed *iii*) the duration of the experiment *iv*) the period of the year when measurements have been carried on. Being the analyzed sites distributed worldwide within several climatic zones, data are firstly grouped according to main ecosystem types: forests, wetlands, managed lands and anthropic environments. Here, forests include several typologies of stands with different structure and species composition, wetlands are areas permanently or seasonally swamped, managed lands include cultivated areas with different type and levels of management, while anthropic environments are those areas fully determined by human activities, such as cities and landfills. An overview of sites main features is given in Appendix A Tables A1 and A2. In order to compare N_2O and CH_4 fluxes from different publications, flux estimates were harmonized and expressed as mg of N_2O or CH_4 m^{-2} h^{-1}. In Appendix A Table A3 flux daily mean and ranges are reported along with the technique employed. Coherently with authors, flux ranges are sometime reported as the standard deviation of the mean, in other cases they refer to minimum/maximum pairs reported either as half-hourly (or hourly) values or as daily averages. Where necessary daily averages were derived from day-time/nigh-time pairs or from long-period averages. In Appendix A Table A4 sensor typologies, measurement accuracy and precision as well as FDL are resumed, as reported by the authors in their studies. As generally accepted, here the term accuracy is used to indicate the proximity of a measurement to the real value of a variable. It is mostly affected by systematic errors. Precision refers to the degree of convergence of several replicates, hence, is mostly affected by random errors. Flux detection limit is the minimum meaningful flux that an instrumental set-up is able to distinguish from its inherent noise. Detection limit (DL) primarily depends on the adopted measurement technique, the instrumental precision and local turbulence characteristics. It is further affected by the chosen sampling strategy (e.g. averaging period, sampling frequency) and to some extent by site-specific characteristics, such as the background gas concentration. An estimation of the FDL is crucial for the selection of the most suitable measuring technique and set-up for obtaining meaningful fluxes from specific ecosystems. Businger and Delany [1989; 1990], suggested an approach to estimate sensor resolution required to make flux measurements with a ±10% uncertainty. The proposed formula took the form

$$R = 0.1|flux|AP \qquad [2.1]$$

where 0.1 represents the 10% uncertainty requirement, flux is the surface flux of the trace gas, and AP an "atmospheric parameter" based on the main atmospheric conditions (stability and friction velocity) describing the uncertainty associated with the chosen technique, EC, FG and REA. Recently Rowe et al. [2010], presented improvements to the method specifying the resolution limits for the covariance method and removing the dependency of the AP parameters to u* (friction velocity).

Nelson et al. [2004] estimated that meaningful N_2O fluxes require an instrumental precision of 1 part-per-thousand of the ambient mixing ratio, while few part-per-thousand of the ambient mixing ratio are often enough for CH_4. The calculation of FDL may be carried out by several approaches. For EC, detection limits are often assessed by estimating the standard deviation of the cross-covariances (between vertical wind speed and the scalar concentration fluctuations) far from the true time lag, e.g., in the region of −50 and +50 s [Kroon et al., 2007; Smeets et al., 2009] following the original proposal by Wienhold et al. [1995]. Alternatively, FDL have been estimated basing on the instrumental noise and the standard deviation of vertical wind speed at the sampling level [Edwards et al., 2001; Pihlatie et al., 2005b; Neftel et al., 2007]:

$$FDL = \frac{\sigma_w \sigma_c}{\sqrt{Tf}} \qquad [2.2]$$

where σ_c is the signal noise of the instrument, σ_w is the standard deviation of vertical wind speed, T is the averaging time and f the measurement frequency.

Differently, for the "slow-methods" such as FG, Griffith et al. [2002] suggest assessing the detection limits by propagating instrumental precision (σ_c) through the flux equations i.e.

$$FDL = -K\rho_a \frac{M_x}{M_a} \frac{d\sigma_c}{dz} \qquad [2.3]$$

were K is the eddy diffusivity, ρ_a is the density of dry air, $d\sigma_c /dz$ is the propagation term of the single measurement precision and M_x and M_a are the molecular masses of species x and dry air. For REA, authors [Beverland et al., 1996b; Pattey et al., 2006; Desjardins et al., 2010] adopted an empirical approach, performing a series of tests (replicates) aiming at quantify the mean concentration differences ($\Delta_c = \bar{c}^+ - \bar{c}^-$) among bags filled with the same ambient air, and compute the FDL integrating such value in the flux equation:

$$FDL = A\sigma_w \Delta_c \qquad [2.4]$$

where A is the empirical parameter dependent on the magnitude of the chosen dead band for the vertical wind speed (generally 0.1 m s^{-1}).

2.2 Flux variability within and between ecosystem categories

Frequency distributions of mean fluxes within and between each land category are showed in Figure 2.1. For what concern N_2O (see also Appendix A Tab. A3), the largest mean fluxes are reported for anthropic environments (min./max. 0.51/4.24 mg m^{-2} h^{-1}, N=2), followed by managed lands (average 0.33 ± 0.55 mg m^{-2} h^{-1}, 0/3.53 mg m^{-2} h^{-1}, N=37) and forests showing a minor contribution (0.013 ± 0.014 mg m^{-2} h^{-1}, 0.005/0.035 mg m^{-2} h^{-1}, N=4). No data are reported for wetlands. In the case of CH_4 more data are reported. Fluxes from anthropic environment are the highest (2103 ± 1962.12 mg m^{-2} h^{-1}, 272.72/5940 mg m^{-2} h^{-1}, N=6), followed by wetlands (3.25 ± 3.9, 0.03/16 mg m^{-2} h^{-1}, N=36), managed lands (0.92 ± 0.88 mg m^{-2} h^{-1}, 0.09/2.46 mg m^{-2} h^{-1}, N=6), and forests (0.43 ± 0.60 mg m^{-2} h^{-1} -0.13/2.19 mg m^{-2} h^{-1}, N=15). Mean fluxes are statistically different (Kruskal-Wallis test, 0.01 significance level) among our ecosystems groups except for CH_4 fluxes from managed lands and from wetlands (inferences referring on groups with very few observation should be used with caution). In the following, a detailed description of the reported N_2O and CH_4 fluxes is presented.

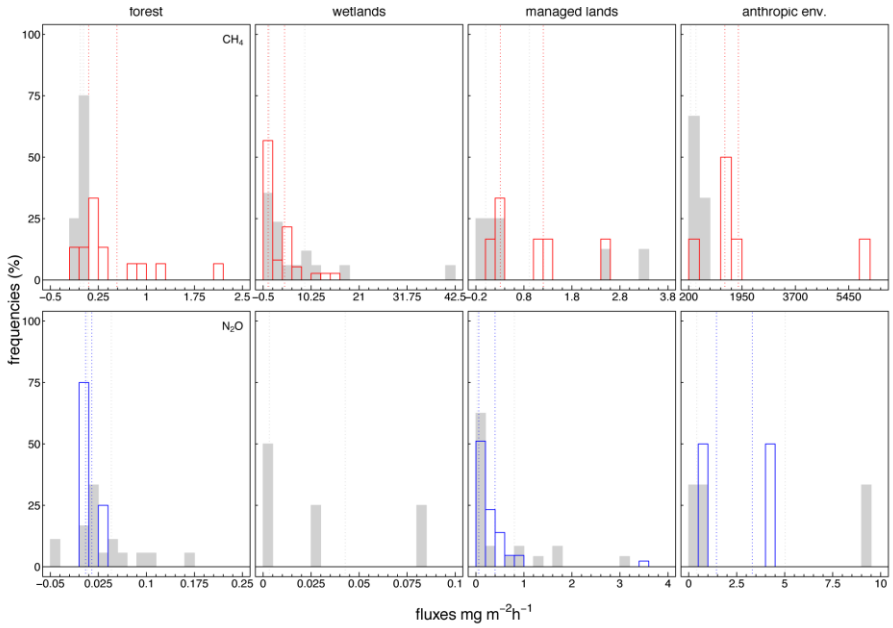

Figure 2.1. Ecosystem frequency distribution of mean CH_4 and N_2O fluxes reported by micrometeorological (red-blue bars) and soil chambers (grey bars) methods. Dashed lines indicate the fluxes interquartile ranges.

Nitrous oxide. About the 89% of N_2O data refer to agricultural ecosystems, only three studies have been reported for forest ecosystems, all included between 47° and 55° latitude, and two studies are in anthropic environments. No studies are reported for wetlands.

The average daily mean N_2O fluxes reported for forests, measured in Denmark, Canada and Switzerland indicate a strong temporal variability within a relatively short period with both high N_2O uptake and emission values. The highest fluxes values reported by Pihlatie et al. [2005b], measured below-canopy, correspond to the period of highest soil water content (around 50% of water filled pore space). Interestingly, this peak was not evidenced using

manual and automated chambers associated to GC in the same period. The latter method was applied with a lower temporal resolution (weekly base) and a limited spatial replication (6 manual and 1 automated chamber), which might explain the differences in the observed results. Small negative fluxes were reported using EC, whereas this was not evidenced with closed chambers. Even higher was the flux variability evidence by Eugster et al. [2007a, b]. A quite high maximum hourly mean was reported in this deciduous forest (3.65 mg N_2O m^{-2} h^{-1}), where an EC system was placed above tree canopy. In this study, the majority of significantly high fluxes were measured within 6.5 h before precipitation events. The authors hypothesized the N_2O production from senescing leaves was stimulated by fog, before precipitation sets in, or by the drizzle, and that this source was as important as soil microbial activity. This underlines the importance of catching the N_2O significant pulses, which might have been missed using discontinuous sampling by enclosure techniques. The distribution of the half hour records of N_2O fluxes, characterized by a quite normal shape centered on a mean value of 0.03 mg m^{-2} h^{-1}, presented a significant amount of fluxes below zero (N_2O uptake). This finding was hypothesized to depend on the presence of the snow cover, as also reported by other authors [Kitzler et al., 2006]. However to the best of our knowledge, a similar distribution in comparable conditions has not been evidence yet using soil enclosures.

The great majority of the N_2O literature analyzed here refers to fluxes from agricultural lands. Without regard to a particularly high value [Denmead et al., 2000], the overall mean (α = 0.02) of the averaged daily flux in these ecosystems is 0.26 ± 0.24 mg m^{-2} h^{-1}. Instantaneous fluxes were extremely variable. Again, as also evidence for the forest sites, the flux variability within site was higher than the flux variability observed among sites, despite the very different management and fertilization loads. In several cases a quite wide range of average N_2O fluxes was reported (App. A, Tab. A3), the highest value (about 5 mg m^{-2} h-1) being reported for an intensively managed grassland in Scotland after periods of fertilization and rainfall events [Di Marco et al., 2004; Flechard et al., 2007].

Extremely variable fluxes were reported by Li et al. [2008] in a maize field (minimum/ maximum hourly values of -4.4/4.8 mg m^{-2} h^{-1}) and in a wheat field (minimum/ maximum hourly values of -2.82/3.59 mg m^{-2} h^{-1}) using two micrometeorological methods, FG and Bowen Ratio (energy balance). Data were only collected after fertilization events or under low wind conditions to maximize detectable N_2O gradients. According to both methods, many negative fluxes were found, even after fertilization. These extreme values, in particular such high negative fluxes, were not reported in most of the analyzed literature with the exception of Flechard et al. [2007], Kroon et al. [2007] and Schrier-Uijl et al. [2010]. The only negative average fluxes, even if very weak (-0.0003 mg m^{-2} h^{-1}), was measured by Maggiotto and Wagner-Riddle [2001] over an unfertilized (control plot) turf grass field in Canada.

Three experiments are available where different techniques were compared. In the first, EC, REA, FG and chambers techniques were used to quantify fluxes from an agricultural field in Denmark [Wienhold et al., 1995; Hargreaves et al., 1996; Christensen et al., 1996; Griffith and Galle, 2000] and results indicated that there was no bias between the different approaches, and the precision of the measurements was mainly related to the spatial variability of the emissions and the variability of each individual technique. In the second study carried on in a lowland in Scotland [Arah, et al., 1994; Galle et al., 1994; Hargreaves, et al., 1994; Smith et al., 1994; Wienhold et al., 1994] a comparison was made using automated

chambers of different size and micrometeorological methods (EC, FG). Measurements were made over similar periods (30 to 60 minutes), however they averaged over different spatial scales and related to different areas of the field. Higher values were obtained by the chamber methods but no conclusive explanation was found for this discrepancy. In the third study a comparison of EC method with chambers measurements was made on a grassland system in central Switzerland [Neftel et al., 2007; Neftel et al., 2010]. The mean background flux measured using both techniques was quite close. N_2O flux temporal variations observed with both methods were also similar, driven by soil temperature and water-filled pore space.
Two studies carried out on the same site (sheep grazed Australian pastures) showed different results using a mass balance (MB) approach (8 days measurements) [Denmead et al., 2000] and an FG approach (15 days measurements) [Griffith et al., 2002]. In the former study, higher fluxes were measured, although a very high emission of 3.53 mg m^{-2} h^{-1} was conditioned by two days of rain in which emissions peaked at about 12.5 mg m^{-2} h^{-1}. In the latter one, significantly smaller fluxes were reported, with an average of 0.09 ± 0.27 mg m^{-2} h^{-1}.
Only two studies report N_2O fluxes measured using micrometeorological techniques in anthropic environments. Famulari et al. [2009] reported the first EC based N_2O flux estimations above a city. Emissions showed a diurnal cycle, following the dynamics of the boundary layer mixing. The overall daily mean flux was 0.52 mg m^{-2} h^{-1}, characterized by three main peaks up to 3.01 mg m^{-2} h^{-1} related to the rush hours of traffic. Rinne et al. [2005] measured N_2O fluxes from the municipal landfill of Helsinki. Average EC-fluxes were 4.24 mg m^{-2} h^{-1}, about 45% of the emissions measured by the soil enclosures.

Methane. More data have been reported for CH_4 fluxes in terrestrial ecosystems (App. A Tab. A1, A2, A3, Fig. 2.1). The majority of investigations in forests refer to boreal coniferous ecosystems. All the analyzed studies were done over short periods of observation (from 2 to 43 days) hence the reported daily average cannot be considered representative for a yearly-based quantification. With just two exceptions [Bowling et al., 2009; Smeets et al., 2009], the reported average CH_4 flux was always positive (net CH_4 emission). In most cases, flux variability between ecosystems was again lower than flux variability within ecosystems. Pattey et al. [2006] measured quite different daily average CH_4 fluxes in the same ecosystem using different techniques (0.73 mg m^{-2} h^{-1} by FG and 2.19 mg m^{-2} h^{-1} by EC). Moreover they also evidenced an extremely high variability between daytime and night-time mean fluxes using the same approach (daytime 1.25 mg CH_4 m^{-2} h^{-1} and night-time 0.21 mg CH_4 m^{-2} h^{-1} by FC and daytime 4.17 mg CH_4 m^{-2} h^{-1} and night-time less than 0.2 mg CH_4 m^{-2} h^{-1} by EC). The coniferous forest in Colorado investigated by Bowling et al. [2009] acted as a net CH_4 sink during the 43 days of observations and no evidence was found for CH_4 emissions from vegetation, even under high UV radiation or after rainy events. A similar result was found by Smeets et al. [2009] in a temperate conifer forest in California, where CH_4 uptake followed a clear diurnal pattern, which would have been unexpected on the base of daily variability of soil characteristics (as they influence gas diffusivity and microbial CH_4 consumption). Only three studies were reported for tropical forests (App. A Tab. A1) during both dry and wet season. In all cases a net CH_4 emission was measured, independently of the season, in the range of 0.08 and 0.85 mg CH_4 m^{-2} h^{-1}.

More data are available for wetlands, many of which are located in boreal regions. These ecosystems have a great impact on atmospheric methane burden. As example Bridgham et al. [2006] estimate that North American wetlands emit around 9 Tg CH_4 yr^{-1}.
The overall mean value distribution of fluxes falls within 0.032 and 16.0 mg m^{-2} h^{-1}, a rather wide range. However the 50% of data are below 1.50 mg m^{-2} h^{-1} and the 75% below 4.36 mg m^{-2} h^{-1}. Studies carried out in tundra show quite consistent results. For example, Wille et al. [2008b] and Sachs et al. [2008] conducted similar experiments measuring CH_4 emission by EC in the Samoylov Island (Siberia) in 2003/2004 and 2006, respectively. Using an averaging interval of 60 minutes, Wille and co-workers derived quality-screened fluxes of about 1.25 mg m^2 h^{-1} during mid-summer and 0.42 mg m^{-2} h^{-1} during the snow cover. Soil temperature and near-surface atmospheric turbulence were recognized as the factors controlling methane emission. Similarly, Sachs et al. [2008] reported average fluxes of 0.78 mg m^{-2} h^{-1} over permafrost. Due to the strong control that near-surface turbulence exerts on methane fluxes, authors argue about the reliability of enclosure-based measurements, which exclude this driver by preventing turbulent exchanges on the sampled surface. Haapanala et al. [2006], using REA technique in a fen in Finland (14 days, growing season) observed a large temporal variation of fluxes within this short period, from 0 to 10.0 mg m^{-2} h^{-1}, with a mean emission of 4.30 mg m^{-2} h^{-1}. These values are in the range reported for the same site by Rinne et al. [2007] using the EC technique. Friborg et al. [1997] compared EC and chamber measurements during spring thaw in a sub-arctic mire in northern Sweden, giving emphasis to the influence of temperature variations and atmospheric conductance on CH_4 fluxes. Beswick et al. [1998] measured CH_4 fluxes in northern Finland utilizing balloon flights for air sampling, applying either FG (mean flux 3.72 mg m^{-2} h^{-1}) or the "box method" (3.85 mg m^{-2} h^{-1}) on the base of local atmospheric stability regime. They also applied EC method obtaining CH_4 fluxes about four times smaller concluding that comparable measurements could be obtained only under suitable conditions for both techniques. Hendriks et al. [2008] demonstrated that simulated 1Hz EC, Disjunct EC and REA fluxes from the same experimental dataset obtained by 10 Hz EC set-up, did not produce significantly different average CH_4 fluxes. Strong seasonal and daily variability was found by Kim et al. [1998a, 1998b] on a prairie marsh in Nebraska using EC approach over a 2 years campaign (seasonal variation from 2.20 to 10.60 mg m^{-2} h^{-1}, with night time to daytime ratio of 0.65-0.90) In the course of the second campaign results were further higher with daytime average fluxes of 25.0 mg m^{-2} h^{-1} and 8.0 mg m^{-2} h^{-1} during night-time, characterized by a strong correlation with near-surface sediment temperature.
Extremely variable fluxes (-16.31 and 31.97 mg m^{-2} h^{-1}) were reported by Mukhopadhyay et al. [2002] in a mangrove forest (India) during 1998-2000 covering three monsoon related seasons. Marked seasonal variation was found to be dependent, apart from biological local process, to meteorological conditions, in particular sensible heat flux and friction velocity. CH_4 flux values for rice fields are within the range of variability of CH_4 fluxes reported for the other analyzed flooded ecosystems. Few CH_4-targeted micrometeorological studies have been made on managed lands, and none of these was aimed at CH_4 flux determination exclusively but always in combination with N_2O flux estimation. All the analyzed sites were characterized by a rather elevated moisture regime of soil, the latter being often organic (peat). In all sites net daily CH_4 emissions were reported. Interestingly, Denmead et al. [2010] recorded a net annual CH_4 emission of about 19.9 Kg CH_4 ha^{-1} over 342 days of observation

(about 0.28 mg m^{-2} h^{-1}) in a sugarcane field, however, enclosure measurements showed essentially zero fluxes. In order to explain this discrepancy the authors assumed that the main CH_4 source was not within the soil but came from the surrounding drains. Their long data set showed no dependence of emissions neither on soil water content nor on soil temperature but a strong relation with rainfall events. In a recent work Dengel et al. [2011] measuring methane fluxes over a pasture by means of EC, observed no clear relationship of fluxes with air temperature or radiation, but a diurnal-trend like behavior, probably driven by sheep grazing.
Six studies are available for anthropic environments. Wagner-Riddle et al. [2006] measured CH_4 fluxes from manure slurry storage tanks at two swine farms in southern Ontario (Canada) by means of a four-tower MB system. By using four methods to integrate horizontal fluxes, they calculated half hourly means ranging 563.40 to 2141.64 mg m^{-2} h^{-1} at one site, and 75.60 to 3937.32 mg m^{-2} h^{-1} at the other site (nitrous oxide fluxes were also targeted but no significant source was detected). A comparison of gas fluxes from liquid manure measured with MB approach and chambers has been recently reported also by Park et al. [2010]. Mean CH_4 flux was 5940.0 mg m^{-2} h^{-1}, about 80% of chambers response. This underestimation was related to the placement of some chambers on hot-spot areas. These extraordinary high emissions peaked to 16632.0 mg m^{-2} h^{-1} and decreased to a minimum rate of 1116.0 mg m^{-2} h^{-1}. Hovde et al. [1995] reports landfill CH_4 emissions (272.72 mg m^{-2} h^{-1}) measured during a very short period (seven half-hourly records collected after a rainstorm). Several years later, Laurila et al. [2005] and Lohila et al. [2007] reported EC measurements based on Gas Chromatograph - Flame Ionization Detector (GC-FID) on a municipal landfill in Finland. Such economical system was also tested against the more expensive system based on Tunable Diode Laser Absorption Spectroscopy (TDLAS) founding comparable responses. Flux strength was strongly dependent on source areas, with differences within wind direction sector of more than 1:4. Lohila and colleagues used an EC set-up to monitor CH_4 fluxes over a 6 months period. Emission rate ranged from 0 to 10800 mg m^{-2} h^{-1} with an average flux of 1908 mg m^{-2} h^{-1}. The high daily variability of fluxes was strictly dependent on flux source area (wind direction) and emission rate was very closely related to CO_2 efflux. Recently also Eugster and Pluss [2010] measured emissions from a sealed landfill in Switzerland. As this site is conceived to avoid gas losses, detected fluxes were negligible respect to the above-mentioned works with daily median values between 5.76 and 39.60 mg m^{-2} h^{-1}. Furthermore during one day a net uptake of -2.23 mg m^2 h^{-1} was recorded.

2.3 Flux detection limits and sensors suitability

From bibliography emerges that about 45% of works were carried out by means of the EC technique, 38% by the FG, 8% by the REA and the remaining 9% by the other techniques. Concerning the gas sensors, 69% of the devices used with EC are based on the Tunable Diode Laser Absorption Spectroscopy (TDLAS), 15% on Cavity Ring-down Spectroscopy (CRDS) and 7 and 6% on Quantum Cascade Laser Absorption Spectroscopy (QCLAS) and Wavelength Modulation Spectroscopy (WMS) respectively. From multiple pair-wise comparison tests (p.value = 0.01), it seems like there is no statistical difference between FDL reported by different sensors, both for methane and for nitrous oxide flux estimates. To have

an indication on micrometeo techniques effectiveness in catching small fluxes, in Figure 2.2 the minimum FDL reported for each sensor/technique (App. A, Tab. A4) is compared with independent measures, absolute minimum flux value, reported for soil enclosure technique (data not shown).

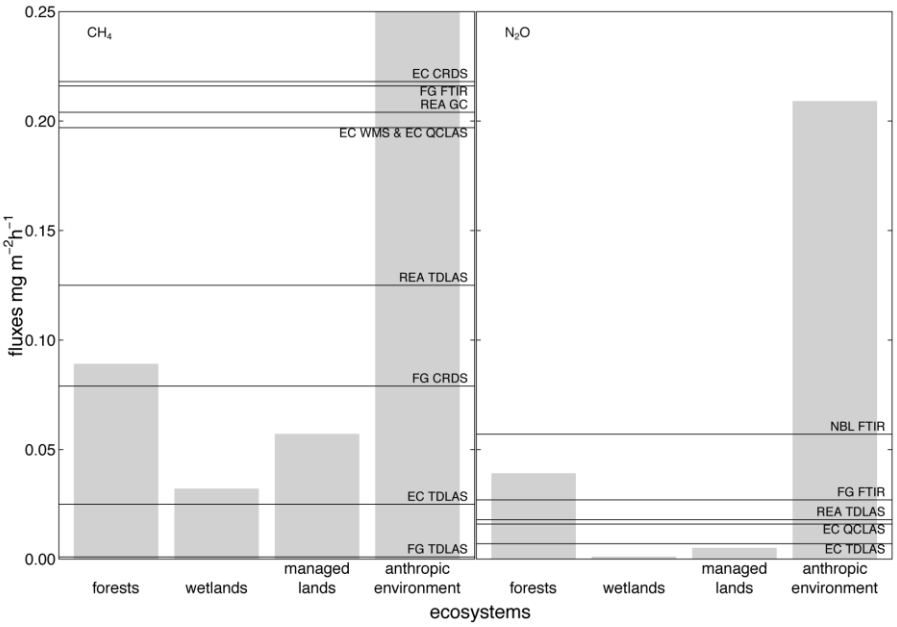

Figure 2.2. Reported minimum flux detection limit FDL (black lines) for each set-up (micrometeorological technique/sensor) plotted against absolute minimum fluxes from soil chambers methods (grey bars). For FDL values refer to the text and Table 4. Acronyms: CRDS - Cavity ring-down spectroscopy; EC - Eddy Covariance; FG - Flux Gradient; FTIR - Fourier Transform Infra-red spectroscopy; GC - Gas Chromatograph; NBL - Nocturnal Boundary Layer; QCLAS - Quantum Cascade Laser Absorption Spectroscopy; REA - Relaxed Eddy Accumulation; TDLAS - Tunable Diode Laser Absorption Spectroscopy; WMS - Wavelength Modulation Spectroscopy.

Even if a direct comparison of these two approaches have to be considered with carefulness, in the case of CH_4 estimation is possible to catch all the significant gas exchange from soil with the current technology, including forests where fluxes are usually very small or even negative (uptake). On the other hand for N_2O it seems that some fluxes can be lost, in particular those from wetlands and managed lands. In order to get an idea about the potential impact of FDL on trace gas fluxes estimates, here an approach, followed by several authors [Edwards et al., 2001; Pihlatie et al., 2005b; Neftel et al., 2007] and based on equation 2.2, is applied to one-year datasets from a clover field and a turkey oak forest at Roccarespampani FLUXNET site (Italy). As it can be seen in Figure 2.3, even during common mixing conditions ($0.2 < \sigma_w < 0.5$) reliability of fluxes must be assessed with care to avoid large errors in estimates.

In the opinion of several authors [Pattey et al., 2006; Edwards et al., 2003], the highest CH_4 flux resolution is achieved using a TDLAS sensors in an EC system (TDLAS-EC), enabling to reach flux detection limits of 0.025-0.042 mg m^{-2} h^{-1}. Within this synthesis, the lowest CH_4 FDL (0.001 mg CH_4 m^{-2} h^{-1}) is reported by Edwards et al. [2001] using FG-TDLAS technique. However, such a low value, may derive from the adopted measurement unit (i.e.

0.026 mg CH_4 m^{-2} day^{-1}, referred to a 30 min averaging period). A FDL of 0.079 mg m^{-2} h^{-1}, is reported by Smeets et al. [2009] using a Fast Methane Analyzer and EC (FMA-EC) set-up. While the minimum FDL using QCLAS-EC set-up is 0.197 mg m^{-2} h^{-1} [Detto et al., 2011; Kroon et al., 2007]. Rather good performances (0.125 mg m^{-2} h^{-1}) were also reached by the TDLAS-REA system [Pattey et al., 2006].

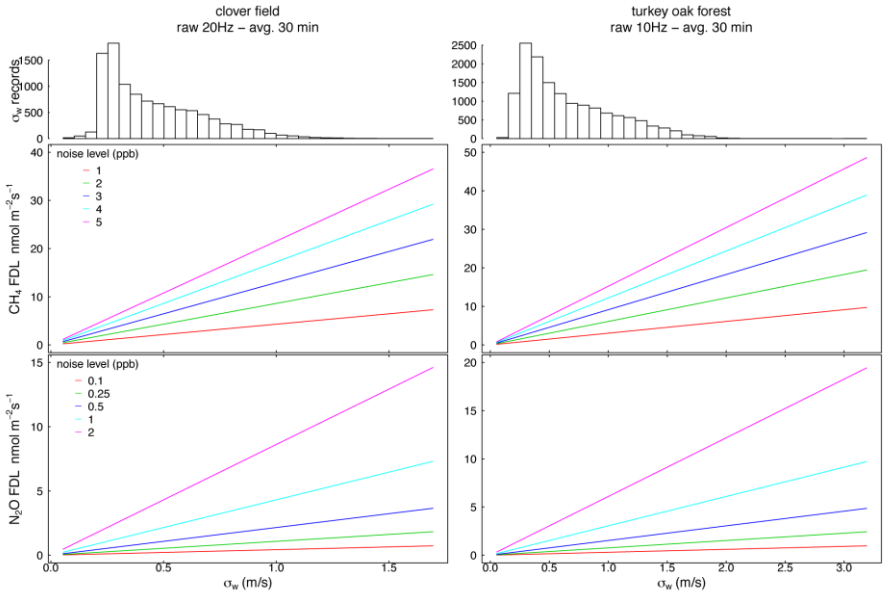

Figure 2.3. Example of flux detection limit (FDL) computation applied to one year raw datasets. Data were measured in 2010 at Roccarespampani (Italy) over a clover field (left side) and a turkey oak forest (right side) by means of eddy covariance towers (h = 2.0 m and h = 15.0 m respectively). FDL is computed using Equation (3) considering 5 levels of instrumental noise level. At the top panels the concerning sw frequency distribution is reported as an indication of the real turbulent intensity.

For N_2O measurements, the lowest FDL was achieved with an TDLAS-EC set-up, showing a detection limit of 0.007 mg m^{-2} h^{-1} for a 30 minutes averaging period [Pihlatie et al., 2005b]. Neftel et al. [2007] with a QCLAS-EC system and Pattey et al. [2007] with a TDLAS-REA achieved twice such value (0.016-0.018 mg m^{-2} h^{-1}). Desjardins et al. [2010] also with a TDLAS-REA system, achieved a slightly higher FDL (0.026 mg m^{-2} h^{-1}). Fast responding sensors, such as TDLAS, QCLAS and FMA, showed comparable achievement. Their performance and stability mainly depends on the instrumental drift. The period over which a laser signal can be averaged to get optimum sensitivity, and thus high precision, determines the quality of the spectrometer [Hendriks et al., 2008]. Such properties can be characterized by a proper signal processing strategy exploring the Allan variance trend [Kroon et al., 2007; Mammarella et al., 2010]. TDLAS and QCLAS devices seem to get analogous precisions. As an example, QCLAS achieves precision 0.1% and 0.2% of ambient concentration for N_2O and CH_4 respectively, thereby resolving fluxes of 0.3 and 4 ppb (1 time RMS noise, 1 second averaging time) [Nelson et al., 2004]. Conversely, TDLAS gives total system noise levels of less than 1 and 4 ppb (1 time RMS noise, 5 second averaging time) for N_2O and CH_4 respectively [Edwards et al., 2003]. The advantages of QCLAS spectrometers are the higher stability of laser frequency and the freedom from cryogenic cooling cycles [Kroon et al.,

2007]. On the other hand, small fluxes may be biased by its sensitivity to water vapor. Neftel et al. [2010] quantify this effects on N_2O fluxes in 0.3 nmol m^{-2} s^{-1} per mmol H_2O m^{-2} s^{-1}, suggesting that drying the air samples could help reducing this problem but this could impact on reactive trace gases measurement and prevent a reliable lag time determination when fluxes are small. Offset drifts in the signal can affect TDLAS estimates, but these could be drive down by active thermal control of the TDL enclosure [Wille et al., 2008a; Mammarella et al., 2010]. FMA seems to be less biased by drifts [Eugster and Pluss, 2010], but sample air should be dried and filtered to avoid contamination of the measurement cell [Hendriks et al., 2008; Wille et al., 2008a]. An interesting comparison between open (WMS device) and closed-path (CRDS device) system is provided, as example, by Detto et al., [2011]. Apart from field versatility, the two systems show comparable FDL. Even if some peculiar problems impact differently on the two systems (air density effects for open-path, synchronization and spectral losses for closed-path), comparison between fluxes magnitude showed good agreement. FTIR shows measurement relative precision of 0.1% ca. of background, resolving concentration of 1 ppb (3 times RMS noise) for N_2O and 6 ppb for CH_4. FTIR is able to measure the concentrations of all gases of interest simultaneously, and because these include water vapor, concentrations can be expressed as mixing ratios relative to dry air, thereby eliminating the need of correcting for air density fluctuations, according to the Webb, Pearman and Leuning theory [Webb et al., 1980]. Open-path FTIR seems to achieve precisions one order of magnitude higher than closed-path FTIR systems and GC-Electron Capture Detector) considering random errors equal to 0.6 and 0.06%, respectively [Kelliher et al., 2002].

2.4 Performances with respect to soil enclosure methods

Frequency distributions of mean fluxes measured with soil enclosure methods over each land category are showed in Fig.2.1. Comparability between micrometeorological and chamber methods is not yet been fully established [Werle and Korman, 2001; Hendriks et al., 2010]. An appropriate footprint analysis, hence atmospheric stability/surface roughness study, and flux source spatial variability assessment within the fetch are needed to compare those methods. The small-scale emissions captured by chambers must be scaled-up at the ecosystem scale by means of suitable models accounting for footprint characteristics and wind regimes, before it can safely compared with micrometeorological fluxes. Anyway, using a non-parametric test (multiple comparison after Kruskal-Wallis test $p = 0.01$), here is made a rough multiple pair-wise comparison between average ecosystem fluxes measured by chambers and micrometeo techniques, founding no statistically significant difference. These two methods are known to yield comparable fluxes when all site elements are considered [Christensen et al., 1996; Laville et al., 1999; Pihlatie et al., 2005b; Schrier-Uijl et al., 2010] but differences up to 50-60% encountered for both N_2O and CH_4 have been usually noticed. This is mainly due to flux spatial variability [Christensen et al., 1996; Schrier-Uijl et al., 2010], as chambers scarcely integrate it over large areas. Discrepancies could generally be assessed by a proper scaling procedure, but short-term natural events, e.g. the water table surfacing [Clement et al., 1995; Hendriks et al., 2008], may alter this evaluation. Enclosure methods may be useful in

the assessment of treatment effects but their use for quantifying spatial and temporal dynamics is limited [Pattey et al., 2007]. Also they could underestimate fluxes when surface roughness is high [Friborg et al., 1997], however are able to catch some changes in environmental conditions in the same way as micrometeorological techniques [Pihlatie et al., 2005b]. Denmead et al. [2010] assert that by chambers is possible to detect fluxes 100 times smaller than FG technique when sources are low and scattered. The ability of this method to detect small fluxes also depends on the chosen gas analyser. Standard or modified GC are normally used, but the FTIR [Galle et al., 1994; Denmead et al., 2010] and Photo Acoustic Spectroscopy (PAS) devices [Hendriks et al., 2007; Neftel et al., 2007; Schrier-Uijl et al., 2010] were also utilized.

As an example, chambers used with GC are reported to detect N_2O fluxes up to 0.001 [Barton et al., 2008; Zhu et al., 2005], 0.002 [Nykänen et al., 2002; Tsuruta et al., 1997] and 0.006-0.009 mg m^{-2} h^{-1} [de Carvalho et al., 2006; Verchot et al., 1999] comparable to FDL achieved with EC and FG-TDLAS. N_2O FDL of 0.017 mg m^{-2} h^{-1}, close to EC-QCLAS performances, are reported by Castaldi et al. [2010] and Laville et al. [2011], while using a FTIR sensor, Smith et al. [1994] detected minimum fluxes of 0.006 mg m^{-2} h^{-1}. For CH_4, FDL of 0.001-0.004 mg m^{-2} h^{-1} [Bubier et al., 2005; West et al., 1999; Langeveld et al., 1997] are reported for chambers-GC set-up, similar to FG-TDLAS performances. PAS sensor can measure concentrations above 100-1000 ppb of CH_4 with a precision of 2 [Hendriks et al., 2007] up to 10 ppb [Schrier-Uijl et al., 2010], giving a FDL of about 0.47 mg m^{-2} h^{-1}. However, as can be seen in Figure 2.2, almost all of the localized fluxes measured with chambers can be detected with an appropriate micrometeorological technique and gas sensor.

2.5 Discussions and conclusions on trace gas flux micrometeorological measurements.

Within forest ecosystems several aspects are still uncertain. Fluxes are small and difficult to quantify even with modern technology. Nitrous oxide fluxes seem to depend mainly on moisture status [Eugster et al., 2007a, 2007b; Pihlatie et al., 2005a, 2005b] and on plants activity, i.e. leafing or senescence instead of rain events, microbial activity and temperature [Simpson et al., 1997]. As far as methane in concerned, forest ecosystems have been observed to act as source or sink, but the dynamics of this equilibrium and their sources are far still from being well characterized. From revised literature, soil physical characteristics emerge as main factors regulating upward and downward exchanges. Indeed, the two sites with a reported CH_4 sink show very dry [Smeets et al., 2009] and moderately dry [Bowling et al., 2009] soil condition and porous texture. Foliar aerobic CH_4 emission under natural condition [Keppler et al., 2006; Wang et al., 2008] still found some concerns in literature [Dueck, et al., 2007; Bowling et al., 2009] and the current review does not confirm such findings. Agreements seem to be instead about N_2O foliar emission [Pihlatie et al., 2005a; Eugster et al., 2007 a, 2007b].

No specific studies on N_2O emissions seems to have been conducted on these ecosystems, even if anaerobiosis and denitrification do exist, thus nitrous oxide emissions may be expected. Methane fluxes are positively correlated with soil temperature and near surface

turbulence and temperature, as they are triggers of soil efflux. A scanty dependence on water table depth was found. The bulk of the fluxes is observed during thaw or re-flooding periods, when the water obstruction to gas circulation in soil pores is removed. Reduction of flux strength is registered under extremely low soil temperatures conditions and when soil lack of substrate for methanogenesis.

Being related to agriculture, hence directly impacted from the human activity, managed lands are the most investigated ecosystems. Presently, it cannot be definitely affirmed whether these ecosystems are a net N_2O and CH_4 sink or source, as management practices can deeply affect the balance. Nevertheless, fluxes on these ecosystems are weak and very variable in time (peaks) and space (hot spots). Especially for nitrous oxide, fluxes are normally low and attenuated from the background mixing ratio, thus difficult to detect accurately, even with modern sensors. Peaks break off this state during disturbance events like rain, grazing, ploughing and, of course, fertilization. A clear relation to temperature – both of air and soil - is not always evidenced. Methane is little investigated in these ecosystems, as usually fluxes are leveled to pretty low values and are extremely variable in space. Apart from rainfall events, there is not an evident dependence on neither water nor organic soil content. The active role of plants in ecosystem emission estimates is a topic that needs in depth investigation [Fowler et al., 2009]. The behavior of herbaceous vegetation is rather assessed, whereas for shrubs and trees the discussion is still open. Literature evidence exist of a substantial role of woody plants in producing and transporting N_2O and CH_4 from soil to atmosphere [McBain et al., 1998; Rusch and Rennenberg, 1998; Gauci et al., 2010]. However, specific field measurements are required to fully assess the mechanisms. Biological processes of oxidation-reduction, regulating the equilibrium between sink and source of these gases are also well identified, although it is still difficult to parameterize them at field scale, but natural and man-induced events can have a significant impact on timing and magnitude of fluxes at different time scales. This thwart our understanding of the driving forces regulating exchanges, but also strengthen the effort to deeper explore the processes, predict variations in future emissions trends in response to climate change and evaluate suitable mitigation options. The large temporal and spatial variations of flux rates are a main source of uncertainty in estimating N_2O and CH_4 fluxes. Temporal trends are well described in literature but, if there is an overall agreement on seasonal patterns, for daily trend there is still lot of ambiguity. This is true for all the ecosystem categories and should be considered while designing a sampling strategy for flux measurements, especially if using sampling systems that do not provide continuous measurements.

Significant progress has been made in measuring non-CO_2 gas fluxes at landscape scales thanks to development in technologies like laser spectroscopy (e.g. WMS, CRDS, QCLAS, TDLAS) and their use in micrometeorological methods. However, also on this topic, there are still open questions. As most authors stress, presently the manual or automatic chambers technique is the most used method for measuring N_2O and CH_4 fluxes. This technique is not expensive, suitable for a wide range of climatic and environmental conditions and can help highlighting the spatial variability of soil gas fluxes at the local scale. On the other hand, spatially-discrete gas sampling precludes the detailed assessment of variability causing incorrect long-term estimates, particularly when strong short-term flux fluctuations occur. Continuous or near-continuous eddy-based measurements improve the accuracy of flux

estimates, detect the short-term variability of fluxes, lead to estimates from site to landscape scales and provide a useful tool to parameterize and validate process-oriented models. The latest development of laser sensors for field applications and the improvement in technological knowledge, allow detecting fluxes in virtually all ecosystem. Measurement reliability can be optimized by an accurate field campaign and an appropriate data processing. Differences between instrument precisions do exist (see App. A Tab. A4) even if small. Apart from the aims of the study and the characteristics of the site, the choice of a sensor (or a system) is yet pretty an economic question. Estimates from the various micrometeorological techniques seem to be in reasonable agreement, especially when comparisons base on accurate footprint analysis. However, the relationship between micrometeorological and chamber method is still a source of divergences among authors. Some found the comparison reliable and concordant in particular when chambers are strategically placed within the footprint area, other found substantial divergence with chambers giving both lower (generally on managed and flooded) and higher (generally on forests) values, with respect to micrometeorological techniques.

From analyzed bibliography, it can be seen an increased year by year progress in CH_4 and N_2O flux measurements leading to improvements on estimates. However assessing the source-sink mechanism in time and space, and the sources and magnitude of errors of estimates are still challenging. In order to visualize the geographical distribution of analyzed studies, they are plotted over the world map (Fig. 2.4) differentiated by ecosystem type.

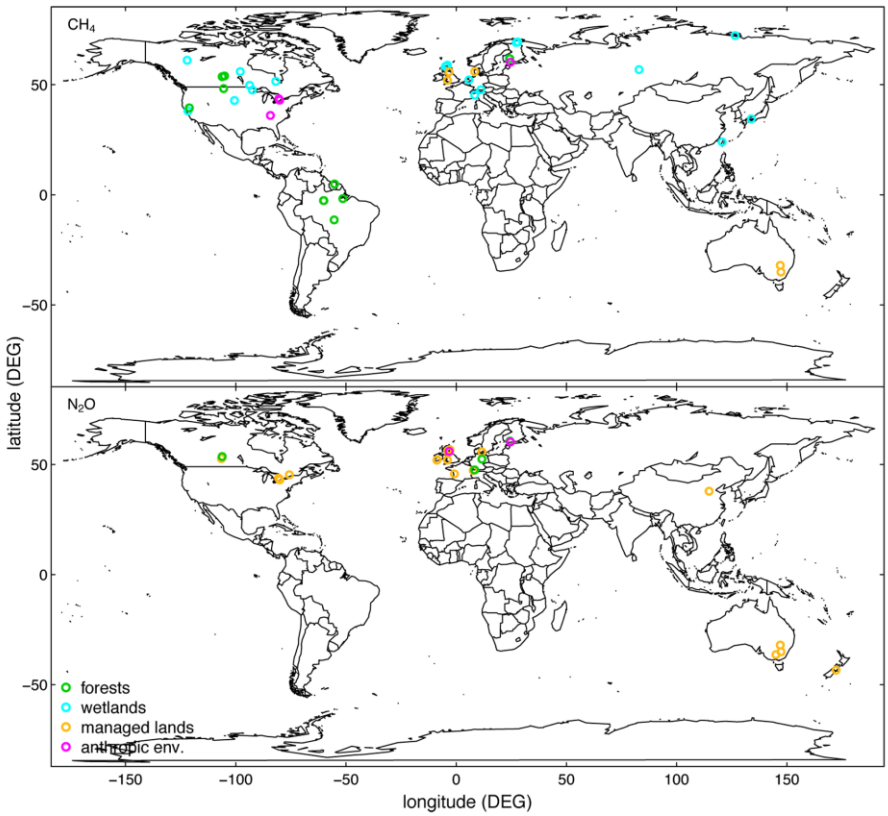

Figure 2.4. Geographical distribution of analysed sites.

As it can be seen, some geographical areas like Africa, Central Asia and South America still remain uncovered form such studies, while more information on trace gas exchange over these regions, especially within their typical ecosystems like forests and wetlands, are becoming today urgent to understand the global cycles of methane and nitrogen. There are still some gap on knowledge (landscape mechanisms, fluxes driving forces, biosphere-atmosphere plant flux mediation) and open questions (identify the best spatial and temporal resolution of measurements, improve the comparison between techniques, improve the uncertainty assessment) that have to be clarified to obtain further unbiased estimates. Micrometeorological methods can contribute to fulfill this gap providing high temporal resolution measurement, continuous long time campaigns and also optimal tool for asses and validate biogeochemical process models. As seen in the analyzed literature, high frequency and very low gas fraction can now be achieved and detected with current technology, but on-going instrument and technique development represent a further challenge for future works.

3 A preliminary assessment of below canopy methane fluxes in a tropical rain forest.

3.1 Introduction

Forest soil and forest understory can have a large importance in the forest scale energy and carbon budget. The sources or sinks strength depends on several parameter. As an example methane production occurs mainly in anoxic environments such as the submerged soils by methanogenic bacteria during the anaerobic degradation of organic matter [Itoh et al., 2009]. This led to suppose that CH_4 uptake/emission rate is regulated by the soil humidity and hence by precipitations. CO_2 production, instead, seems to be attenuated by high soil water content and enhanced by temperature increasing [Bowden et al., 1998]. There have been many studies that reports CH_4 sink in temperate forest ground and most of these were conducted in regions with low precipitation [Singh et al., 1997; Livesley et al 2011]. Anyway other studies have demonstrated that forest soils can also emit CH_4 [The et al., 2005; Livesley et al 2011]. The tropical forest soils are generally well drained but it depends on the surface horizons type, the sloping of the terrain and the plant species composition. This highlight the big variability that can occur in methane uptake/emissions, frequently scattered in hot spots. Most of the studies are still conducted through soil chambers [e.g. Castaldi et al., 2010] strictly linking the estimate to the selected sampling points or area. Eddy covariance below canopy measurements can help override such difficult by sampling over a relatively wide area. While the EC method is routinely used to measure carbon and energy fluxes above vegetation canopies, it has also been adopted for trunk-space measurements [Baldocchi et al., 1986; Subke and Tenhunen, 2004; Philatie et al., 2005; Mammarella et al., 2010]. The feasibility of sub-canopy EC measurements is anyway related to some assumptions [Baldocchi and Meyers 1991] and mainly depends on the develop of the turbulence. As stated in the previous chapters, below canopy turbulence can be intense but intermittent and no universal theory on it do exists [Launianen et al., 2005]. Turbulent transport is regulated by sporadic gusts that penetrate the canopy layer reaching the forest floor, hence is dependent also on the forest structure.

In this chapter, the results from two EC measurement campaigns conducted at the forest floor of Ankasa are reported. Measurements took place in April 2011 during the dry season and in October 2011 during the rain period. The main object of this study is to assess the applicability of trunk space EC to measure CH_4 and CO_2 exchange in such a complex ecosystem, discuss the problem and uncertainty and provide an estimation of the magnitude of fluxes.

3.2 Materials and methods

3.2.1 Site description

Measurements were carried out at the Ankasa forest reserve, about 300 m far from the main tower. The sampling site (05° 16' 13.400" N; 02° 41' 29.101" W; 100 m a.s.l.) is on a seasonally swamped lowland area characterized by a quite flat orography and a dense understory vegetation covered from dominants trees having a mean height of 30 m (for soil description and the species compositions refers to Sect. 1.3).
A sketch of the measurement site and set-ups is showed in Fig. 3.1.

Figure 3.1. Left panel: aerial image of the below canopy measurement site (white triangle) showing its proximity to the main tower (red square). The middle panel shoe the system set-up for April (in the dry season) and the panel on the right the set-up for October (wet season). Note the difference in the soil water content below the instruments: in October there was a water layer of about 20 cm thickness.

The first experiment was conducted from 11 to 14 April 2011 at the end of the dry season and, as can be seen from Fig 3.1 (middle panel) also the soil was nearly dry. During the sampling period, the average air temperature was 26.7 °C, the average relative humidity 91.2 % and no rainy events were recorded (Fig. 3.2).

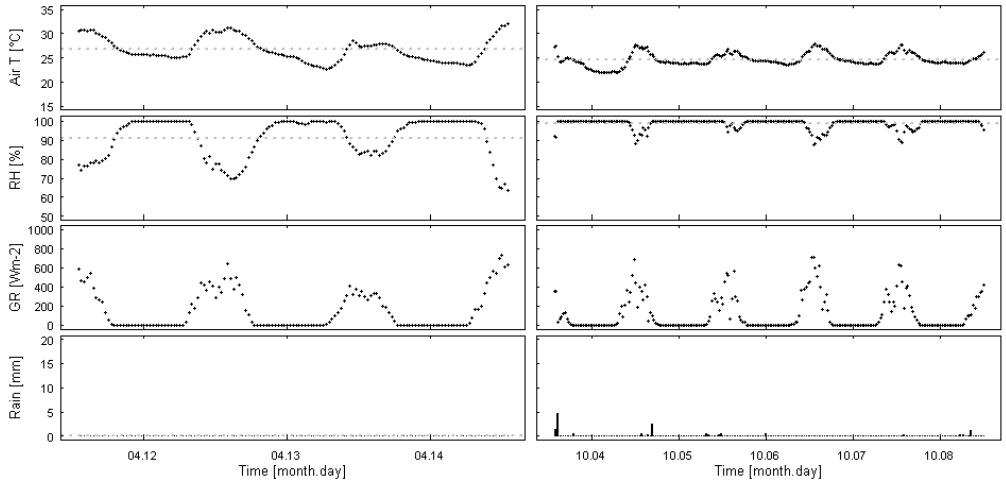

Figure 3.2. Meteorological conditions during the measurement campaign of April (left side) and October (right side). The air temperature was higher in April (about 27 °C) than in October (25°C). Instead the air relative humidity was lower, even if more than 90% on average. In April no rainy events were recorded.

The second experiment was conducted from 3 to 8 October 2011 in the middle of the rainy season, during a period of flooding when the soil under the system was completely inundated (Fig 3.1 right panel). The average air temperature was 24.6 °C, the average humidity 98.7 % and sporadic rainy events were recorded.

3.2.2 Eddy covariance measurement system

The system set-ups slightly differ for the two campaigns (Fig. 3.1). In April the system was composed by a Wind-Master Pro 3D sonic anemometer (Gill Instruments Ltd., UK), a LI-7500 CO_2/H_2O open path gas analyser and the new LI-7700 CH_4 open path analyser (LI-COR Bioscience, Lincoln, NE, USA). Gas signals were acquired in analogue, synchronized with wind and sonic temperature signal from the anemometer and logged to an industrial computer by a serial communication at a sampling rate of 10 Hz. The logging process was implemented by Ecco-Catch, a software developed at the University of Tuscia. In October the system comprised a Wind-Master Pro 3D anemometer, the new LI-7500-A CO_2/H_2O open path gas analyser and the LI-7700. This time the analogue signal from the anemometer was acquired and integrated with gas measurement by the control box of the gas sensors (LI-7550, LI-COR Bioscience), which also directly store the data in a memory device. This configuration allowed bypassing the computer with a sensible power requirement reduction and an improvement of the system stability.
The sensors were installed at an height of 2.5 m from the soil and horizontally positioned at a distance suitable to minimize spectral losses but contemporary avoid reciprocal interference and wind flow distortions.

3.2.3 Eddy covariance data processing

Raw data analysis was carried out following the procedure described in Sect. 1.2.2. Erroneous data caused by electronic failures were removed. To minimize the effect of sloping terrain and anemometer misalignment a double rotation was performed on the wind components. The vertical fluxes were calculated by equation 1.13 considering the molar densities of fluxes as measured by the gas sensors. Averaging time for flux calculations was 30 min and block average was used as detrending method. Time lags were computed by the covariance maximization method using a default windows previously computed on sensor physical distance. As commonly accepted [Aubinet et al., 1999] negative fluxes are considered as sink while positive as source. To account for density fluctuations [Webb et al., 1980] the CO_2 fluxes were corrected using Eq. [1.38] that in the case of CH_4 measured by the LI-7700 becomes:

$$F_{CH4} = A\left\{\overline{w'\rho'_{cm}} + B\mu\frac{\overline{\rho_{cm}}}{\overline{\rho_d}}\overline{w'\rho'_v} + C(1+\mu\sigma)\frac{\overline{\rho_{cm}}\,\overline{w'T'}}{\overline{T}}\right\} \qquad [3.1]$$

where ρ_{cm} is the methane mass density calculated as $\rho_{cm} = m_c\,\rho_c$ with m_c being the molecular weight of methane and ρ_c is measured raw number density, *A*, *B*, *C* are instrument specific

multipliers respectively accounting for spectroscopic effects of temperature, pressure, and water vapour on methane density, spectroscopic correction to the latent heat flux term for pressure and water vapour and for spectroscopic correction to the sensible heat flux term for temperature, pressure and water vapour [LI-COR 2010]. Spectral correction for high-pass and low-pass filtering effects were both analytically computed as in Moncrieff et al. [2004] and in Moncrieff et al. [1997].

Once corrected fluxes were computed, further filters have been applied to time series. The LI-COR 7700 output some diagnostic values to flag records during instrument malfunctioning; here the received signal strength indicator (RSSI, an indicator of the laser sampling path cleanliness) was used rejecting half-hours records when the mean RSSI were below 10%. Also half-hours corresponding to rain records higher than 2 mm were removed.

Then data were storage corrected using the discrete approach, where the CO_2 concentration measured at instrument level is considered to nullify at ground level. Spike fluxes were removed in two steps using the median of absolute deviation about the median (MAD) [Papale et al., 2006] and the probability distribution of the fluxes series, eliminating records lower than the 0.25% and higher than 99.75% of the distribution. Both despiking method were applied to day-time and night-time fluxes separately to account for their different magnitude. The daily partitioning was made on a global radiation threshold of 20 W m^{-2}.

It is known that eddy flux measurements can underestimate the net ecosystem exchange during periods with low turbulence and thus limited air mixing [Aubinet et al., 1999; Goulden et al., 1996; Gu et al., 2005]. Normally the $u*$ value is used as criterion to quantify turbulence strength and discard data below a certain threshold [Gu et al., 2005; Papale et al., 2006] but in the trunk-space, assumptions made on this approach are hardly met. In these situations a low turbulence discriminating criterion based on standard deviation of vertical wind speed σ_w it is often used [Launiainen et al., 2005; Pihlatie et al., 2005b]. Anyway in this study it was not possible to use such method as fluxes showed weak dependence on σ_w. Fluxes during low mixing (mostly during night) were individuated and marked but not eliminated as they have a small impact on flux daily means, the aim of this work.

3.2.4 Methane flux detection limit of the eddy covariance system

As CO_2 atmospheric concentration it is relatively high, it is not difficult to resolve its fluctuations with the current gas sensors. It is not so for trace gases like CH_4. Requirements to resolve fluctuations of such gases depends both on atmospheric turbulence and the nature of fluxes. The standard error of flux estimate is given by [Edwards et al., 2003]

$$\sigma_F = \sum \sqrt{\frac{Sw(f)Sc(f)}{4\pi f T_a}} \qquad [3.2]$$

where T_a is the averaging period (e.g. 1800 s), *Sw(f)* is the variance spectrum of the vertical wind, *Sc(f)* is the variance spectrum of the scalars signal and f is the measurement frequency (in Hz). Considering *Sc(f)* as the analyser noise it is possible to determine the contribution of the analyser to the total uncertainty. This value is often considered as the flux detection limit

(FDL) of the estimate [Edwards et al., 2003; Pihlatie et al., 2005b; Neftel et al., 2007]. For a direct computation here it is used the equivalent formula reported in the previous chapter (equation [2.2]).

3.3 Results

3.3.1 The magnitude and variability of energy, carbon dioxide and methane fluxes

The pattern of energy fluxes clearly shown that both sensible (H) and latent heat (LE) are strongly influenced by the local atmospheric and microclimatic conditions (Fig. 3.3). Except for LE in April the diurnal variations does not follow the classical diurnal course.

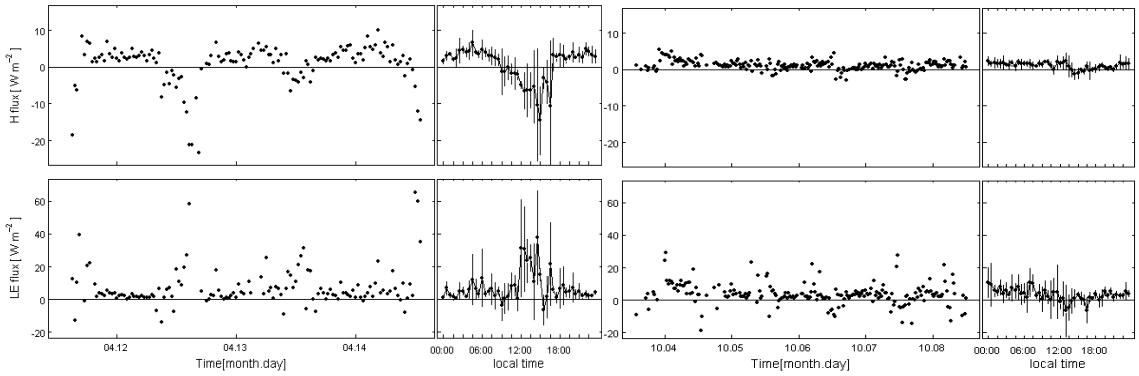

Figure 3.3. Patterns of sensible heat flux (H) and latent heat flux (LE) for April (left panels) and October (right panels) 2011. Right side frames shown the flux diurnal pattern.

In April H vary mostly from -20 to 10 W m^{-2} reaching its minimum in the early afternoon, while in October its variation seems to be strongly attenuated (-5 to 5 W m^{-2}) without any clear peak. These unusual patterns could probably be related to the difference in the trunk space air temperature and the above canopy temperature. At midday such gap reach its maximum when the lower below canopy temperature, together with the relatively low soil heating due to the screen effect of the dense vegetation, enhance the downward vertical temperature gradient. This is more clear in April, while in October the worst climatic condition and cloudy sky damp the temperature differences and thus gradients. Evapotranspiration (linked to LE) in April shown the classic diurnal pattern with higher values (around 40 W m^{-2}) in the afternoon driven by the high temperature and the lower soil water content. In October the LE variation seems dumped again, probably due to the higher humidity of both soil (that was flooded) and air joined to the lower temperatures. Also the relative humidity of air could play a significant role being almost always around 100%.
Carbon dioxide fluxes shows a distinct seasonal behaviour (Fig 3.4). In April fluxes are generally higher with half-hourly values ranging from -18 to 48 μmol m^{-2} s^{-1}. The period average is 9.4 ± 0.01 μmol m^{-2} s^{-1} corresponding to an emission of 3.5 g m^{-2} d^{-1}. With the exception of few points no sinks were recorded. Emission peaks at noon after a rapid increase

in the early morning. This pattern may be due to several reasons. The soil respirations is the dominant process during this period. Even if no rains occurred, the litter was humid with soil humidity values around 30-60% and temperatures were high. Such condition promotes litter decomposition and soil respiration largely prevails on photosynthesis. During night-times soil respiration decreases but CO_2 emission are now supported by respiration of plants. In the morning, when vertical mixing is enhanced after sunrise, a portion of the CO_2 stored close to the soil surface during the night is flushed upwards and, together with the temperature-driven restart of soil bacteria activity, determine the rapid increase.

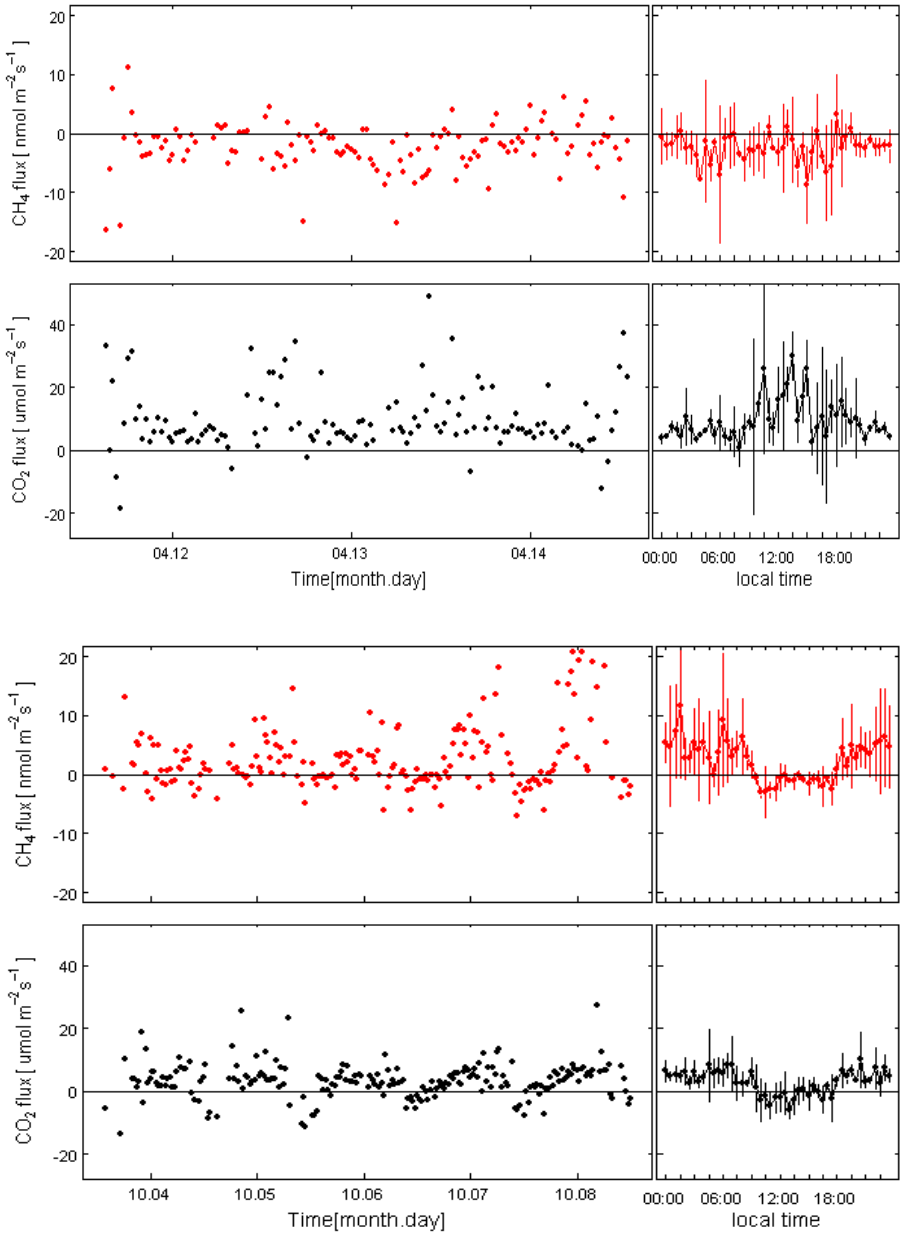

Figure 3.4. CH_4 and CO_2 time series for the dry (upper panels) and wet season (lower panels). Right side frames shown the average flux diurnal pattern, vertical error bars stand for ± standard deviation of the mean.

In October fluxes are smaller ranging from -13 to 27 μmol m^{-2} s^{-1} and an average of 3.2 ± 0.005 μmol m^{-2} s^{-1} corresponding to a net daily emission of 1.2 g m^{-2} d^{-1}. During this period the soil surface was completely flooded (water layer up to 20 cm) and the water, generating an anoxic environment, dimmed the soil respiration. In fact the diurnal pattern seems to be governed by the plants activity, following the behaviour of the above canopy CO_2 fluxes with sinks during the sunny hours (about -0.5 μmol m^{-2} s^{-1}).

Methane fluxes also show a distinct seasonal behaviour. In April half-hourly means range from -16.3 to 11 nmol m^{-2} s^{-1} with an average value of -2.2 ± 0.02 nmol m^{-2} s^{-1} corresponding to a net sink of 0.13 mg m^{-2} h^{-1}. High temperatures and limited soil moisture enhance CH_4 uptake that seems to dominate over the 24 hours. In October fluxes ranges between -7.0 and 32.3 nmol m^{-2} s^{-1}, with and average daily value of 2.67 ± 0.05 nmol m^{-2} s^{-1} thus a net source of about 0.15 mg m^{-2} h^{-1}. The diurnal variability is higher showing a weak day time CH_4 sink averaged to 0.4 nmol m^{-2} s^{-1}, and night time emissions to 4.7 nmol m^{-2} s^{-1}. Variation in CH_4 fluxes was greater during night-time than during day-time. Also for CH_4 the anoxic condition of soil induced by the water layer is the main driving force leding to an improve in methanogens bacteria activity.

While in April there is no a clear dependence of CH_4 fluxes to wind direction, in October it seems there is a prevailing sector, south-east, from which higher fluxes come (Fig 3.5). Anyway the overall frequency distribution shown that most of the fluxes measured by the EC system are from north.

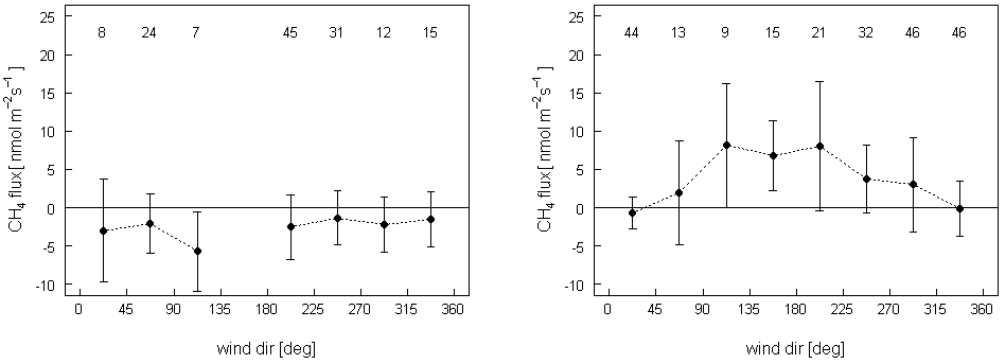

Figure 3.5. CH_4 fluxes from different wind direction sectors from the eddy covariance mast (left panel refers to April right panel to October). Dots represent the mean flux from each of 45° sector, error bars stand for ± standard deviation of the mean. Numbers in the top stand for the absolute frequency from each wind sector.

3.3.2 Consistency of methane fluxes estimates

The flux detection limit of the system was calculated form Eq. [2.2] considering an instrument noise level of 5 ppb [LI-COR 2010] and 30 min averaging period with 10 Hz measurement frequency. In April the average standard deviation of vertical wind speed at 2.5 m height was 0.05 m s^{-1} leading to a FDL ranging from 0.02 to 0.3 nmol m^{-2} s^{-1} (0.08 nmol m^{-2} s^{-1} on average). Generally day-time FDL was 40% higher than night-time. In October the average standard deviation of vertical wind speed decreased to 0.03 m s^{-1} reflecting a lower FDL ranging from 0.02 to 0.11 nmol m^{-2} s^{-1} without any sensible difference over the full day period.

An example of spectra and co-spectra are shown in Fig. 3.6. Normalized spectra of vertical wind speed (w) and sonic temperature (Ts) reflect the turbulence characteristics of the trunk space. Spectral density is pretty noisy and shifted to the highest frequencies almost forming a second energy peak. The frequency dependence in the inertial sub-range generally follow the expected $f^{-2/3}$ law but sometimes seems less pronounced. Normalized co-spectra of CH_4 and w and CO_2 and w are even more noisy but still shown an energy shift to higher frequency. As can be seen, the frequency dependence of the measured fluxes is less pronounced than the $f^{-4/3}$ behaviour, leading to a relatively higher contribution of high frequency (small scale) eddies to the measured flux.

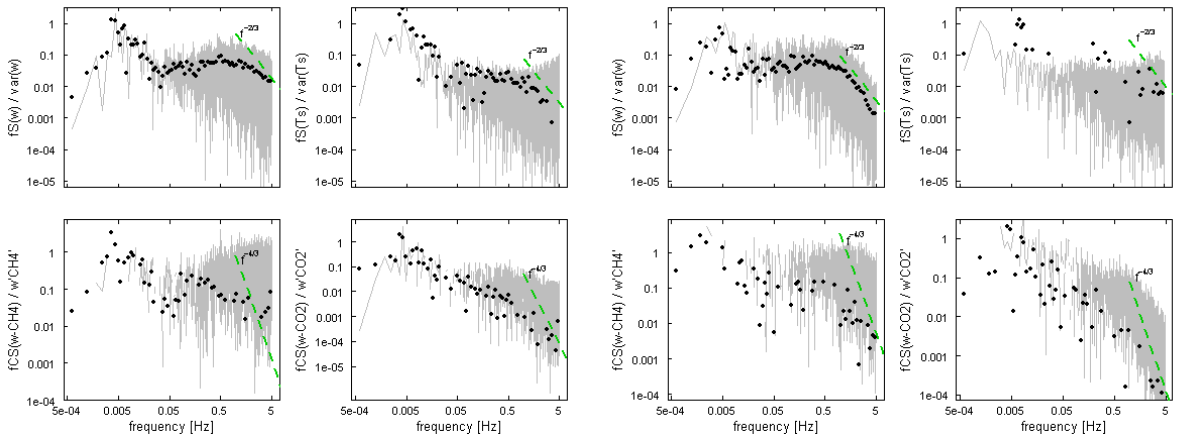

Figure 3.6. Example of normalized spectra of w and sonic temperature (upper panels) and normalized co-spectra of CH_4 and w and CO_2 and w. The 4 plot block on the left refers to April 12 at 14:30 with a mean wind of 0.15 m s^{-1} and a σ_w of 0.08 m s^{-1}. The blocks on the right refers to October 08 at 10:00, mean wind of 0.14 m s^{-1}, σ_w of 0.03 m s^{-1}. Grey lines are the full(co)spectra and the dots are the binned (means of 90 records) values calculated by the hamming tapering window.

3.4 Conclusions

From the bibliography it seems that this is the first attempt to measure CH_4 fluxes by means of eddy covariance technique below a tropical rain forest canopy.

Both methane and carbon dioxide below canopy fluxes shown a clear seasonal behaviour. In the dry season (April) the forest understory act as net sink for CH_4 (-0.13 mg m^{-2} h^{-1}) and as net source for CO_2 (3.5 g m^{-2} d^{-1}). In the wet season (October), when the soil surface was completely flooded, it is observed a net daily source of CH_4 (0.15 mg m^{-2} h^{-1}) and an attenuation of the CO_2 emission (1.2 g m^{-2} d^{-1}) with a weak sink in the noon. As a comparative examples (conducted with soil chambers) Priemé and Christensen [1999] measured a weaker CH_4 sink of 0.34 mg m^{-2} d^{-1} (about -0.015 mg m^{-2} h^{-1}), during the wet season in a forest soil in Ghana, while Singh et al. [1997] have measured an even stronger sink during both dry (-0.46 to -0.95 mg m^{-2} h^{-1}) and wet (-0.2 to -0.32 mg m^{-2} h^{-1}) season in India. Exactly the same pattern reported in this study was observed by Verchot et al. [2000] in a primary forest in the eastern Amazon: during the dry season a net CH_4 sink of 0.04 mg m^{-2} h^{-1} while in the wet season an emission of 0.001 mg m^{-2} h^{-1}. The decreasing in CO_2 emissions at highest soil moisture as well as its increasing with higher temperature in tropical forest floor material is also reported by some authors [Bowden et al., 1998]. Wet season campaign

also shown that when radiation penetrate the dense canopy layer, part of the CO_2 emitted from the soil is balanced from photosynthesis.

The analysis on reliability of CH_4 shows that most of the measured fluxes were above the FDL and the system is thus adequate to resolve most of the fluxes. The FDL ranged between 0.3 - 4.0 ng m^{-2} s^{-1} in the dry season and 0.3 - 1.5 ng m^{-2} s^{-1} in the wet season. Edwards et al. [2003] using a tunable diode laser trace gas analyser with a noise level of 8 ppb (almost twice respect to LI-7700 noise) estimates a FDL of 7 - 12 ng m^{-2} s^{-1} that is consistent with the analysis reported here.

Spectral analysis reveals that measurements are affected by a general high noise. The energy density is shifted to the higher frequency demonstrates the big contribution of the smallest eddies. It is also visible a second energy peak with a break in the middle. This can be due to the nature of below canopy turbulence characterized by small scale eddies and the large, coherent turbulent eddies that occur because of quick sweeps and ejections [Baldocchi and Meyers, 1991]. Also radiation penetrating the canopy may induce thermals near the forest floor causing intermittent biases in the fluxes [Subke and Tenhunen, 2004].

The results of this study confirm that eddy covariance measurement can be performed below a closed canopy but it is needed to face with problematic conditions [Baldocchi and Meyers, 1991; Subke and Tenhunen, 2004]. Insufficient atmospheric mixing, affects measurements especially at night-time, and also leads to a violation to the assumptions underlying the EC theory. Data quality tests had shown that a considerable part of data suffers from insufficient turbulence and longer series are thus required to discriminate valid measurements. Turbulence was generally low with u_* ranging from 0.01 – 0.2 m s^{-1} in April and 0.01 – 0.12 m s^{-1} in October while σ_w ranged between 0.01 and 0.2 m s^{-1} in April and 0.02 and 0.07 in October. Measurement in such conditions generally underestimates fluxes [Janssens et al., 2000].

4 The impact of the storage term on above canopy CO_2 and CH_4 fluxes.

4.1 Introduction

The estimate of surface-atmosphere gas exchange by eddy covariance involves the calculation of two terms, the aerodynamic fluxes (F_c) and the storage flux (S_c) (see Sect. 1.2.1). The net ecosystem exchange (*NEE*), also referred to as biotic flux, can thus be expressed as:

$$NEE = F_c + S_c \qquad [4.1]$$

The storage intensity varies with the degree of turbulence and follows a diurnal cycle: during night (when stable stratification occurs), trace gases emitted by plants and/or soil accumulate in the space beneath the EC sensors, while when thermal convection restarts in the morning this storage is depleted [Aubinet et al., 1999]. The storage flux can be computed by Eq. [34] and is expressed as a flux density (generally μmol m^{-2} s^{-1}). It is given by difference in the instantaneous profiles of the gas concentration, $c(z, t)$ at the beginning and end of the averaging period divided by the averaging interval T. Normally the instantaneous difference are replaced by the difference between time-averaged vertical profiles centred on the beginning and the end of the flux-averaging period [Finnigan, 2006].

Some authors adopt a different approach to calculate the storage [Greco and Baldocchi, 1996; Knohl et al., 2003]. This method assumes the profile gas concentrations to be constant in the space beneath the EC system and the storage is thus calculated from the time change of the gas concentration at the top of the tower. Nevertheless, this method could underestimate the real storage fluxes, especially over tall forests, as the above-canopy variation of gas concentrations can be decoupled from concentration changes in the below-canopy space [Iwata et al., 2005].

Considering a full diurnal cycle, storage fluxes become negligible compared to aerodynamic fluxes and can be approximate to zero as the night-time accumulation equals the day-time loss of the scalar [Aubinet et al., 1999]. Thus, the storage flux have no detectable impacts on long term budgets studies, while it can makes a significant contribution and must be accounted for if one wants to analyse fluxes over shorter periods or investigate their physiological controls [Iwata et al., 2005; Aubinet et al., 2012].

In this study, the diurnal variation in CO_2 concentration beneath the eddy covariance system is examined, to understand how storage fluxes vary with atmospheric conditions and turbulence, and how important the half-hourly storage values are in determining the *NEE*. The potential of using the single-point approach and how its results relate to the storage calculated from profile measurements are also evaluated. Furthermore, based on a few days of methane concentrations measurements, it is evaluate the possibility to correlate storage fluxes of the

two gases (CO_2 and CH_4) and the feasibility to correct single-point CH_4 storage flux estimates using CO_2 as a proxy.

4.2 Site and measurements

Data used in this study were collected in the Ankasa forest reserve (5° 16' 06.5" N; 2° 41' 38.8" W, 119 m a.s.l.) during the full year 2011. A detailed site description is reported in Sect. 1.3.

Figure 4.1. Left panel: aerial image of the main tower (red square) location. Right panel: a perspective from the tower base. The storage system air inlets are placed on the north side of the tower structure at 0.4, 0.8, 8.5, 18,. 24, 48.9 and 64 m from the soil.

The CO_2 EC system is placed almost at the top of the tower (at 50 m height) and consists of a LI-6262 closed-path IRGA, sampling the air at a constant rate of 8 l min^{-1}, a Wind-Master sonic anemometer and a set of standard meteorological sensors. Data were sampled at 10 Hz and raw data screening and processing followed the procedure described in Sect. 1.2.2.
The gas analyzer for the CO_2 profile is placed at the base of the tower and comprises a LI-820 closed-path IRGA connected to a multi-input manifold through which the air is collected from 7 sampling levels placed at 0.4, 0.8, 8.5, 18, 24, 48.9 and 64 m along the tower structure. Air is sampled at a constant flow rate of 10 l min^{-1} and Teflon filters (Gelman Acro 50, 1 µm) are placed at the tube inlet to avoid contamination of the optical chamber. The automatic system cycles through the entire profile every half hour, sampling each level for about 3 minutes after 1 min of flushing to remove residual air from the tubes and avoid sample mixing.
Methane profile measurements were performed during three sampling campaigns in April 2011 (dry season), July 2011 (season transition) and October 2011 (rainy season). Within each campaign, data were collected for two days, manually cycling through the entire profile every 2 hours. For each level, after 1 min flushing, air was collected for 1 min in a 10 l Teflon bag (SKC Inc., PA USA) then re-sampled from the bag and stored in 20cl vials. CH_4 concentration was measured within two weeks from the sampling by means of a gas chromatograph (Trace GC ultra, Thermo Finnigan Inc.) equipped with a FID detector. Each vial was analysed performing three replicates.

4.3 Calculation of the storage fluxes

The CO_2 and CH_4 storage are calculated from concentration profiles approximating derivatives in Eq. [1.14] by finite differences between two successive measurements, and the integrals by sums [Aubinet et al., 2001; de Araujo et al., 2010] as

$$Sc = \frac{P_a}{\Re T_a} \sum_{0}^{h} \frac{\Delta c}{\Delta T} \Delta z \qquad [4.2]$$

where P_a is the atmospheric pressure (bar), R is the molar gas constant (m^3 bar K^{-1} mol^{-1}), T_a is the air temperature (K), h is the maximum measurement height (m), c is CO_2 (µmol mol^{-1}) or CH_4 concentration (nmol mol^{-1}), T is the averaging time (s), and z is the averaging height (m). Measured half-hourly CO_2 concentrations were vertically interpolated (Δz = 0.5 m) up to 50 m, the EC system height, by means of a cubic spline function and then summed (a comparison with linear interpolation showed insignificant differences) while CH_4 measured concentration were first interpolated in time to achieve half-hour resolution and then linearly interpolated in space and summed.
Prior to be used in the analysis storage data were screened to eliminate records during system failures, bad readings, spikes and the alike.

4.4 Results

Figure 4.2 (left panel) shows full-year daily trends of CO_2 concentration at each sampling level. Below canopy CO_2 daily pattern clearly anti-correlates to that of temperature (Fig. 4.2 right panel) and systematically decreases moving from the soil to the tower top. During the night such offset increases due to the reduced mixing while during day-time, except for the two level close to the ground (below 1 m), concentrations are very similar demostrating that the turbulent mixing extends down to some meters within the canopy layer (about 20 m).

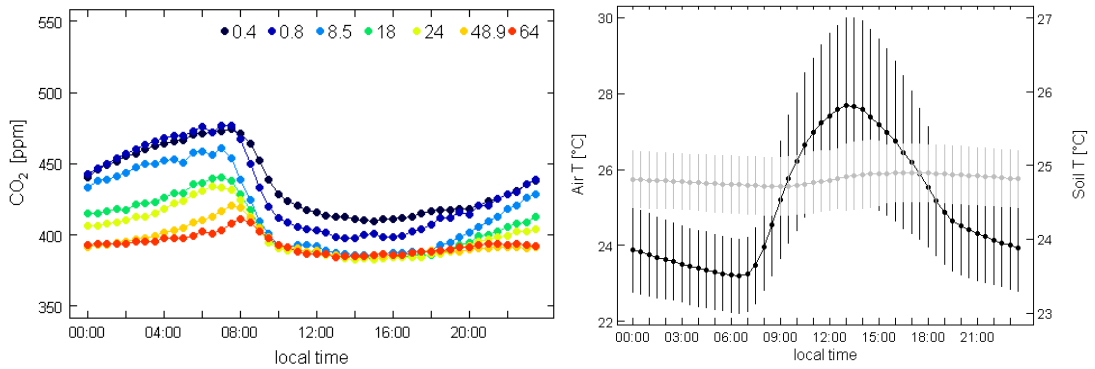

Figure 4.2. Left panel: CO_2 daily mean concentration trends(µmol mol^{-1}) at each sampling level. Error bars were omitted for clearness. Right panel: daily trend of air temperature (black lines) and soil temperature (grey line) below the forest canopy. Note the very low diurnal excursion, especially for T_{soil}.

In the late evening (18:00 - 19:00) CO_2 increases almost linearly until reaching, prior to dawn, mean values of the order of 30 - 70 µmol mol^{-1} above the daytime values. Then, between7:00 and 9:00, a steep decrease of CO_2 concentration occurs attesting the onset of turbulence and release of CO_2 that had built up during the night.

To analyse fluxes, the full year dataset was divided into 4 three-month period, Q1, Q2, Q3 and Q4, following the rain regime patterns: dry, wet, moderately dry, and moderately wet respectively.

Figure 4.3 shows the diurnal patterns of CO_2 eddy fluxes (F_c), storage (S_c) and NEE ($F_c + S_c$). The *Fc* daily means are -14.65, -8.56, -4.68 and -6.58 mg CO_2 m^{-2} d^{-1} for the four periods, showing that the Ankasa forest always act as a net CO_2 sink. Analysing half-hourly values, from midnight until around 7:00 a.m, *Fc* is always positive (ecosystem respiration). The observed mean effluxes are quite small ranging from 1.86 µmol m^{-2} s^{-1} of the Q4 period to 3.3 µmol m^{-2} s^{-1} in Q1. After that, temperature increases until convective turbulence breaks the thermal stratification and within about an hour and half, an emission peak is observed reaching 6.00 µmol m^{-2} s^{-1} during dry period (Q1). This peak does not occurs in Q3. The photosynthesys effect become visible around 8:00 – 9:00 determining the ecosystem day-time CO_2 absorption that peaks with fluxes of -23.8, -15.15, -13.8, -13.5 µmol m^{-2} s^{-1} for the four periods respectively. *Fc* goes back to positive values after sunset around 19:00 with no significant deviations from the night means.

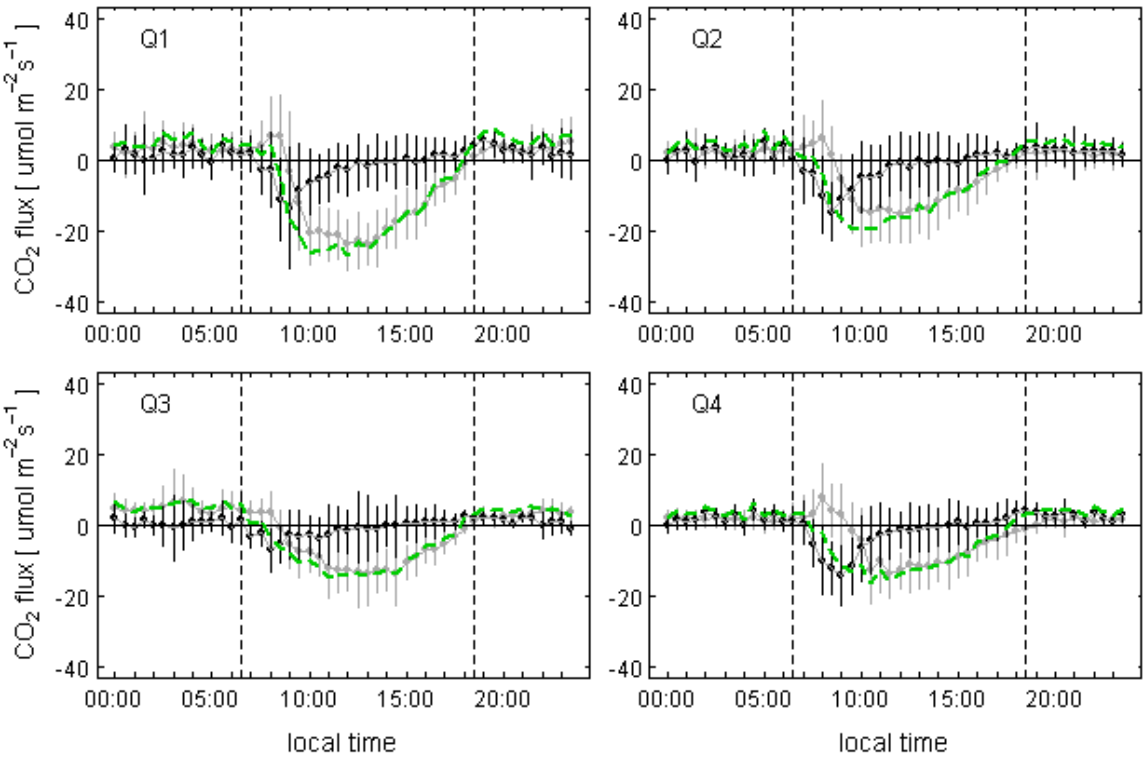

Figure 4.3 Seasonal daily trend of the CO_2 eddy flux (*Fc*, grey line), the storage flux (*Sc*, black line) and the biotic flux (NEE, green dashed line).Vertical bars represent the standard deviation of the means. Each plot represent 3 months means. Dashed vertical lines indicate sunrise and sunset. The period starting in January (Q1) comprises most of the dry season, periods starting in April (Q2) and October (Q3) comprise rainy periods while the quarter starting in July (Q3) represent a dry transition period between rains.

As far as storage fluxes are concerned, from midnight to about 7:00 CO_2 accumulation occurs in the below canopy layer determining average positive storage fluxes of 1.78, 1.5, 0.5 and 1.85 μmol m^{-2} s^{-1} during the four quarters. Such fluxes account for 10% of the NEE in the Q3 period, around 35% in Q1 and Q2 and reach 50% in Q4. Then, storage flux has a steep decrease, due to the CO_2 depletion, that peaks within 4-5 hours. In this time gap, the storage term makes the highest contribution to the NEE accounting for 55 to 90% of the total biotic flux. After midday storage fluxes are negligible until sunset when it reaches positive night values. In the first half of the night, suddenly after sunset, *Sc* fluxes – and thus NEE - shows the highest nocturnal intensity and than decrease slowly until the morning.
The importance of half-hourly storage fluxes relative to eddy fluxes is visible in Fig. 4.4, where the daily course of their ratio is shown. It can be observed that S_c supplies its major contribution during night-time, when the ratio S_c/F_c is often around or above the unity.

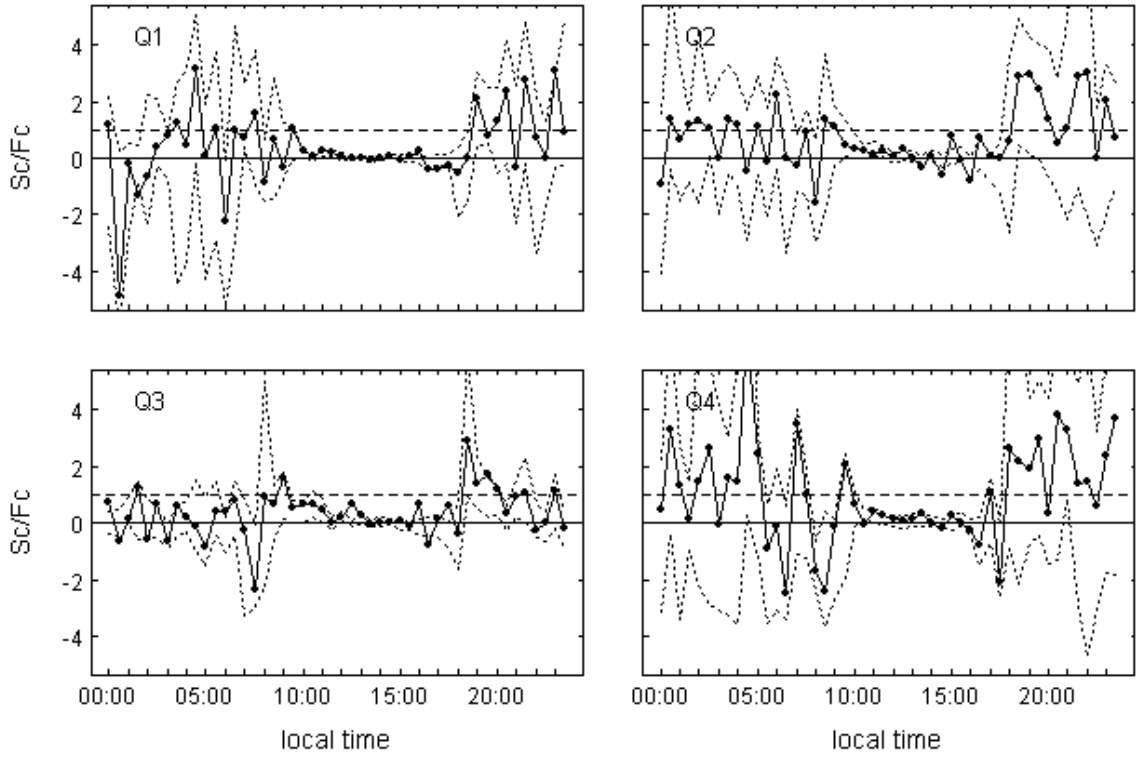

Figure 4.4. Seasonal daily trend of mean (black line) and inter-quartile range (dotted lines) ofthe storage (*Sc*) to eddy flux (*Fc*) ratio. The unity, representing the same flux intensity, is indicated by the horizontal dashed line.

To explore which environmental variable acts as main driver of S_c, several correlations analysis were performed. Storage flux variations were analysed respect to changes of shear stress (u_*), atmospheric stability (z/L), air and soil temperatures and solar radiations (global radiation and PAR). Further analyses were also made by defining range-classes of such explicative variables and by separating night and day records. None of those variables was found to have a significant descriptive value. To confirm the result, it was applied the approach proposed by Iwata et al. [2005], assessing whether total night-time storage S_{cNtot} was

more predictable than half-hour values. Linear and logarithmic regressions were tested between S_{cNtot} and the previous variables averaged over the night and also in this case, no clear relation was found.

Daily trend of CO_2 storage calculated by the discrete approach (S_{c1P}) is showed in Fig. 4.5 for each season. The CO_2 concentration measured by the IRGA of the EC system was used for the computation. The S_{c1P} trend generally follows the daily pattern of S_c but, on average, S_{c1P} underestimates both CO_2 accumulation and depletion.

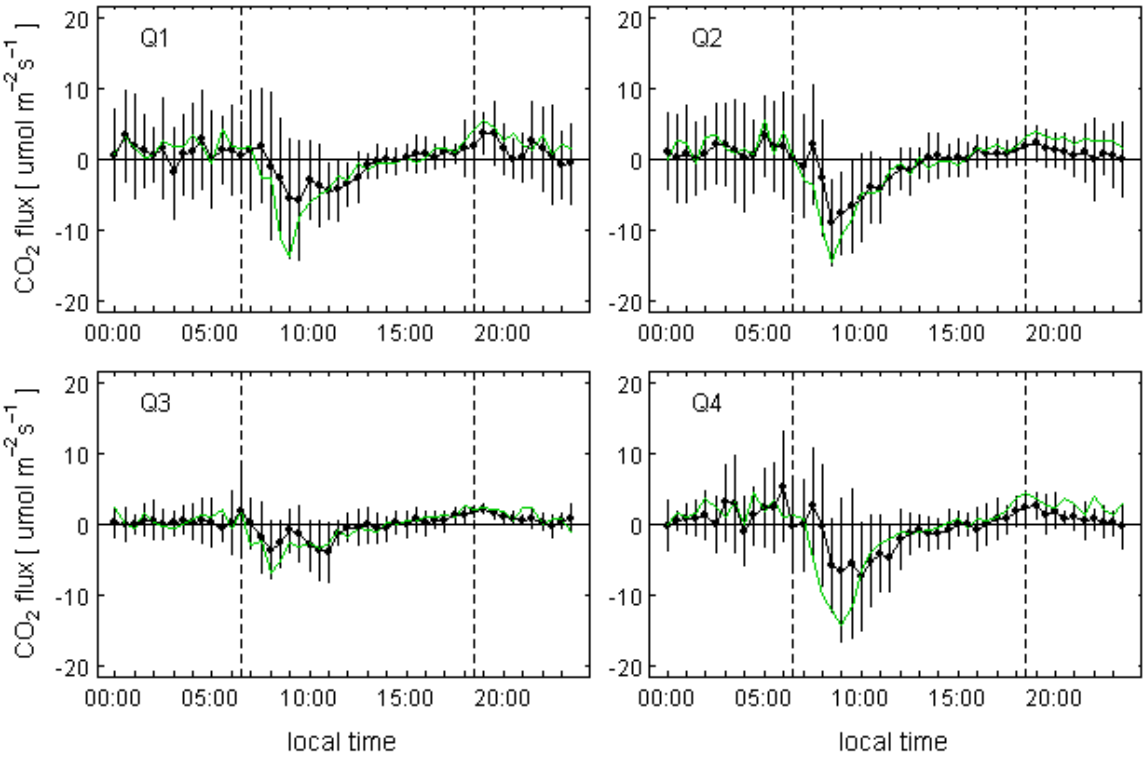

Figure 4.5. Seasonal daily trend of the CO_2 storage calculated by with the single-point approach (S_{c1P}, black line). The comparison with *Sc* (green line) evidences the general underestimation of the CO_2 accumulation (positives values) and depletion (negative values) provided by S_{c1P}.

Between midnight and 7:00 a.m., S_{c1P} losses about 20-38% of the more accurate storage estimation provided by S_c. The morning depletion peak is underestimated on average by 37-58%, then until the sunset the bias is sensibly reduced. Anyway after 19:00 the underestimation increases again up to 25-65%. From half-hourly values frequency distribution of S_c and S_{c1P} (Fig. 4.6) it is possible to evaluate the average difference between the two approaches, but also that daily trends are similar, indicating that the two measures are linked by the same drivers. The inter-quartile range of *Sc* spans within -3.46 – 3.64 µmol m^{-2} s^{-1} while for S_{c1P} this range is -1.58 – 1.82 µmol m^{-2} s^{-1}.

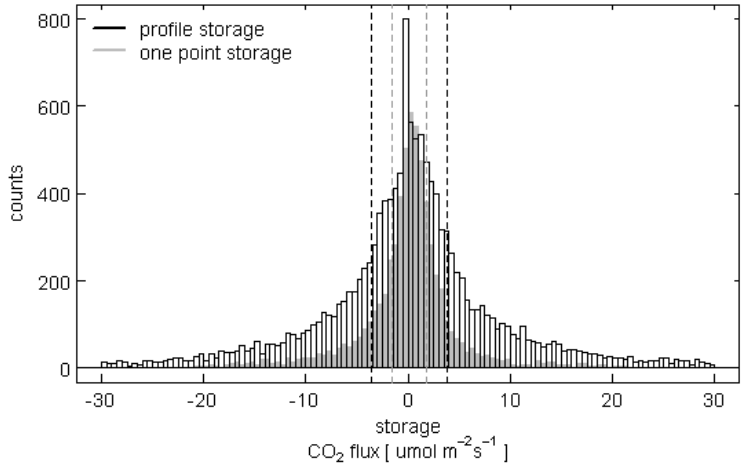

Figure 4.6. Comparison of the half-hourly records frequency distribution of *Sc* (empty bars) and Sc_{1P} (grey bars).

The accuracy of predicting the "real" storage term (assuming S_c as its best estimation) from the storage calculated with the single-point approach was evaluated.
The relation $S_c = f(u_*) \cdot S_{c1P}$ was tested over the four periods, sorting data in u_* classes of 0.1 m s^{-1} as this parameter was deemed to be the more explicative of such relation. It can be observed in Fig 4.7 that the dispersion of the distributions is so large that no tendency in S_c/S_{c1P} ratio with increasing values u_* is noticeable.

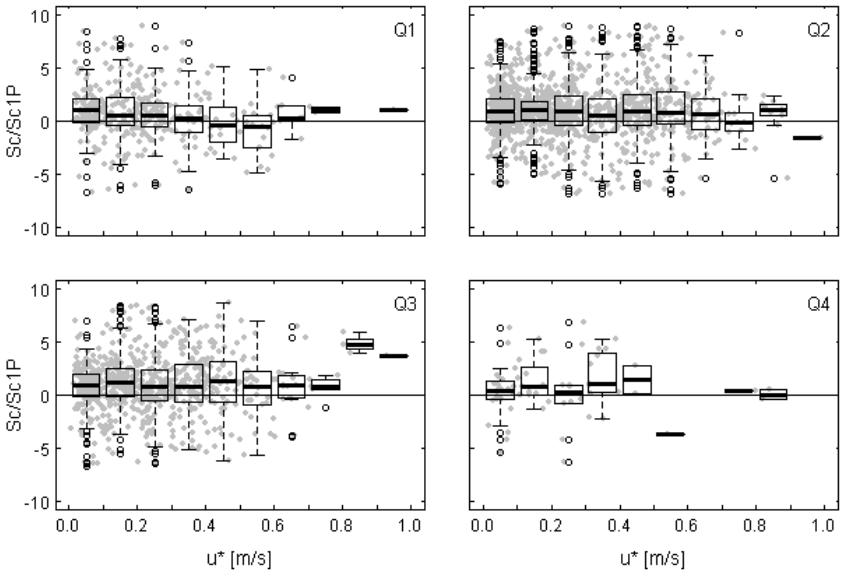

Fig 4.7. Distribution of the S_c / S_{c1P} ratio as a function of friction velocity u_*. Annual data were divided in sub-period (as for the previous analysis). Scatterplots represent the original data while the boxplots the distribution of the ratio within each u_* class of 0.1 m s^{-1}.

To investigate further into this topic, the relation $S_c = f(S_{c1P}, u_*)$ was tested. A regression analysis by linear models was carried out both for the whole dataset and separating day-time and night-time records. The result for the whole dataset is shown in Fig 4.8. It can be

observed that the correlations are still weak especially for the higher $u*$ classes (from 0.5 to 0.8 m s^{-1}).

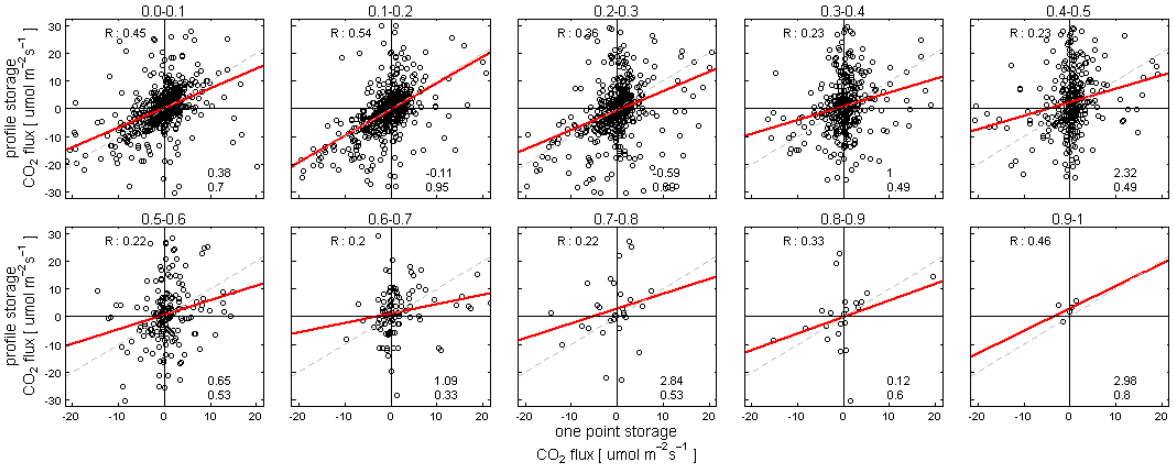

Figure 4.8. Linear regression analysis between *Sc* (y-axis) and Sc_{1P} (x-axis). Data were separated by $u*$ classes of 0.1 m s^{-1} (classes range is showed over the upper side of each plot). Red lines are the linear models, dashed grey lines represent the 1:1 ratio. Numbers at the top-left corners are the correlation values while on the bottom right corner there are the intercept (first number) and the slope (second number) of the fitted model.

As any of the previous relations was fond to be consistent, the S_c/S_{c1P} ratio was analyzed in function of the time. The hypotesys was that the two estimates were both linked to the period of the day, as also suggested by Fig. 4.5. The mean diurnal variation of S_c and S_{c1P} is plotted in Fig. 4.9 as well as the S_c/S_{c1P} ratio (*CF*). As can be seen, S_{c1P} underestimates the night-time CO_2 accumulation and also the morning depletion (07:00-10:00 a.m.), while for the rest of the day is very similar to S_c. Such biases are captured by the S_c/S_{c1P} ratio being higher with increasing underestimation.

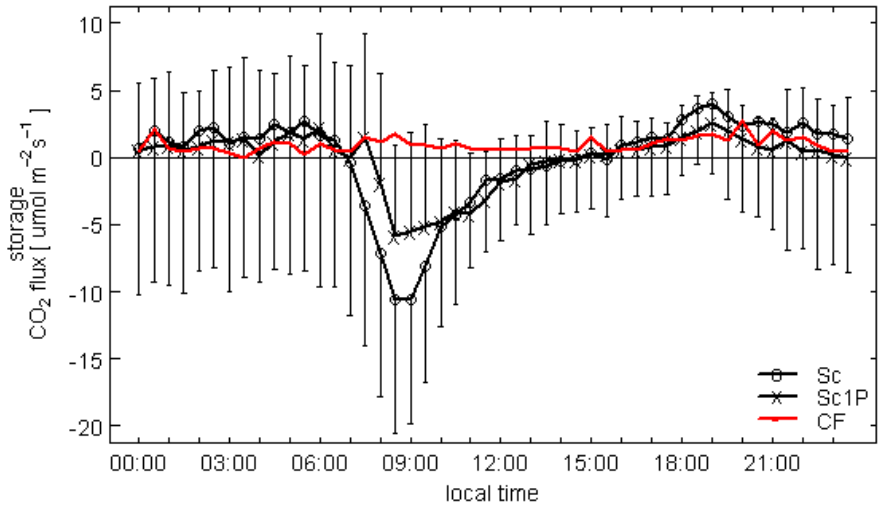

Figure 4.9. Mean diurnal variation of the storage flux calculated from profile measurements *Sc* (—o—) and from the top of the tower *Sc1P* (—x—). Their ratio (red line) nice follows the *Sc1P* storage underestimation. Bars represent the standard deviation of the means.

The S_c/S_{c1P} ratio even if not directly linked to any environmental or atmospheric variable, takes account of their global effect on the storage as co-vary all with the hour of the day. Thus, in absence of full profile measurements, such parameter can be used to correct the storage estimates made from the tower top.

Methane concentration patterns during the sampling days is shown in Fig 4.10. The variability was very high as also evidenced by the nearly random behaviour of the plot density. Mean CH_4 concentration varies in April from 1751 to 2300 ppb, in July 1730 – 2520 ppb while in October 1710 – 2071 ppb. Such spans are generally larger than the range of 1790 – 1840 ppb measured by Querino et al., [2011] in a similar ecosystem. The standard deviation of the replicates ranged 2–100 ppb but there were measures with more than 100% of uncertainty. The latters were discarded for storage computation.

Despite few cases in which the plume with high CH_4 concentration leaves the soil and rises up (e.g. in 2011.10.20 at 20:00), plumes seem to come from areas far from the sampling point. Also the canopy effect is sometimes visible (e.g. in April and October) but in most cases CH_4 diffusion seems to be not affected by the plants.

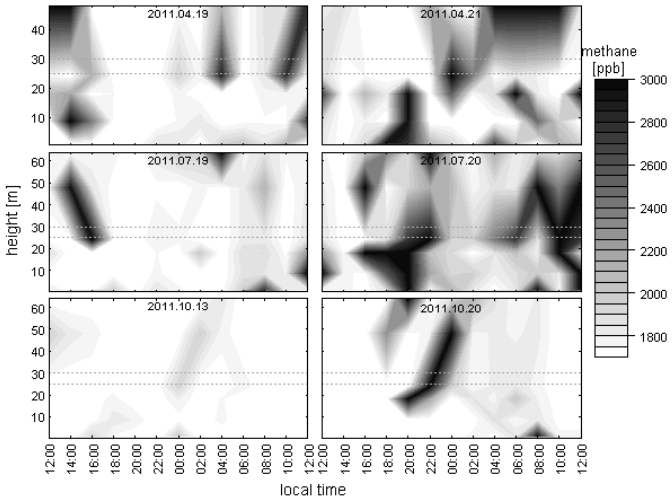

Figure 4.10. Contour plot of the measured CH_4 concentrations along the profile system. The data at the top of each plot indicate the first day of sampling. The pairs of dotted grey lines indicate the dominant canopy layer. Note that samplings start at 12:00.

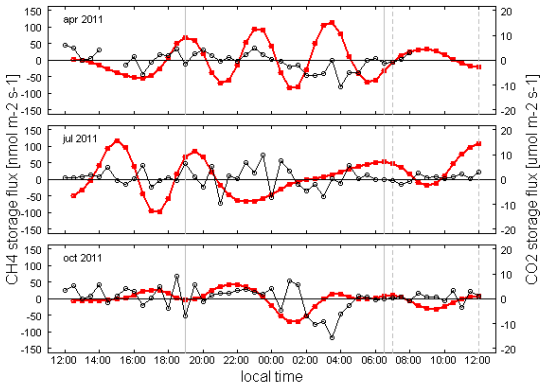

Figure 4.11. Averaged daily trend of CH_4 storage (red curves) for the three sampling campaigns. The curves are smoothed as the 2 hours lapsed measurements were interpolated at half-hourly resolution by a cubic spline function. The concurrent CO_2 storage (black lines) is also shown to evaluate similitudes.

Half hourly values of CH_4 storage (S_{CH4}) are shown in Fig. 4.11. No clear pattern is evidenced, probably due to the fact that values were averaged over only 2 days, hence natural variability is not sufficiently smoothed away. Indeed, looking at the concurrent S_c values, the pattern shown in Fig. 4.3 and 4.5 vanish as well.

4.5 Conclusions

The diurnal variation in CO_2 concentration beneath the eddy covariance system shows a significant vertical gradient during the night. Prior to dawn, CO_2 mean values are of the order of 30 - 70 μmol mol^{-1} above the daytime mean values. Then, the onset of the turbulence around 7:00 a.m determines a sudden release of the CO_2 accumulated during the night and the CO_2 gradient along the profile smooth out. This is not true for the first meter above the ground, were the influence of soil respiration is strong, alimenting the concentration gradient in this layer.

The CO_2 storage daily trends, observed in the different rain seasons, show the characteristic pattern reported also in other works on tropical forests [Grace et al., 1996; Malhi et al., 1998; Iwata et al., 2005]. The S_c peak in the first hour of the night was also observed by de Araujo et al. [2010] and van Gorsel et al [2007]. They demonstrated that differences in S_c between the first and second halves of the night were related to suppression of turbulence, stability of the flow regime within the canopy and gravity currents that drain CO_2 enriched air away.

The CO_2 accumulation at night was higher during the dry periods accounting for up to 50% of the total biotic flux. According to de Araujo et al. [2010], this demonstrates the large underestimation of the ecosystem respiration that can occur in such ecosystems. As expected, half-hourly storage terms have scant importance relative to the eddy flux during sunny hours, while they can be as high as the measured flux during low turbulence conditions. Anyway, the CO_2 accumulated at night is released in the morning and captured by the EC measurement system thus, as also asserted by Aubinet et al. [2012], this event can induce a bias on half hourly flux estimates, but it is without impact on long-term budget.

The functional relationships between S_c and atmospheric and environmental variables did not reveal any significant correlation, perhaps due to the complexity of the Ankasa ecosystem. Despite storage computation is straightforward its modelling could be problematic as many of factors can contribute. Also, interactions of multiple causes with different weights can impact on storage changes. In addition to the ecological causes, also the complex orography of the forest plays a significant role. Such challenging issue, is common in tropical ecosystems as also evidenced by other authors [van Gorsel et al., 2009; de Araujo et al, 2010]. As example they argued that because of the too small temperature range (one of the main driver of *Sc*) in the tropics, it is difficult to build a satisfactory relationship. A more detailed analysis – including a rigorous data screening - is needed, to better understand this phenomenon and it is the aim of future work.

To properly evaluate the hourly NEE, especially in dense and tall forests, it is necessary to quantify the storage from profile measurements. Indeed, it is found that the S_c estimate by means of the single-point approach (i.e. from the CO_2 concentrations measured at the EC level) could be biased.

The relations between S_c and S_{c1P} demonstrate that none of the environmental drivers can clearly explicates discrepancies between the two estimates. A similar conclusion was also reported by Iwata et al. [2005], who however were able to find relationships between the total night time storage and the morning depletion. Here neither this relation has shown significant results. The reason could be either in the distance of the EC system that is about 20 m above the canopy layer or, more likely, the presence of a considerable advection in the trunk space. In fact the complexity of the Ankasa forest soil can enhance this phenomenon. The presence of advection causes the respired CO_2 to be removed from the ecosystem and not detected by the measurement system. In this case, data correction by advection measurements becomes necessary not only for half hourly estimates but also for long-term budgets. An experiment aimed to quantify the advection strength at Ankasa is currently implemented. When advection data are not available, an accurate data filtering removing records during low turbulence conditions, joined to an appropriate gap filling procedure, could help resolving the problem.
However, a good relation was found for the mean diurnal variation of S_c and S_{c1P}. Their ratio in function of the hour of the day was found to be a good descriptor for the S_{c1P} storage underestimation.
The high variability of the below canopy CH_4 concentrations, and the absence of a long and continuous dataset, determined the impossibility to directly couple CO_2 and CH_4 storages. Except for some events, the observed CH_4 plumes in the trunk air space seem to come from upwind areas around the tower (it has to be note that, to be captured by the first air inlets of the profile system, a plume must to be formed just below the tower), and not confined to a certain period of the day. This phenomenon was also observed by Querino et al., [2011], suggesting that such episodes may be not caused by local source but by advection of air enriched of CH_4 remotely. Anyway, the limited length of the sampling period is probably the main cause of the low correlation found between half-hourly values of S_c and S_{CH4} as the measured CH_4 concentrations were too much variable.
Due to such lack of trustful relationship, the possibility to directly correlate storage fluxes of the two gases (CO_2 and CH_4) was found to be impractical. On the other hand, the necessity to correct the CH_4 measured flux by the storage term is also demonstrated.
Hence, to better assess the CH_4 storage flux estimates in absence of profile measurements, here it is proposed an approach based on the S_c/S_{c1P} ratio of the CO_2. In fact, without considering any environmental variable as proxy, it was found that such relation can be used to estimate the magnitude of the storage underestimation made by S_{c1P}. Then, assuming that transport processes for both gases are similar [Carmo et al., 2006], it is possible to retrieve a correction factor (CF) for the single-point CH_4 storage estimate. This is feasible as only the magnitude of the underestimation it is considered and the latter it is supposed to be of the same intensity for both gases as it is linked to the local conditions. This approach is free from a direct link between CO_2 and CH_4 emission patterns. For example, consider the case of a huge below canopy storage of CO_2 and a low concentration at the tower top resulting in a high CF. If in the same time there is a low storage of CH_4, the measured CH_4 concentration at the top would be also low, determining a near zero single-point storage estimate. Thus correcting this low value with a high CF would cause in any case a low value of S_{CH4}.
Anyway the approach presented here is primarily intended as practical method to correct the single point storage estimates in case of unavailability of profile measurements. Its feasibility

have to be verified in accordance to the local conditions. As example in sites with stronger variation of environmental variables, a method able to find complex relations, as the artificial neural networks method [Papale and Valentini, 2003], should be evaluate before.
Continuous sampling with *in situ* CH_4 measurements is currently planned at Ankasa and will be the base of a future investigation.

5 CH_4 and CO_2 fluxes over a tropical forest in Africa.

5.1 Introduction

The carbon exchange between biosphere and atmosphere is governed by consumption through photosynthetic and methanotrophic organism and release (respiration) through autotrophic and heterotrophic organism. The magnitudes of these processes vary from biome to biome, but some of the largest fluxes are expected to be in tropical rain forests [Malhi et al., 1998]. Nevertheless, such ecosystems have been less studied than temperate or boreal ones. The important role of tropical forests in CO_2 exchange is currently verified [e.g. Phillips et al., 1998; Simon et al. 2009] and source-sink mechanism is understood even if some debates are still on [Clark 2004; Tan et al., 2010]. In a recent paper, Malhi [2012] reports a range for tropical forest gross primary productivity (GPP i.e. the total canopy photosynthesis) between 30 and 40 Mg C ha^{-1} $year^{-1}$.

In the matter of CH_4, there are still significant uncertainties in source and sink dynamics. In particular, there is scientific debates over both the magnitude and direction of the CH_4 flux between forests and the atmosphere, and the major uncertainties regard tropical ecosystems [Smeets et al., 2009]. The active role of plants in CH_4 emission was recently investigated [Keppler et al. 2006, Vigano et al. 2008] to help explain the surprisingly high CH_4 concentrations observed by satellite over tropical forests in south America [Frankenberg et al., 2005]. The authors concluded that plants may be direct emitters of CH_4. Anyway, these findings have been under severe debate [Duek et al., 2007; Ferretti et al., 2007]. The critics assert that the previously published global emission values (62 – 236 Tg CH_4 yr^{-1}) were strongly overestimated. Thus, the contribution of terrestrial plants to global methane emission is to be reviewed, and the role of tropical forests in this mechanism have to be further investigated.

The eddy covariance (EC) technique is appropriate for continuous flux measurements over forest, integrating over landscape and measuring fluxes along environmental conditions changes. CO_2 and CH_4 fluxes measures over temperate and boreal forest canopy are recently improved [e.g. Smeets et al., 2009; Eugster and Pluss 2010; Philatie et al., 2010] but very few regards tropical forest [e.g. Querino et al., 2011].

In this work CH_4 and CO_2 fluxes are measured by means of the EC technique at the Ankasa forest reserve in Ghana. The goal is to investigate on the CH_4 sink-source mechanism on a local scale, quantify CH_4 and CO_2 flux magnitudes ad its diurnal changes, and provide an estimation of the long term budgets of such gases.

5.2 Measurement site, set-up and meteorological conditions

The EC measurements were carried out at the Ankasa forest reserve station in Ghana. The tower (05° 16' 13.400" N; 02° 41' 29.101" W; 119 m a.s.l.) is the first facility in the African continent collecting data on trace gases exchange over a tropical primary forest. The surrounding area is characterized by a rather complex orography, with a broad flat terrain interrupted by plateaus and small valleys with a maximum difference in altitude of 50-70 m

dig by the hydrographical grid. About 300 m far from the tower, in the North-East direction, there is the seasonal waterlogged area in which below canopy measurements were made (see Chap. 3). The forest has a dense canopy layer with a mean height of 30 m (for a detailed description refers to Sec. 1.3). Measurement site and set-up are showed in Fig. 5.1.

Figure 5.1. Outlooks of the Ankasa EC tower station. At the top, a panorama from the tower spanning from north to east. At the bottom from the left an aerial picture of the tower, a view from the tower top and a particular of the measuring sensors (note that the second anemometer is part of a concurrent measurement system)

The EC system was installed at an height (z) of 50 m from the soil, about 20 m above the canopies. The required energy is provided by 9 solar panels mounted along the tower structure and connected to a pack of 8 batteries of 200 A each (the energy reserve during nights and cloudy days). The instrumentation consist of a 3-D sonic anemometer Wind-Master Pro (Gill Instruments Ltd., UK), a LI-7500-A open-path CO_2/H_2O analyser and a LI-7700 open-path CH_4 analyser (LI-COR Bioscience, Lincoln, NE, USA). Raw data were sampled at 10 Hz and stored through the control box of the gas sensors (LI-7550) into a removable memory device. The needed prognostic data (air and soil temperatures, air pressure, air and soil humidity, precipitation, and direct, reflected and diffuse solar radiations) were collected by a multiplexer and a CR-1000 data logger (Campbell Scientific, Inc.) on half-hourly base.
Measurements started on April 2011 and ended on February 2012. Anyway, due to technical problems with the system, data up to October had to be discarded. Thus, the dataset presented here cover the period from 9 October 2011 to 2 February 2012.
The meteorological conditions for the measurement period are showed in Fig. 5.2. The air temperature varied within a narrow range with a period mean of about 26 °C. Also the soil temperature fluctuates around 25 °C with some temporary deviations. The rain intensity, as well as the relative humidity of the air, showed a progressive decline. This is a sign of the transition from the rain to the dry period.

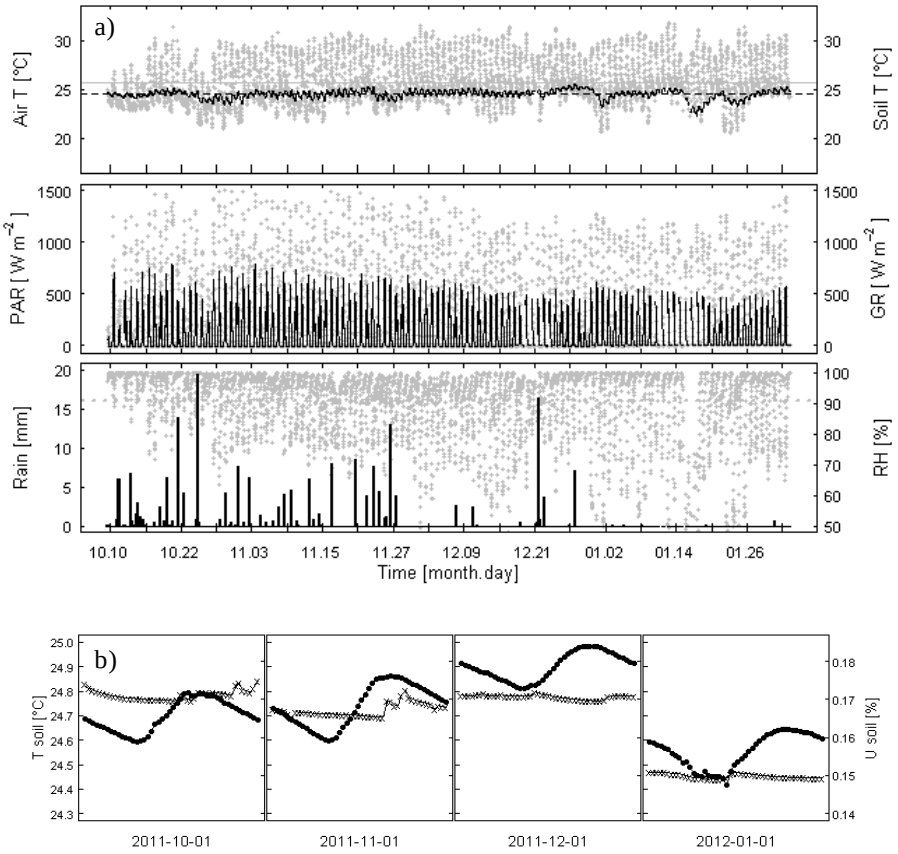

Figure 5.2. a) Meteorological conditions at the Ankasa forest reserve (Ghana) during the measurement period. Time series of air (grey dots) and soil (black dots) temperature are showed in the upper panel. The middle panel reports the photosynthetically active solar radiations (PAR, grey dots) and the global radiation (black line). At the bottom it is reported the total precipitations (black bars) and the air relative humidity (grey dots). b) Monthly averaged diurnal cycles of soil temperature (full circles) and humidity (crosses).

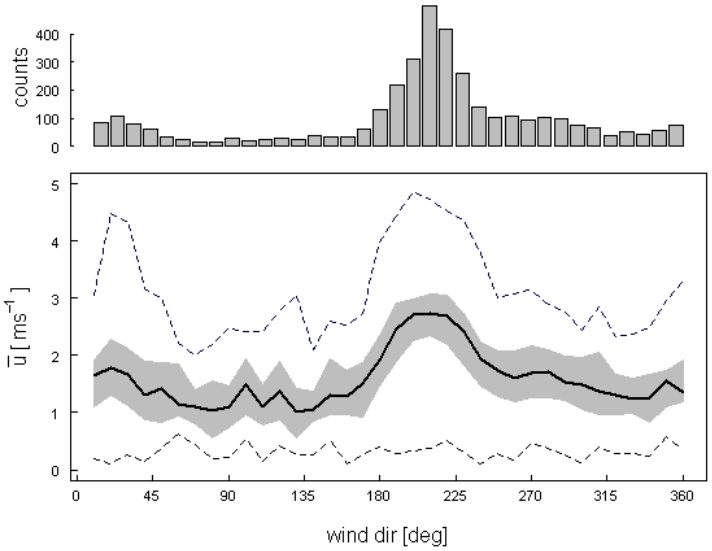

Fig 5.3. Horizontal wind speed as a function of wind direction. Data were aggregated for wind direction sectors of 10°. Median (bold line), interquartile range (shaded area; 50% of all values), and maximum and minimum values (dashed lines) are shown.

The analysis of the wind (Fig. 5.3) revealed that mean wind velocity mostly ranged between 1 and 3 m s^{-1}. The dominant wind direction is from south-west as also evidenced by highest wind speeds.

5.3 Data processing and screening

As the system was placed above the tall canopies a zero reference level *d*, the so called displacement height, was considered and approximated to 0.67 times the canopy height (30 m) thus the effective measurement height becomes $z - d = 29.9$ m.

Data processing was done following the steps reported in Sec. 1.2.2 using the EddyPro™ software (LI-COR Inc.). In particular, fluxes were calculated as half-hour covariances using block averaging. The wind vector was rotated prior to flux calculations by the planar fit method [Wilczak et al., 2001]. Physical separation between sensor was corrected by the covariance maximization procedure. To compensate for air density fluctuation the WPL correction was applied to the measured scalar fluxes, and for CH_4 it was also applied the LI-7700 correction for spectroscopic effect [McDermitt et al., 2011]. Both high-pass and low-pass filtering effects were corrected by fully analytic methods [Moncrieff et al., 1997; Moncrieff et al., 2004]. Data quality control [Aubinet et al., 1999; Foken 2008] was executed during the processing routine. Flags on half-hourly values were determined by the statistical tests on raw data (see Sec. 1.2.2) in conjunction with the stationarity and integral turbulence tests. The latter aim to assess the validity of the EC measurements and ifthe necessary turbulent conditions are met [Kaimal and Finnigan,1994; Foken and Wichura, 1996]. A further customized flagging policy was set basing on diagnostic outputs of the gas sensors. These are the automatic gain control (AGC, 0-100%), an index of cleanliness in the optical path of the LI-7500A, and for the LI-7700, the residual signal strength indicator (RSSI, 0-100%) and the diagnostic value (DIAG, 0-65535). The former accounts for the cleanliness of the instrument mirrors and the latter for the correct instrument functioning. During post-processing bad flagged records were rejected. Then fluxes data were first storage corrected. For CO_2 the storage (*Sc*) was directly computed from concurrent profile measurements (Chap. 4), while for CH_4, as continuous profile measurements were not available, the biased storage term estimated from the tower top (see e.g. Aubinet et al., [2012]) was corrected by a factor resulting from the ratio of S_c to the concurrent single-point estimate (see Chap. 4), assuming that transport processes for both gases between forest trunk space and the overlying atmosphere are similar [Carmo et al., 2006].

Then, a flux spike detection technique based on the absolute deviation from the median [Papale et al., 2006] was applied. Often in the night time it is observed a dependence of the measured CO_2 efflux to friction velocity u_* rising, suggesting an underestimation of ecosystem respiration under poor mixing conditions. Plotting the eddy flux, the storage flux and their sum (the biotic flux) against u_* it is possible to evaluate this [Grace et al., 1996; Dolman et al. 2002]. In Fig. 5.4 the average night-time fluxes, normalized by air temperature, are plotted against u_* (u_* partition was based on quantiles so each class is equally represented). It is apparent from this figure that NEE is constant at low friction velocity as expected from theory. The storage flux seems to compensate for the potential flux loss. On

this basis, no correction for low u^* was made to avoid a flux overestimation (note that the most of the low turbulent conditions were eliminated by the steady state and stationarity tests flags).

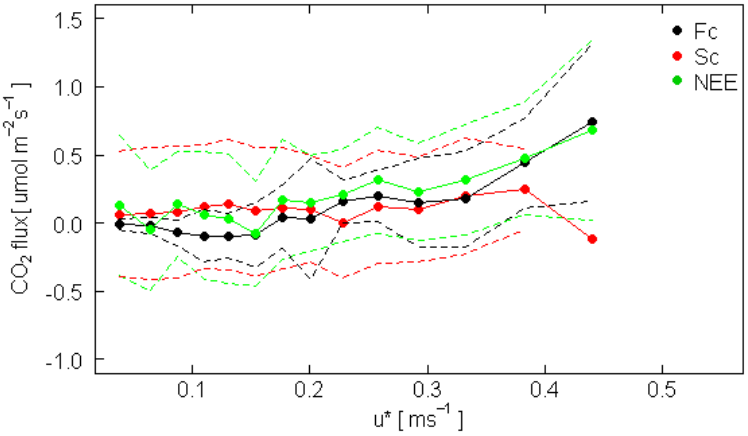

Figure 5.4. Relation of night-time CO_2 eddy-covariance flux (*Fc*), storage (*Sc*), and biotic flux (*NEE*) with friction velocity u_*. Fluxes are normalized by air temperature to eliminate the covariation between temperature and u_*.

After applying the above mentioned data filtering and corrections, a gap-filling procedure was performed to replace gaps on half-hourly time series. The technique used to fill gaps is based on the method proposed by Reichstein et al. [2005] that consider both the co-variation of fluxes with meteorological variables and the temporal auto-correlation of the fluxes. For the CO_2 the explicative variables were air temperature, global radiation and water vapour pressure deficit, while for CH_4 the latter was substituted by the soil temperature.
Then, to locate the source area distribution of measured fluxes, the estimated footprint distance based on the model by Korman and Meixner [2001], were considered in function of the wind direction. In addition the quality of the EC measurements was check by spectral analysis and the flux detection limit of the system was estimated by the method proposed e.g. by Edwards et al. [2003].

5.4 Results

5.4.1 Variability of CO_2 and CH_4 mixing ratio

The diurnal variation of CO_2 and CH_4 mixing ratio was investigated for each month (Fig. 5.5). A clear diurnal pattern is evident for both gases. The morning increase of CO_2 (due to the depletion of the CO_2 accumulated in the stand during night) is more pronounced than that of CH_4, with the latter being less steep. In fact the CH_4 starts to increase after sunset and lasts almost linearly until the early morning. The average diurnal amplitude is around 35 ppm for CO_2 and 40-50 ppb for CH_4 with a progressive reduction throughout the measurement period.

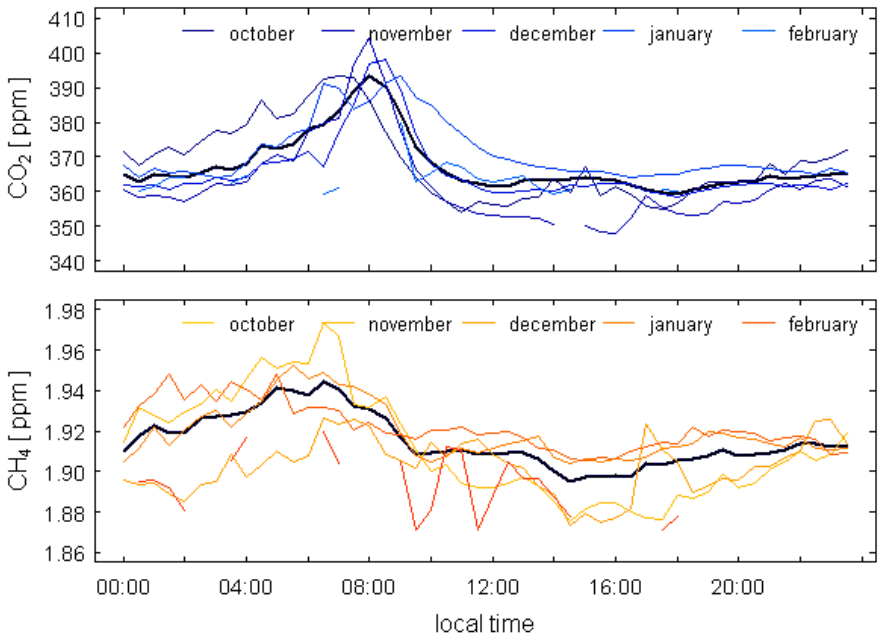

Figure 5.5. Monthly mean diurnal variation of CO_2 and CH_4 mixing ratio (µmol $mol^{-1}_{dry\ air}$) for the measurement period. Gaps on series are due to system failures.

5.4.2 Energy and scalar fluxes

Time series of sensible (H) and latent heat (LE) are showed in Fig. 5.6. Only corrected and filtered records are reported.

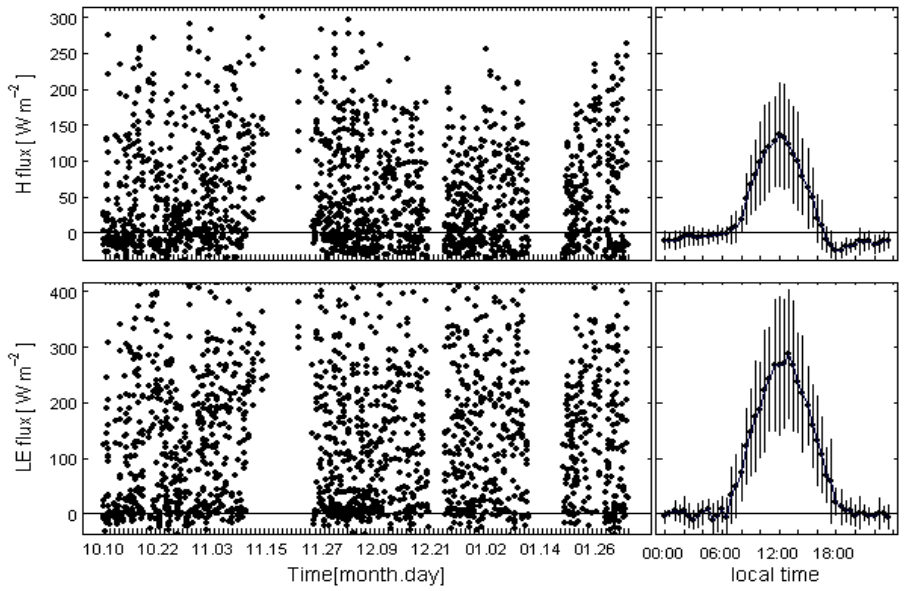

Figure 5.6. Time series of sensible (H) and latent heat (LE) fluxes. The boxes at the right side show the respective daily trends.

The diurnal variations of the energy fluxes were closely related to the intensity of solar radiation. It is also visible a decrease in the energy density during measurements. The sensible

heat flux reaches the maximum at noon, and is typically below zero at night, with the highest negatives values just after sunset. The latent heat flux reaches the maximum a little bit later (around 13:00) and approached zero at night. On average H reaches 150 Wm^{-2} while LE peaks up to 300 Wm^{-2}.

Figure 5.7 shows the time series of the screened and storage corrected scalar fluxes.

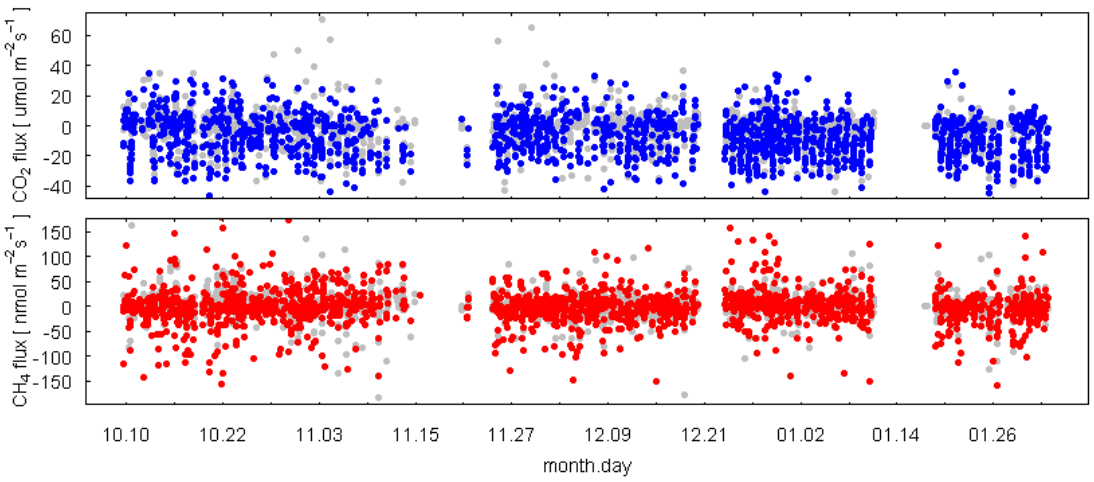

Figure 5.7. Time series of CO_2 (blue dots) and CH_4 (red dots). The corrected values are plotted over the measured values (grey dots) in function of time. Gaps are due to system crasches.

The interquartile range of the half-hours CO_2 fluxes ranged between -11.2 and 3.6 µmol $m^{-2}s^{-1}$ while the CH_4 fluxes showed higher variation with a range of -6.7 to 8.3 nmol $m^{-2}s^{-1}$ and sporadic peaks at ± 200 nmol $m^{-2}s^{-1}$.

The mean diurnal variation for the whole period (Fig. 5.8) shows a typical pattern for the CO_2 with an average night-time respiration efflux of 3.4 µmol $m^{-2}s^{-1}$ and a day-time average sink (downward flux) of 9.7 µmol $m^{-2}s^{-1}$ with a peak around 10:00 a.m. that often reach 20 µmol $m^{-2}s^{-1}$. For the whole measurement period the forest acted as a net CO_2 sink with a daily mean value of -3.1 µmol $m^{-2}s^{-1}$ (-11.8 g CO_2 $m^{-2}d^{-1}$).

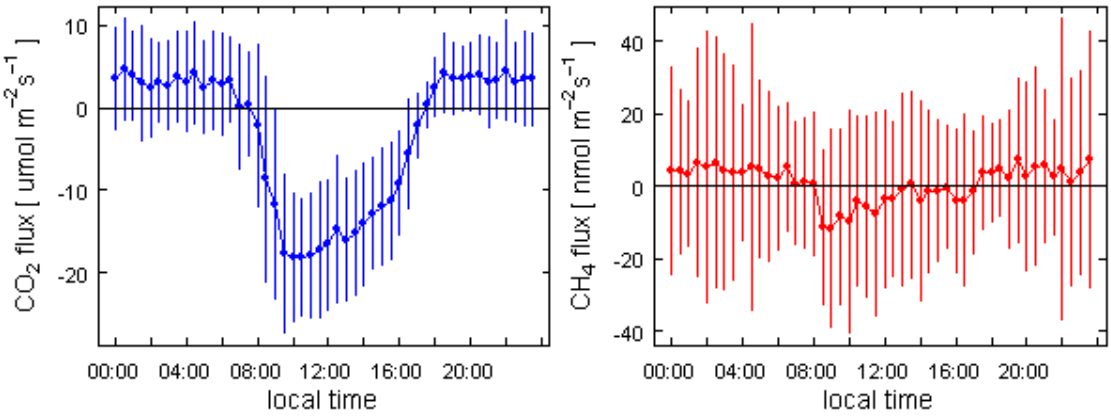

Figure 5.8. Mean diurnal variation of CO_2 (left) and CH_4 fluxes (right) for the whole period. Vertical bars represents the standard deviation within each half-hour.

The daily cycle of CH_4 flux appears more noisy but a trend is visible. During the night an average CH_4 emission of 4.5 nmol $m^{-2}s^{-1}$ was observed, though during day the fluxes become negatives with a mean of -2.7 nmol $m^{-2}s^{-1}$. The daily mean value for the whole period was 0.9 nmol $m^{-2}s^{-1}$ (1.25 mg CH_4 $m^{-2}d^{-1}$). Considering this daily emission it is possible to estimate a yearly net emission of 4.56 Kg ha^{-1}-y^{-1}. This value is to some extent smaller than the result obtained by soil chambers of 21 Kg ha^{-1}-y^{-1} (Castaldi pers. com.) but anyway comparable considering that the latter estimate is obtained from an integration on bry and wet season.

Daily trends were analysed for each month (Fig. 5.9). As can be seen, CO_2 fluxes repeat the same diurnal pattern with some variation on emission intensity at night and a quite constant absorption during the sunny hours. The monthly averages are hence determined mostly by the respiration rate and are -1.6, -4.2, -2.5 and -3.7 µmol $m^{-2}s^{-1}$ from October to January respectively. Indeed CH_4 shows a marked monthly variation with a different pattern in November. A similar variability was also observe by Querino et al., [2011] even if they recorded mainly CH_4 emissions. The average values for each month are 1.3, -0.7, 4.3 and -1.6 nmol $m^{-2}s^{-1}$. The highest nocturnal emission was observed in October and December, with peaks in the early morning and around midnight that exceed 20 nmol $m^{-2}s^{-1}$. Also the late morning sink was more evident in these months though in the rest of the period seems more scattered.

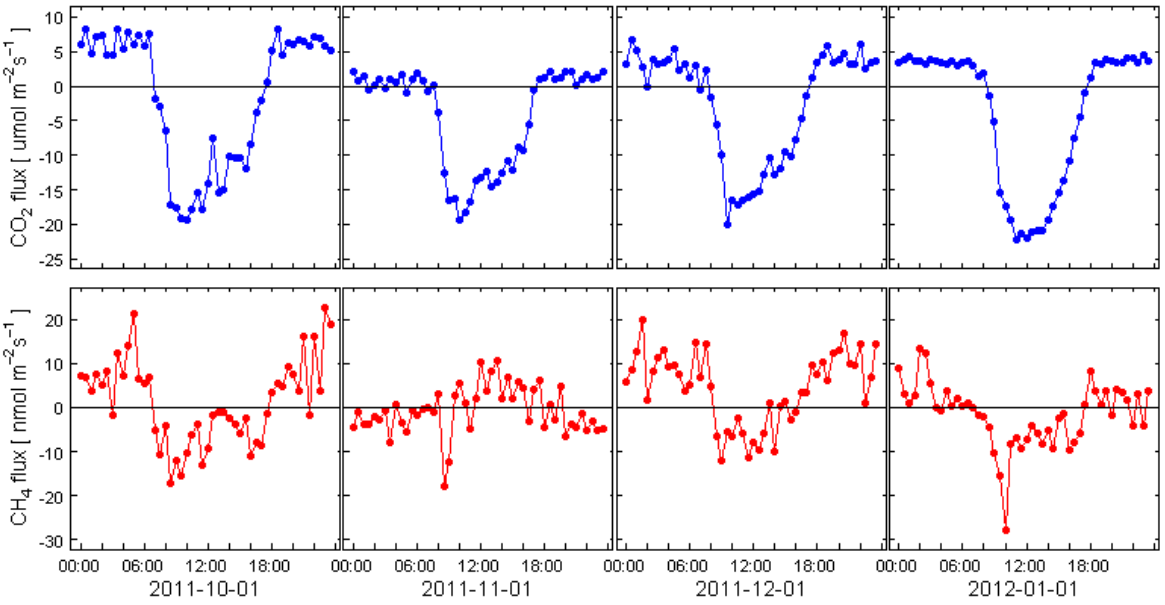

Figure 5.9. Monthly averaged diurnal cycles of CO_2 (upper panels) and CH_4 flux (lower panels). February was not considered in this analysis as few days were sampled.

The daily integrated biotic fluxes (F_c + S_c) for the full measurement period are showed in Fig. 5.10. While for CO_2 there is a progressive increase of the sink with just an inflection in December, the daily cumulative values of CH_4 presents a considerable scatter. To allow comparison between the impact of the two gases on the Ankasa ecosystem (and on the atmosphere) the CH_4 values are expressed as g CO_2 equivalents m^{-2} considering a global

warming potential with a 100-year time horizon (See Chap. 1) The net CO_2 sink for the measurement period was about 65.7 Kg CO_2 m^{-2}, reduced only by 0.17 Kg CO_2 eq m^{-2} from the CH_4 emission (0.26%).

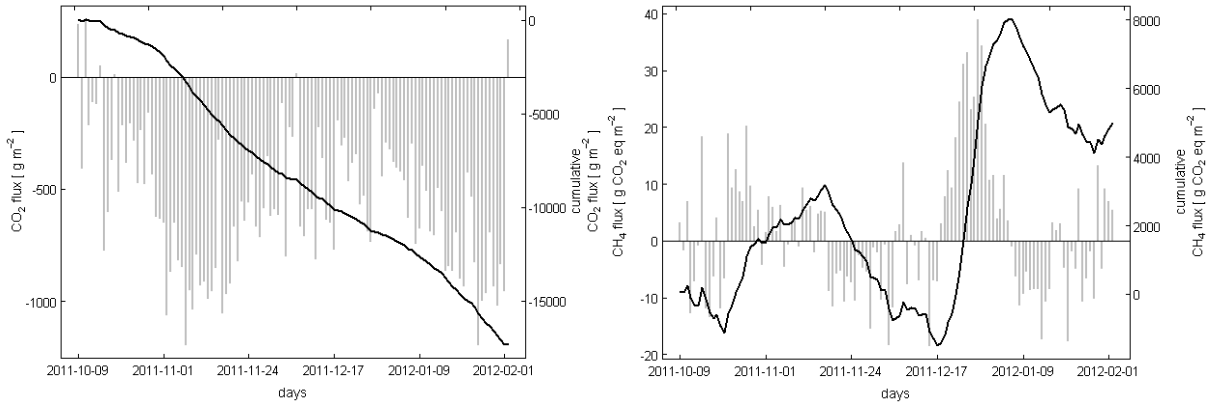

Figure 5.10. Daily sum and cumulative CO_2 (left) and CH_4 flux (right) at for the full measurement period at Ankasa tropical forest. CH_4 fluxes are expressed as g CO_2 equivalents considering 100-year time horizon.

5.4.3 Data screening and measurement quality

Of the total half-hourly records, about 35% were discarded due to instrument failures, AGC, RSSI and DIAG bad flags, about 20% were excluded due to statistical tests (steady state and developed turbulence included) and a further 1.8% were filtered as recorded during rains.
The quality of the EC system measurements was tested by the spectral analysis of fluxes. In Fig. 5.11 it is shown an example of averaged and normalized binned spectra ($fS(x)/var(x)$) and cospectra ($fC(wx)/(\overline{w'x'})$) of sensible heat, CO_2 and CH_4 for 9 hours obtained under slightly unstable conditions ($z\text{-}d/L$ = -0.3 ± 0.2). The natural frequency was used to plot (co)spectra as wind speed variation within the data selection was small ($\bar{u}$ = 3.1 ± 0.7 m s^{-1}). In the inertial subrange spectra start to follow the $f^{-2/3}$ law [Kaimal et al., 1972] up to about 0.25 Hz then spectral values for CH_4 fluxes starts to increase with a slope of f^{+1} [Stull, 1997]. This type of behaviour is due to a relatively high signal noise (the so called white noise) present in the CH_4 mixing ratio measurements. Anyway, such noise is random and does not correlate with vertical wind speed variations hence has few impact on EC measurements [Tuzson et al., 2010]. In fact, the co-spectra of sensible heat, CO_2 and CH_4 (Fig. 5.11) overlap and compare well to the universal Kansas curve for unstable conditions [Kaimal et al., 1972]. This is a proof for the good quality of the EC measurements [Smeets et al, 2009], and in particular, the shape and noise of the CH_4 co-spectrum compares well to the others confirming the quality of the CH_4 flux measurement However, for the highest frequencies, the values are still a little bit irregular due to the influence of the relatively high signal noise as discussed before.
To verify if the chosing averaging period, i.e. 30 min, was adequately long to capture the the low frequency part of the fluxes, the ogive test [Foken 2008] was implemented. The flux ogive represents the cumulative contribution of the turbulent eddy frequencies to the flux (i.e. the cumulative co-spectrum) so if the value of this integral aproaches a constant value at low frequency it means that the averaging period is satisfactory.

As can be seen in Fig. 5.12 both the CO_2 and CH_4 ogives converge within 0.005 Hz (with some delete for CO_2), thus most of the flux is reached within a time scale of 200 s.

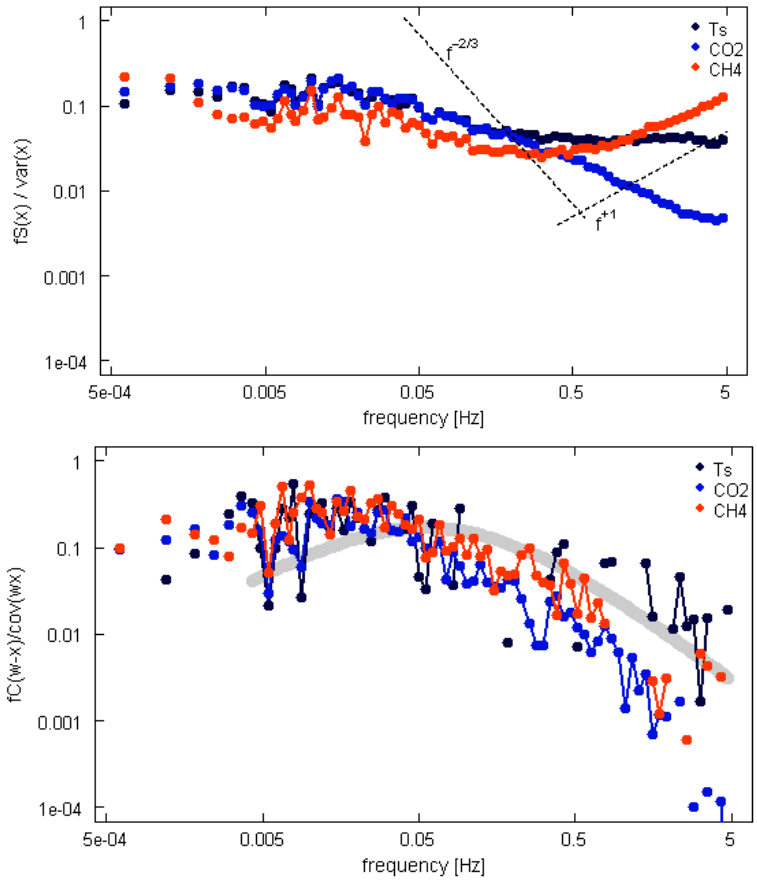

Figure 5.11. Comparison of normalized averaged spectra and co-spectra of sensible heat (*Ts*, dark blue points), CO_2 (light blue points) and CH_4 (red points) for 9 hours under slightly unstable conditions (z-d/L = -0.3 ± 0.2, u= 3.1 ± 0.7 m s^{-1}).

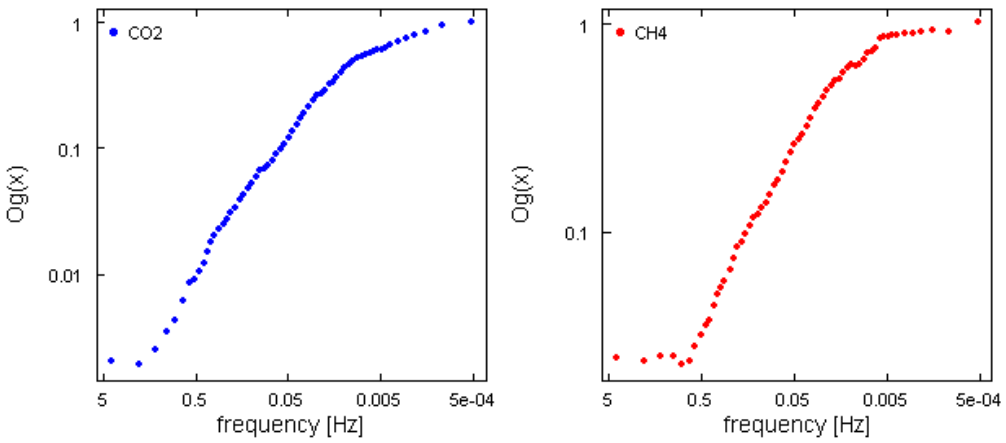

Figure 5.12. Converging ogives for CO_2 (left) and CH_4 (right) for the (co)spectra selection of Fig. 5.11. Most of the flux is reached within 200 s.

The estimated flux detection limit for CH_4 flux measurement ranges between 0.01 and 1.3 nmol m^{-2} s^{-1} with an average value of 0.43 nmol m^{-2} s^{-1}, thus most of the time smaller than the measured fluxes. As it is expressed as the product of the standard deviation of the vertical wind (σ_w) and of the instrument noise in the trace gas concentrations measure (σ_c) divided by the square root of number of independent measurements, the flux detection limit varies between night and day being on average 0.6 and 0.25 nmol m^{-2} s^{-1} respectively.

5.4.4 Flux footprint

The footprint of the measured fluxes during unstable conditions (Fig 5.13) shows that the main sources are located within 600-800 m from the tower.

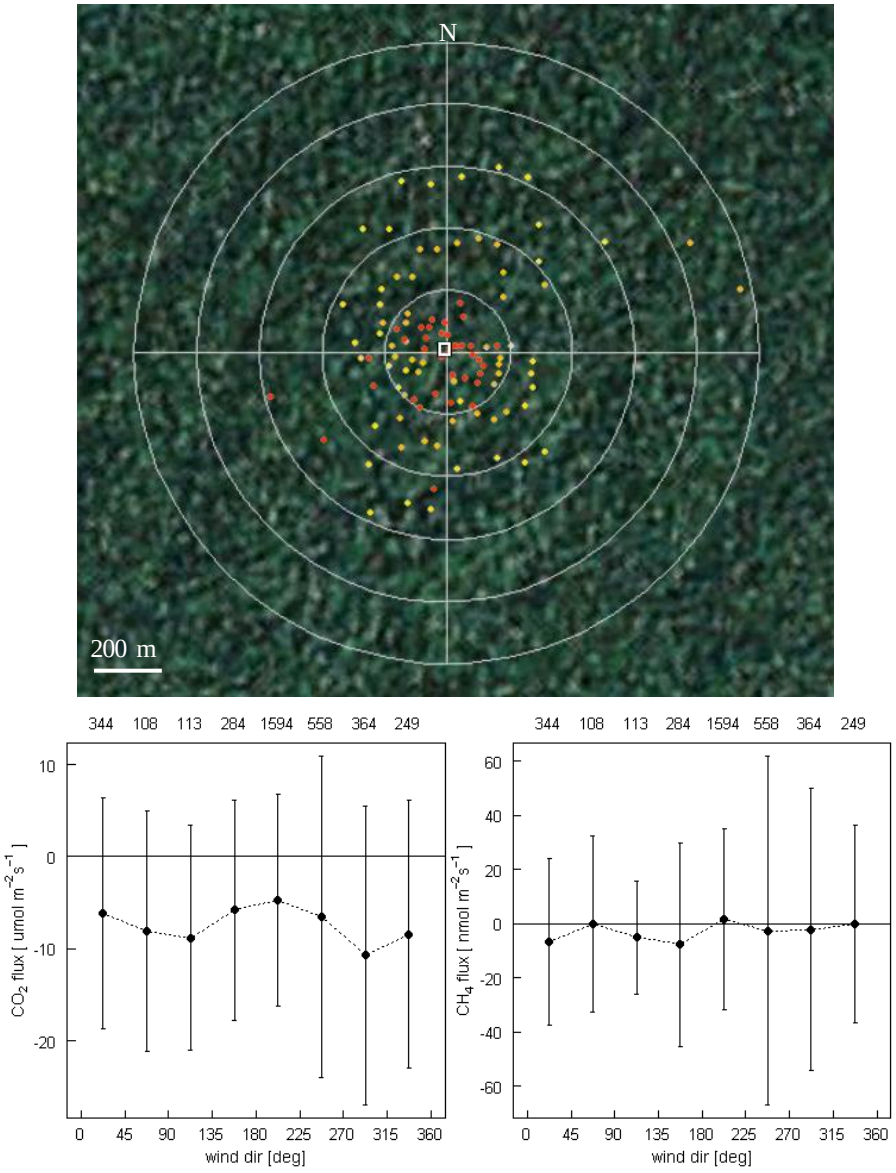

Figure 5.13. Upper frame: aerial image of the Ankasa forest with an overlapped representation of the flux footprint area. The radial grid extends to 1000 m. The 70% and 50% cumulative crosswind-integrated contribution and footprint peaks (yellow, orange and red points) represent the source area. Data were averaged considering wind sectors of 10°. Bottom plots: CO_2 (left) and CH_4 (right) flux dependency on wind direction, aggregated in 45° wind sectors. Numbers at the top of the frame are the number of records within each class.

Distances increase with stability (almost twice) but footprint model estimates during stable conditions are not robust [Kljun et al., 2004]. The 70% contribution to the measured half-hourly flux (cumulative crosswind-integrated contribution) often occur within 600 m from the tower, while the largest relative crosswind-integrated contribution (footprint peak) is localized within 200 m and drift away up to 400 within the south-west sector (Fig 5.13).
To investigate if the magnitude of fluxes has a connection with a prevailing direction, flux mean and standard deviation was calculated for each 45° wind sector (Fig. 5.13 bottom panels). Is almost evident that most of the fluxes comes from the south-west sector, but there is not a clear relation with their intensity. This is expected for CO_2 as forest density is pretty homogenous in the surrounding area of the tower. For CH_4 it seems that the most of negative fluxes comes from the east side (from north to south) but a cross-check with independent measurements (e.g. soil chambers) is needed to validate this findings.

5.5 Discussions and conclusions

Mixing ratios measurements above the canopy revealed a clear diurnal cycle of both CO_2 and CH_4. With regard to CO_2 the night time concentrations increase almost linearly until the early morning when a rapid intensification bring the concentrations at the daily maximum. This peak is followed by a rapid decrease to the background values. This pattern is also reported in other studies conducted above tropical forests [Grace et al. 1996; Malhi et al. 1998] and is attributed both to the plants activity and to the diurnal evolution of the boundary layer, with the latter having a predominant role [Culf et al., 1997]. The CH_4 concentration is subject to same atmospheric forces (the plant contribution is null) thus the diurnal evolution is similar: the shallow stable boundary layer at night retains the surface emissions in the below canopy space and the evolution of the mixed boundary layer, caused by the surface heating, determines the break of the nocturnal layer, the temporary increase of the CH_4 concentration as it arise from the forest, and the subsequent dilution to background levels. Quantitatively, the CH_4 concentration showed a decreasing in diurnal amplitude during the measurement period passing from 80 ppb in October to near 40 in January. CH_4 concentration measured in this study compares with values observed by Querino et al. [2011] over a similar forest in Brazil but on average are 10 ppb higher.
The difference observed in the energy fluxes - the latent heat is on average nearly two times the sensible heat - is an indication that the incoming solar radiation, partitioned into the two energy streams, is used mainly for the evapotranspiration. This is also confirmed by the Bowen ratio (H/LE) that during the measurements showed a median value of 0.2.
The diurnal cycle of CO_2 flux compares very well with analogous studies. In this experiment it was measured a mean daily flux of -3.1 $\mu mol\ m^{-2}\ s^{-1}$ with absorption peaks around 10:00 a.m. that reach 20 $\mu mol\ m^{-2}\ s^{-1}$ coinciding with the maximum photosynthetic activity. Very similar to the absorption peaks measured by Fan et al., [1990], Grace et al., [1996] or Malhi et al. [1998] in Brazil while somewhat higher than Querino et al. [2012] and de Araujo et al. [2011].
The error of the daily means was assessed by the method proposed by Moncrieff et al., [1996]. For the actual dataset constituted by 117 days, assuming a pessimistic 20% random

errors per half-hour value, the overall random error on the net carbon dioxide flux is 0.20 μmol m^{-2} s^{-1} i.e. 6.7 % of the daily means.

The CH_4 diurnal cycle showed considerable more scatter. In general the increase of CH_4 emission starts after sunset (around 18:00 local time) and lasts linearly until the early morning. The morning venting peak is not always clear. In fact it is visible in October and December while in the other moths is not. After the develop of the mixed boundary layer, the fluxes begin to decrease until reaching a negative peak around 9:00-10:00 a.m.. After that fluxes return to small values around zero more quickly than CO_2 as they are not influenced by the photosynthetic uptake. On average the night time emission were estimated to be 4.5 nmol m^{-2} s^{-1} (6.2 mg m^{-2} d^{-1}) in contrast to a diurnal sink of 2.7 nmol m^{-2} s^{-1} (3.7 mg m^{-2} d^{-1}). The overall daily flux was estimated to be 0.9 nmol m^{-2} s^{-1} or 1.25 mg m^{-2} d^{-1}.

Smeets et al. [2009] measured a diurnal sink over a forest in California of about 6 mg m^{-2} d^{-1}, resulting in a daily (downward) mean flux of 2.5 mg m^{-2} d^{-1}. A more suitable comparison could be done with Querino et al. [2011] that measured an average flux of 2.8 mg m^{-2} d^{-1} over a tropical forest in Brazil. In general they observed more positive fluxes, even during the sunny hours, and a higher morning peak that on average reaches a value on 6 nmol m^{-2} s^{-1}.

Using the same criteria adopted for CO_2, the random error assessment of the CH_4 daily means gave a value of 0.4 nmol m^{-2} s^{-1} that, in this case, means about 44% of the daily value.

The substantial variability observed in CH_4 flux is not so straightforward to explicate as it may come from several sources. As an example looking at the meteorological conditions of Fig. 5.2, the high variation found in the daily cycle within each month is not fully explainable. While CO_2 showed a clear response to net radiation, CH_4 seems to be insensitive (Fig. 5.14). The same was found for air temperature (data not sown). A similar behaviour is reported by Dengel et al., [2011]. The rain intensity seems to potentially have an impact on CH_4 fluxes but further confirm by longer dataset are needed.

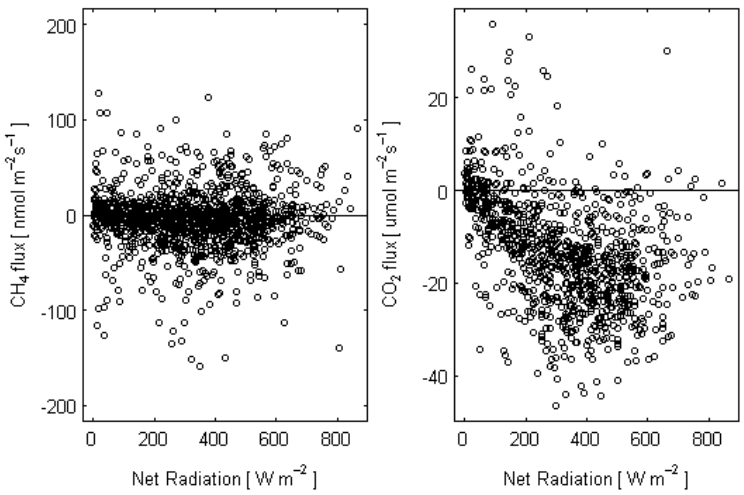

Figure 5.14. Response of CH_4 and CO_2 fluxes to net radiation. CH_4 shows no variation while CO_2 shows a typical light-response curve.

The system flux detection limit (FDL) shows that for most conditions the 7700 sensitivity is adequate for measuring CH_4 fluxes by EC over the Ankasa forest. The estimated value was

0.43 nmol m^{-2} s^{-1} that corresponds to 6.9 ng m^{-2} s^{-1} with a range of variation between 0.01 to 20 ng m^{-2} s^{-1}. The mean value is pretty similar to the mean FDL, 7 - 12 ng m^{-2} s^{-1}, reported from Edwards et al. [2003]. Anyway such values are somewhat smaller than 8 – 35 ng m^{-2} s^{-1} reported from Querino et al. [2011], or 22 ng m^{-2} s^{-1} by Smeets et al. [2009] using a different approach for the computation.

The data collected in this experiments suggest that the Ankasa forest acts, on average, as a source of CH_4 to the atmosphere. Periods of sink also occurs mainly prior to the noon. This emission only compensate for 0.26% of the total C fixed by the forest as CO_2. As no evidence for aerobic CH_4 emission from canopies was found, it is assumed that the major contribution to the CH_4 balance comes from the soil. Anyway, a detailed investigation with continuous profile measurement is needed to completely asses this aspect.

From the footprint estimation it seems that most of the fluxes come from the south-west sector and a general increase of the distances is visible in the north north-east part. This could be an indication that the main CH_4 sources are localized at the south of the tower but further sampling at the soil level are needed to verify this finding.

The feasibility of CH_4 EC measurement is confirmed even if the dilution of CH_4 concentration during the day makes the resolution of the small concentration difference a challenging task.

6 General discussions

The structure of this thesis, composed of autonomous chapters, allowed the discussion of each topic at the end of each session. In this chapter there will be reported the overall conclusions on the work and some perspective for the future researches.

From analysed bibliography, it can be seen an increased year by year progress in non-CO_2 flux measurements, in particular for methane, leading to improvements on estimates. However assessing the source-sink mechanism in time and space, and the sources and magnitude of errors of estimates are still challenging.
Forest ecosystems have been observed to act either as source or sink, but the dynamics of this equilibrium is far still from being well characterized. Soil characteristics emerge as main factors regulating upward and downward exchanges, indeed no indication for the active role of plants were found.

This study confirmed that eddy covariance measurement can be performed below a closed canopy but it is needed to face with some problematic conditions. Insufficient atmospheric mixing, affects measurements especially at night-time, and also leads to a violation to the assumptions underlying the EC theory. Data quality tests had shown that a considerable part of data suffers from insufficient turbulence conditions. Anyway, the results of the measurement campaigns in the trunk space of the Ankasa forest revealed that the soil water content acts as main driver on CH_4 emissions with measured fluxes being of opposite sign during dry and wet season. Longer series are required to discriminate valid measurements, perform a deeper error assessment and set functional relationship with environmental variables.

The same perspectives are valid for CH_4 storage estimates. Despite storage computation is straightforward, its modelling could be problematic as many of factors can contribute. The interaction of multiple causes, the complex orography of the forest soil and the weak variation on meteorological conditions typical of tropical ecosystems contribute to the difficult in building satisfactory relationships. A more detailed analysis – including a rigorous data screening - is needed, to better understand this phenomenon and it will be the aim of future works. At the moment, to better assess the CH_4 storage flux estimates in absence of profile measurements, it is proposed an approach based on the Sc/Sc1P ratio of the CO_2. In fact, without considering any environmental variable as proxy, it was found that such relation can be used to estimate the magnitude of the storage underestimation made by Sc1P. Hence, assuming that transport processes for both gases are similar, it is possible to retrieve a correction factor (CF) for the single-point CH_4 storage estimate.

Finally this thesis tested the hypothesis whether eddy covariance (EC) flux measurements technique can represents a useful resource to estimate CH_4 fluxes over the forest canopy.
Results confirmed the feasibility of such approach even if the natural variability of CH_4 emissions and the low ambient concentrations strongly impact on the uncertainty of the

estimates. The relative 30 min EC flux uncertainty, dependent on the flux magnitude, could be much larger than 100%. However, emission estimates are usually made over longer time period. In that case, the uncertainty in the estimate will decrease since all uncertainties are random. Here it was estimated that the uncertainty in daily CH_4 emission estimates it is around 44% in comparison to 7% for CO_2.

The emissions of CH_4 were clearly lower than the sink of CO_2 in this tropical forest. Anyway the emissions of this gas are not trivial when a full GHG balance has to be calculated. It is therefore important to decrease the uncertainties in the estimates and obtain accurate observations. The eddy covariance technique can substantially contribute to this aim with the condition of an appropriate data processing and a careful error assessment.

References

Arah, J. R. M., I. J. Crichton, K. A. Smith, H. Clayton, and U. Skiba, 1994. Automated gas chromatographic analysis system for micrometeorological measurements of trace gas fluxes, J. Geophys. Res., 99 (D8), 16593–16598, doi: 10.1029/94JD00316.

Aubinet M., Grelle A., Ibrom A., Rannik Ü., Moncrieff J., Foken T., Kowalski A.S., Martin P.H., Berbigier P., Bernhofer C., Clement R., Elbers J., Granier A., Grünwald T., Morgenstern K., Pilegaard K., Rebmann C., Snijders W., Valentini R., Vesala T., 1999. Estimates of the Annual Net Carbon and Water Exchange of Forests: The EUROFLUX Methodology. Advances in Ecological Research, 30, 113–175.

Aubinet M., Vesala T., Papale D., 2012. Eddy Covariance: A Practical Guide to Measurement and Data Analysis. Springer Atmospheric Sciences, Dordrecht Heildeberg London New York ISBN-10: 9400723504.

Baldocchi D., 1997. Flux footprint within and over forest canopies. Boundary-Layer Meteorology 85, 273–292.

Baldocchi, D. D. and Meyers, T. P., 1991. Trace gas exchange above the floor of a deciduous forest 1, Evaporation and CO2 efflux, J. Geophys. Res., 96, D4, 7271–7285.

Baldocchi, D. D., Verma, S. B., Matt, D. R., and Anderson, D. E., 1986. Eddy-correlation measurements of carbon dioxide efflux from the floor of a deciduous forest, J. Appl. Ecol., 23, 967–975.

Baldocchi, D., E. Falge, L. Gu, R. Olson, D. Hollinger, S. Running, P. Anthoni, C. Bernhofer, K. Davis, R. Evans, J. Fuentes, A. Goldstein, G. Katul, B. Law, X. Lee, Y. Malhi, T. Meyers, W. Munger, W. Oechel, K. T. Paw U, K. Pilegaard, P. Schmid, R. Valentini, S. Verma, T. Vesala, K. Wilson, and S. Wofsyn, 2001. FLUXNET: A new tool to study the temporal and spatial variability of ecosystem–scale carbon dioxide, water vapour, and energy flux densities, Bull. Amer. Meteor. Soc., 82, 2415–2434, doi: 10.1175/1520-0477(2001)082<2415:FANTTS>2.3.CO;2.

Beswick, K., T. Simpson, D. Fowler, T. Choularton, M. Gallagher, K. Hargreaves, M. Sutton, and A. Kaye, 1998. Methane emissions on large scales, Atmos. Environ., 32 (19), 3283-3291, doi: 10.1016/S1352-2310(98)00080-6.

Beverland, I., D. ONeill, S. Scott, and J. Moncrieff, 1996b. Design, construction and operation of flux measurement systems using the conditional sampling technique, Atmos. Environ., 30 (18), 3209-3220, doi: http://dx.doi.org/10.1016/1352-2310(96)00010-6.

Beverland, I.J., J. Moncrieff, D. H. ONeill, K. J. Hargreaves, and R. Milne, 1996a. Measurement of methane and carbon dioxide fluxes from peatland ecosystems by the conditional-sampling technique, Q. J. R. Meteorolog. Soc., 122, 819-838, doi: 10.1002/qj.49712253203.

Bowden R.D., Newkirk K.M., Rullo G.M., 1998. Carbon dioxide and methane fluxes by a forest soil under laboratory-controlled moisture and temperature conditions. Soil Biology & Biochemistry, 30(12), 1591-1597.

Bowling, D.R., J. B. Miller, M. E. Rhodes, S. P. Burns, R. Monson, and D. Baer, 2009. Soil and plant contributions to the methane flux balance of a subalpine forest under high ultraviolet irradiance, Biogeosciences Discuss. 6, 4765–4801, doi:10.5194/bgd-6-4765-2009.

Bridgham, S.D., J. P. Megonigal, J. K. Keller, N. B. Bliss, and C. Trettin, 2006. The carbon balance of North American wetlands, Wetlands, 26 (4), 889–916, doi: http://dx.doi.org/10.1672/0277-5212(2006)26[889:TCBONA]2.0.CO;2.

Burba, G., A. Schmidt, R. L. Scott, T. Nakai, J. Kathilankal, G. Fratini, C. Hanson, B. Law, D. K. McDermitt, R. Eckles, M. Furtaw, and M. Velgersdyk, 2012. Calculating CO2 and H2O eddy covariance fluxes from an enclosed gas analyzer using an instantaneous mixing ratio. Global Change Biology, 18, 385–399, doi: 10.1111/j.1365-2486.2011.02536.x.

Businger, J. A. and A. C Delany, 1989. Sensor resolution requirements for the accurate measurement of atmosphere/biosphere fluxes for the range of atmospheric conditions., Our Changing Atmosphere, Proceedings of the 28th Liève International Astrophysical Colloquium, Cointe-Ougree, Belgium, 487-492.

Businger, J. A. and A. C. Delany, 1990. Chemical sensor resolution required for measuring surface fluxes by three common micrometeorological techniques, J. Atmos. Chem., 10, 399-410, doi: 10.1007/BF00115782.

Cao, M., K. Gregson, and S. Marshall, 1998. Global methane emission from wetlands and its sensitivity to climate change, Atmos. Environ., 32 (19), 3293-3299, doi: 10.1016/S1352-2310(98)00105-8.

Carmo J. B., Keller M., Dias J. D., Camargo P. B., and Crill, P., 2006. A source of methane from upland forests in the Brazilian Amazon, Geophys. Res. Lett., 33, L04809. doi:10.1029/2005GL025436.

Castaldi S., de Grandcourt A., Rasile A., Skiba U. and. Valentini R., 2010. CO2, CH4 and N2O fluxes from soil of a burned grassland in Central Africa. Biogeosciences, 7, 3459–3471.

Chiti, T., Certini, G., Grieco, E. & Valentini, R. 2010. The role of soil in storing carbon in tropical rainforests: the case of Ankasa Park. Ghana Plant Soil 331, 453–461., doi:10.1007/s11104-009-0265-x)

Christensen, S., P. Ambus, J. Arah, H. Clayton, B. Galle, D. Griffith, K. J. Hargreaves, L. Klemedtsson, A. M. Lind, M. Maag, A. Scott, U. Skiba, K. Smith, M. Welling, and F. Wienhold, 1996. Nitrous oxide emission from an agricultural field: comparison between measurements by flux chamber and micrometerological techniques, Atmos. Environ. 30 (24), 4183-4190.

Clark D., 2004. Sources or sinks? The responses of tropical forests to current and future climate and atmospheric composition. Phil. Trans. R. Soc. Lond. B, 359, 477–491.

Clement, R., S. Verma, and E. Verry, 1995. Relating chamber measurements to eddy correlation measurements of methane flux, J. Geophys. Res., 100 (D10), 21047-21056, doi: 10.1029/95JD02196.

Crutzen, P. J., E. Sanhueza, and C. A. M. Brenninkmeijer, 2006) Methane production from mixed tropical savanna and forest vegetation in Venezuela, Atmos. Chem. Phys. Discuss., 6, 3093–3097, doi: 10.5194/acpd-6-3093-2006.

Culf A.D. , Fisch G., Malhi Y., Nobre C.A., 1997. The influence of the atmospheric boundary layer on carbon dioxide concentrations over a tropical forest. Agricultural and Forest Meteorology 85, 149-158.

Davidson E.A. and J. P. Shimel, 1995. Microbial process of production and consumption of nitric oxide, nitrous oxide and methane, in Biogenic trace gases: measuring emissions from soil and water, edited by P.A. Matson and R. C. Harriss, pp. 327-357, Blackwell Science Ltd, UK.

de Araujo A.C., Dolman A.J., Waterloo M.J, Gash J.H.C., Kruijt B., Zanchi F.B., de Lange J.M.E., Stoevelaar R., Manzi A.O., Nobre A.D., Lootens R.N. and Backer J., 2010. The spatial variability of CO2 storage and the interpretation of eddy covariance fluxes in central Amazonia. Agricultural and Forest Meteorology 150, 226–237.

Dengel S., Levy P. E., Grace J., Jones S. K., Skiba U. M., 2011. Methane emissions from sheep pasture, measured with an open-path eddy covariance system. Global Change Biology, 17 (12), 3524–3533.

Denmead, O.T. 2008. Approaches to measuring fluxes of methane and nitrous oxide between landscapes and the atmosphere, Plant Soil, 309, 5-24, doi: 10.1007/s11104-008-9599-z.

Denmead, O., R. Leuning, I. M. Jamie, and D. W. T. Griffith, 2000. Nitrous oxide emissions from grazed pastures: measurements at different scales, Chemosphere, 2, 301-312, doi: http://dx.doi.org/10.1016/S1465-9972(00)00035-0.

Denmead, O., B. Macdonald, G. Bryant, T. Naylor, S. Wilson, D. Griffith, W. Wang, B. Salter, I. White, and P. Moody, 2010. Emissions of methane and nitrous oxide from Australian sugarcane soils, Agric. For. Meteorol., 150 (6), 748-756, doi: 10.1016/j.agrformet.2009.06.018.

Desjardins R. L., 1974. A technique to measure CO2 exchange under field conditions. International Journal of Biometeorology, 18 (1), 76-83, DOI: 10.1007/BF01450667.

Desjardins, R.L., E. Pattey, W. Smith, D. Worth, B. Grant, R. Srinivasan, J. Macpherson, and M. Mauder, 2010. Multiscale estimates of N2O emissions from agricultural lands, Agric. For. Meteorol., 150 (6), 817-824, doi: 10.1016/j.agrformet.2009.09.001.

Detto, M., J. Verfaillie, F. Anderson, L. Xu, and D. Baldocchi, 2011. Comparing laser-based open- and closed-path gas analyzers to measure methane fluxes using the eddy covariance method, Agric. For. Meteorol., 15 (10), 1312-1324, doi: . 10.1016/j.agrformet.2011.05.014.

Di Marco, C., U. Skiba, K. Weston, K., Hargreaves, and D. Fowler, 2004. Field scale N2O flux measurements from grassland using eddy covariance, Water Air Soil Pollut. Focus, 4, 143-149, doi: 10.1007/s11267-005-3024-x.

Dolman A.J., Moors E.J., Elbers J.A., 2002. The carbon uptake of a mid latitude pine forest growing on sandy soil. Agricultural and Forest Meteorology, 111, 157–170.

Dueck, T.A., de Visser R., Poorter H., Persijn S., Gorissen A., de Visser W., Schapendonk A., Verhagen J., Snel J., Harren F. J. M., Ngai A. K. Y., Verstappen F., Bouwmeester H., Voesenek L. A., and van der Werf A., 2007. No evidence for substantial aerobic methane emission by terrestrial plants: a 13C-labelling approach. New Phytol., 175, 29-35, doi: 10.1111/j.1469-8137.2007.02103.x.

Edwards, G. C., H. H. Neumann, G. Den Hartog, G. W. Thurtell, and G. Kidd, 1994. Eddy correlation measurements of methane fluxes using a tunable diode laser at the Kinosheo Lake tower site during the Northern Wetlands Study (NOWES), J. Geophys. Res., 99 (D1), 1511-1517, doi: 10.1029/93JD02368.

Edwards, G. C., G. M. Dias, G. W. Thurtell, G. E. Kidd, N. T. Roulet, C. A. Kelly, J. W. M. Rudd, A. Moore, and L. Halfpenny-Mitchell, 2001. Methane Fluxes from a Wetland using the Flux-Gradient Technique The Measurement of Methane Flux from a Natural Wetland Pond and Adjacent Vegetated Wetlands using a TDL-Based Flux-Gradient Technique, Water Air Soil Pollut. Focus, 1 (5-6), 447-454, doi: 10.1023/A:1013110112173.

Edwards G.C. , G.W. Thurtell, G.E. Kidd, G.M. Dias, C. Wagner-Riddle, 2003. A diode laser based gas monitor suitable for measurement of trace gas exchange using micrometeorological techniques. Agricultural and Forest Meteorology, 115, 71–89.

Ehhalt, D., M. Prather, F. Dentener, R. Derwent, E. Dlugokencky, E. Holland, I. Isaksen, J. Katima, V. Kirchhoff, P. Matson, P. Midgley, and M. Wang, 2001. Atmospheric Chemistry and Greenhouse Gases, in Climate Change 2001: The Scientific Basis, Third Assessment Report of the Intergovernmental Panel on Climate Change, edited by F. Joos and M. McFarlan, Cambridge University Press, Cambridge, United Kingdom and New York, NY, USA.

Eugster, W., K. Zeyer, M. Zeeman, P. Michna, A. Zingg, N. Buchmann, and L. Emmenegger,, 2007a) Methodical study of nitrous oxide eddy covariance measurements using quantum cascade laser spectrometery over a Swiss forest, Biogeosciences, 4, 927-939, doi: 10.5194/bg-4-927-2007.

Eugster, W., K. Zeyer, M. Zeeman, P. Michna, A. Zingg, N. Buchmann, and L. Emmenegger, 2007b. Nitrous oxide net exchange in a beech dominated mixed forest in Switzerland measured with a quantum cascade laser spectrometer, Biogeosciences Discuss., 4 (2), 1167-1200, doi:10.5194/bgd-4-1167-2007.

Eugster, W. and P. Pluss, 2010. A fault-tolerant eddy covariance system for measuring CH4 fluxes, Agric. For. Meteorol., 150 (6), 841-851, doi: 10.1016/j.agrformet.2009.12.008.

Famulari, D., E. Nemitz, C. Di Marco, G. J. Phillips, R. Thomas, E. House, and D. Fowler, 2009. Eddy-covariance measurements of nitrous oxide fluxes above a city, Agric. For. Meteorol., 150 (6), 786-793, doi: 10.1016/j.agrformet.2009.08.003.

Fan S.M., Wofsy S. C., Bakwin P. S., Jacob D. J., Fitzjarrald D. R., 1990. Atmosphere-Biosphere Exchange of CO2 and O3 in the Central Amazon Forest. J. Geophys. Res., 95(D10), 16851–16864, doi:10.1029/JD095iD10p16851

Fan, S.M., S.C. Wofsy, P. S. Bakwin, and D. J. Jacob, 1992. Micrometeorological measurements of CH4 and CO2 exchange between the atmosphere and subartic tundra, J. Geophys. Res. Atmos., 97 (D15), 16627–16643.

Ferretti1 D. F. , Miller J. B., White J. W. C., Lassey K. R., Lowe D. C. and D. M. Etheridge, 2007. Stable isotopes provide revised global limits of aerobic methane emissions from plants. Atmos. Chem. Phys., 7, 237–241.

Finnigan J., 2000. Turbulence in plant canopies. Annu. Rev. Fluid Mech, 32, 519–571.

Finnigan J., 2006. The storage term in eddy flux calculations. Agricultural and Forest Meteorology 136, 108–113.

Flechard, C. R., P. Ambus, U. Skiba, R. M. Rees, A. Hensen, A. Van Amstel, A. Van Den Pol-van Dasselaar, J. F. Soussana, M. Jones, J. Clifton-Brown, A. Raschi, L. Horvath, A. Neftel, M. Jocher, C. Ammann, J. Leifeld, J. Fuhrer, P. Calanca, E. Thalman, K. Pilegraard, C. Di Marco, C. Campbell, E. Nemitz, K. J. Hargreaves, P. D. Levy, B. C. Ball, S. K. Jones, W. C. M. Van De Bulk, T. Groot, M. Blom, R. Dominguez, G. Kasper, V. Allard, E. Ceschia, P. Laville, P. Cellier, C. Henault, F. Bizouard, M. Abdalla, M. Williams, S. Baronti, F. Berretti, and B. Grosz, 2007. Effects of climate and management intensity on nitrous oxide emissions in grassland systems across Europe, Agric. Ecosyst. Environ., 121 (1-2), 135-152, doi: 10.1016/j.agee.2006.12.024.

Foken, T., 2008: Micrometeorology. Springer-Verlag, Berlin Heidelberg, Germany.

Foken T., G. Skeib, S. H. Richter, 1991. Dependence of the integral turbulence characteristics on the stability of stratification and their use for Doppler-Sodar measurements. Z. Meteorol., 41, 311-315.

Foken T., Wichura B., 1995. Tools for quality assesment of surface-based flux measurements. Agricultural and Forest Meteorology, 78, 83-105.

Forster, P., V. Ramaswamy, P. Artaxo, T. Berntsen, R. Betts, D.W. Fahey, J. Haywood, J. Lean, D.C. Lowe, G. Myhre, J. Nganga, R. Prinn, G. Raga, M. Schulz and R. Van Dorland, 2007. Changes in Atmospheric Constituents and in Radiative Forcing, in Climate Change 2007: The Physical Science Basis, Contribution of Working Group I to the Fourth Assessment Report of the Intergovernmental Panel on Climate Change edited by S. Solomon, D. Qin, M. Manning, Z. Chen, M. Marquis, K.B. Averyt, M.Tignor, H.L. Miller, Cambridge University Press, Cambridge, United Kingdom and New York, NY, USA.

Fowler, D., K. Hargreaves, U. Skiba, R. Milne, M. S. Zahniser, J. B. Moncrieff, I. J., Beverland, and M. W. Gallagher, 1995. Measurements of CH4 and N2O fluxes at hte landscape scale using micrometeorological methods, Philos. Trans. R. Soc., A, 351 (1696), 339-355, doi: 10.1098/rsta.1995.0038.

Fowler, D., K. Pilegaard, M. A. Sutton, P. Ambus, M. Raivonen, J. Duyzer, D. Simpson, H. Fagerli, S. Fuzzi, J. K. Schjoerring, C. Grainer, A. Neftel, I. S. A. Isaksen, P. Laj, M. Maione, P. S. Monks, J. Burkhardt, U. Daemmgen, J. Neirynck, E. Personne, R. Wichink-Kruit, K. Butterbach-Bahl, C. Flechard, J. P. Tuovinen, M. Coyle, G. Gerosa, B. Loubet, N. Altimir, L. Gruenhage, C. Ammann, S. Cieslik, E. Paoletti, T. N. Mikkelsen, H. Ro-Poulsen, P. Cellier, J. N. Cape, L. Horvath, F. Loreto, U. Niinemets, P. I. Palmer, J. Rinne, P. Misztal, E. Nemitz, D. Nilsson, S. Pryor, M. W. Gallagher, T. Vesala, U. Skiba, N. Brueggemann, S. Zechmeister-Boltenstern, J. Williams, C. O'Dowd, M. C. Facchini, G. De Leeuw, A. Flossman, N. Chaumerliac, and J. W. Erisman,, 2009. Atmospheric composition change: Ecosystems-Atmosphere interactions, Atmos. Environ., 43 (33), 5193-5267, doi: 10.1016/j.atmosenv.2009.07.068.

Frankenberg C., Meirink J. F., Van Weels M., Platt U., and Wagner, T., 2005. Assessing methane emissions from global space-borne observations. Science, 308, 1010–1014, doi:10.1126/science.1106,644.

Friborg, T., T. R. Christensen, and H. Soegaard, 1997. Rapid response of greenhouse gas emission to early spring thaw in a subarctic mire as shown by micrometeorological techniques, Geophys. Res. Lett., 24 (23), 3061-3064, doi: 10.1029/97GL03024.

Friborg, T., H. Soegaard, T. R. Christensen, C. R. Lloyd, and N. R. Panikov, 2003. Siberian wetlands: Where a sink is a source, Geophys. Res. Lett., 30 (21), 1999-2002, doi:10.1029/2003GL017797.

Galle, B., L. Klemedtsson, and D. Griffith, 1994. Application of a Fourier transform IR system for measurements of N2O fluxes using micrometeorological methods, an ultralarge chamber system, and conventional field chambers, J. Geophys. Res., 99 (D8), 16575-16583, doi: 10.1029/94JD00264.

Ganzeveld, L., L. Changsheng, L. Càrdens, J. Hawkins, and G. Kirkman, 2004. Nitrogen emission from soil, in Emission of atmospheric trace compounds, edited by L. Grainer, P. Artaxo, C. E. Reeves, pp 711-225, Kluwer Academic Publisher, Dordrecht, The Netherlands.

Gauci, V., D. J. Gowing, E. R. Hornibrook, J. M. Davis, and N. B. Dise, 2010. Woody stem methane emission in mature wetland alder trees, Atmos. Environ., 44 (17), 2157-2160, doi: 10.1016/j.atmosenv.2010.02.034.

Goulden M., Munger J., Fan M., Daube B., Wofsy S., 1996. Measurements of carbon sequestration by long-term eddy covariance: methods and a critical evaluation of accuracy. Global Change Biology, 2, 169-182.

Grace J., Malhi Y., LLoyd J., McIntyre J., Miranda A., Meir P., Miranda H. S., 1996. The use of eddy covariance to infer the net carbon dioxide uptake of Brazilian rain forest. Global Change Biology, 2, 209-217.

Grant, R.F. and E. Pattey, 1999. Mathematical modeling of nitrous oxide emissions from an agricultural field during spring thaw, Global Biogeochem. Cy., 13 (2), 679-694, doi: 10.1029/1998GB900018.

Grant, R. F. and E. Pattey, 2003. Modelling variability in N2O emissions from fertilized agricultural ?elds, Soil Biol. Biochem., 35, 225–243, doi: http://dx.doi.org/10.1016/S0038-0717(02)00256-0.

Greco S. and Baldocchi, D., 1996. Seasonal variations of CO2 and water vapour exchange rates over a temperate deciduous forest. Global Change Biology, 2, 183-197.

Griffith, D. W. T. and B. Galle, 2000. Flux measurements of NH3, N2O and CO2 using dual beam FTIR spectroscopy and the flux–gradient technique, Atmos. Environ. 34, 1087-1098, doi: 10.1016/S1352-2310(99)00368-4.

Griffith, D. W. T., R. Leuning, O. T. Denmead, and I. M. Jamie, 2002. Air–land exchanges of CO2, CH4 and N2O measured by FTIR spectrometry and micrometeorological technique, Atmos. Environ., 36, 1833-1842.

Gu L., Falge E.M., Boden T.A., Baldocchi D.D., Black A.T., Saleska S.R., Suni T., Verma S.B., Vesala T., Wofsy S.E., Xu L., 2005. Objective threshold determination for nighttime eddy flux filtering. Agricultural and Forest Meteorology, 128, 179-197.

Gu L., Massman W. J., Leuning R., Pallardy S. G., Meyerse T., Hanson P. J., Riggs J. S., Hosman K. P., Yang B., 2012. The fundamental equation of eddy covariance and its application in flux measurements. Agricultural and Forest Meteorology, 152, 135– 148.

Haapanala, S., J. Rinne, K. Pystynen, H. Héllen, H. Hakola, and T. Riutta, 2006. Measurements of hydrocarbon emissions from a boreal fen using the REA technique, Biogeosciences, 3, 103-112, doi: 10.5194/bg-3-103-2006.

Hargreaves, K.J., U. Skiba, D. Fowler, J. Arah, F. G. Wienhold, L. Klemedtsson, and B. Galle, 1994. Measurement of nitrous oxide emission from fertilized grassland using micrometeorological techniques, J. Geophys. Res., 99 (D8), 16569–16574, doi: 10.1029/94JD00269.

Hargreaves, K. J., F. G. Wienhold, L. Klemedtsson, J. R. M. Arah, I. J. Beverland, D. Fowler, B. Galle, D. W. T. Griffith, U. Skiba, K. A. Smith, M. Welling, and G. W. Harris, 1996. Measurement of nitrous oxide emission from agricultural land using micrometeorological methods, Atmos. Environ., 30 (10-11), 1563-1571, doi: 10.1016/1352-2310(95)00468-8.

Hargreaves, K.J., and D. Fowler, 1998. Quantifying the effect of water table and soil temperature on the emission of methane from peat wetland at the field scale, Atmos. Environ., 32 (19), 3275-3282, doi: 10.1016/S1352-2310(98)00082-X.

Hargreaves, K.J., D. Fowler, C. E. R. Pitcairn, and M. Aurela, 2001. Annual methane emission from Finnish mires estimated from eddy covariance campaign measurements, Theor. Appl. Climatol., 70, 203-213, doi: 10.1007/s007040170015.

Haslwanter A., Hammerle A., Wohlfahrt G., 2009. Open-path vs. closed-path eddy covariance measurements of the net ecosystem carbon dioxide and water vapour exchange: A long-term perspective. Agricultural and Forest Meteorology 149 (2) 291–302.

Hendriks, D. M., J. van Huissteden, A. J. Dolman, and M. van der Molen, 2007. The full greenhouse gas balance of an abandoned peat meadow, Biogeosciences, 4, 411-424, doi: 10.5194/bg-4-411-2007.

Hendriks, D. M., A. J. Dolman, M. van der Molen, and J. van Huissteden, 2008. A compact and stable eddy covariance set-up for methane measurements using off-axis integrated cavity output spectroscopy, Atmos. Chem. Phys., 8, 431-443, doi: 10.5194/acp-8-431-2008.

Hendriks, D. M., J. van Huissteden, and A. J. Dolman, 2010. Multi-technique assessment of spatial and temporal variability of methane fluxes in a peat meadow, Agric. For. Meteorol., 150 (6), 757-774, doi: 10.1016/j.agrformet.2009.06.017.

Herbst, M., T. Friborg, R. Ringgaard, and H. Soegaard, 2011. Interpreting the variations in atmospheric methane fluxes observed above a restored wetland, Agric. For. Meteorol., 151 (7), 841–853, doi: 10.1016/j.agrformet.2011.02.002.

Horst, T.W., 1997. A simple formula for attenuation of eddy fluxes measured with first-order response scalar sensors. Boundary-Layer Meteorology 82,219-233

Hovde, D. C., A. C. Stanton, T. Meyers, and D. R. Matt, 1995. Methane Emissions from a Landfill Measured by Eddy Correlation Using a Fast Response Diode Laser Sensor, J. Atmos. Chem., 20, 141-162, doi: 10.1007/BF00696555.

IPCC, 2001: Climate Change 2001: The Scientific Basis. Contribution of Working Group I to the Third Assessment Report of the Intergovernmental Panel on Climate Change [Houghton, J.T., et al. (eds.)]. Cambridge University Press, Cambridge, United Kingdom and New York, NY, USA, 881 pp.

Iqbal, J., S. Lin, R. Hu, and M. Feng, 2009. Temporal variability of soil-atmospheric CO2 and CH4 fluxes from different land uses in mid-subtropical China, Atmos. Environ., 43 (37), 5865-5875, doi: 10.1016/j.atmosenv.2009.08.025.

Itoh M., Ohte N., Koba K., 2009. Methane flux characteristics in forest soils under an East Asian monsoon climate. Soil Biology & Biochemistry, 41, 388–395.

Iwata H., Malhi Y., von Randow C., 2005.. Gap-filling measurements of carbon dioxide storage in tropical rainforest canopy airspace. Agricultural and Forest Meteorology, 132, 305–314.

Janssens I. A., Kowalski A. S., Longdoz B. and Ceulemans R., 2000. Assessing forest soil CO2 efflux: an in situ comparison of four techniques. Tree Physiology, 20, (1), 23-32. doi: 10.1093/treephys/20.1.23

Judd, M., F. M Kellier,. M. J. Ulyatt, K. R Lassey, K. R Tate, D. Shalton, M. J. Harvey, and C. F. Walkers, 1999. Net methane emissions from grazing sheep, Global Change Biol., 5, 647-657, doi: 10.1046/j.1365-2486.1999.00264.x.

Kaimal J. C., Wyngaard J. C., Izumi Y., Cot'e O. R., 1972: Spectral characteristics of surface-layer turbulence. Quart. J. R. Met. Soc., 98, 563–589

Kaimal, J. C., Finnighan, J. J., 1994, Atmospheric Boundary Layer Flows. Their Structure and Measurement. Oxford University Press, New York, Oxford.

Kelliher, F.M., A. R. Reisinger, R. J. Martin, M. J. Harvey, S. J. Price, and R. R. Sherlock, 2002. Measuring nitrous oxide emission rate from grazed pasture using Fourier-transform

infrared spectroscopy in the nocturnal boundary layer, Agric. For. Meteorol., 111, 29-38, doi: 10.1016/S0168-1923(02)00007-2.

Keppler, F., J. T. G. Hamilton, M. Brass, and T. Röckmann, 2006. Methane emissions from terrestrial plants under aerobic conditions, Nature, 439 (7073), 187-191, doi: 10.1038/nature04420.

Kim, J., S. B. Verma, and D. Billesbach, 1998a. Seasonal variation in methane emission from a temperate Phragmites-dominated marsh: effect of growth stage and plant-mediated transport, Global Change Biol., 5 (4), 433-440, doi: 10.1046/j.1365-2486.1999.00237.x.

Kim, J., S. B. Verma, D. Billesbach, and R. Clement, 1998b. Diel variation in methane emission from a midlatitude prairie wetland: Significance of convective throughflow in Phragmites australis, J. Geophys. Res. Atmos., 103 (D21), 28029–28039, doi: 10.1029/98JD02441.

Kitzler, B., S. Zechmeister-Boltenstern, C. Holtermann, U. Skiba, and K. Butterbach-Bahl, 2006. Controls over N2O, NOx and CO2 ?uxes in a calcareous mountain forest soil, Biogeosciences, 3, 383-395.

Kljun N., Calanca P., Rotach M. W. and Schmid H. P., 2004. A simple parameterisation for flux footprint predictions. Boundary Layer Meteorology, 112, 503-523.

Knohl A., Schulze E., Kolle O., Buchmann N., 2003. Large carbon uptake by an unmanaged 250-year-old deciduous forest in Central Germany. Agricultural and Forest Meteorology, 118, 151–167.

Kormann R. and Meixner F. X., 2001. An analytical footprint model for nonneutral stratification. Boundary Layer Meteoroogy, 99, 207–224.

Kormann, R., H. Muller, and P. Werle, 2001. Eddy flux measurements of methane over the fen 'Murnauer Moosa' 11°11' E, 47°39' N, using a fast tunable diode laser spectrometer, Atmos. Environ., 35, 2533-2544, doi: 10.1016/S1352-2310(00)00424-6.

Kroon, P.S., A. Hensen, H. J. J. Jonker, M. S. Zahniser, W. H. van't Veen, and A. T. Vermeulen, 2007) Suitability of quantum cascade laser spectroscopy for CH4 and N2O eddy covariance ?ux measurements, Biogeosciences, 4, 715–728, doi: 10.5194/bg-4-715-2007.

Launianen S., Rinne J., Pumpanen J., Kulmala L., Kolari P., Keronen P., Siivola E., Pohja T., Hari P., Vesala T., 2005: Eddy covariance measurements of CO2 and sensible and latent heat fluxes during a fully year in aboreal pine forest trunk-space. Boreal Environment Research, 10, 569-588.

Laurila, T., J. P. Tuovinen, A. Lohila, J. Hatakka, M. Aurela, T. Thum, M. Pihlatie, J. Rinne, and T. Vesala, 2005. Measuring methane emissions from a landfill using a cost-effective micrometeorological method, Geophys. Res. Lett., 32, L19808, doi:10.1029/2005GL023462.

Laville, P., C. Jambert, P. Cellier, and R. Delmas, 1999. Nitrous oxide fluxes from a fertilised maize crop using micrometeorological and chamber methods, Agric. For. Meteorol., 96 (1-3),19-38, doi: 10.1016/S0168-1923(99)00054-4.

Le Treut, H., R. Somerville, U. Cubasch, Y. Ding, C. Mauritzen, A. Mokssit, T. Peterson and M. Prather, 2007: Historical Overview of Climate Change. In: Climate Change 2007: The Physical Science Basis. Contribution of Working Group I to the Fourth Assessment Report of the Intergovernmental Panel on Climate Change [Solomon, S., D. Qin, M. Manning, Z. Chen, M. Marquis, K.B. Averyt, M. Tignor and H.L. Miller (eds.)]. Cambridge University Press, Cambridge, United Kingdom and New York, NY, USA

Leahy, P., G. Kiely, and T. M. Scanlon, 2004. Managed grasslands: A greenhouse gas sink or source?, Geophys. Res. Lett., 31, L20507, doi:10.1029/2004GL021161.

Li, J., X. Tong, Q. Yu, Y. Dong, and C. Peng, 2008. Micrometeorological measurements of nitrous oxide exchange above a cropland, Atmos. Environ., 42, 6992–7001, doi: 10.1016/j.atmosenv.2008.04.040.

LI-COR 2010. LI-7700 Methane analyzer user manual. LI-COR Bioscience, Lincoln, NE, USA

Livesley S. J., Grover S., Hutley L. B., Jamali H., Butterbach-Bahl K., Fest B., Beringer J., K. Arndt J. S., 2011. Seasonal variation and fire effects on CH4, N2O and CO2 exchange in savanna soils of northern Australia. Agricultural and Forest Meteorology, 151, 1440–1452.

Lohila, A. T. Laurila, J.-P. Tuovinen, M. Aurela, J. Hatakka, T. Thum, M. Pihlatie, J. Rinne, and T. Vesala, 2007. Micrometeorological Measurements of Methane and Carbon Dioxide Fluxes at a Municipal Landfill, Environ. Sci. Technol., 41, 2717-2722, doi: 10.1021/es061631h.

Maggiotto, S. R. and C. Wagner-Riddle, 2001. Winter and spring thaw measurements of N2O, NO and NOx fluxes using a micrometeorological method, Water Air Soil Pollut. Focus, 1, 89-98, doi: 10.1023/A:1013174214957.

Malhi Y., 2012. The productivity, metabolism and carbon cycle of tropical forest vegetation. Journal of Ecology 2012, 100, 65–75.

Malhi Y., Nobre A. D., Grace J., Kruijt B., Pereira M.G.P., Culf A., Scott S., 1998. Carbon dioxide transfer over a Central Amazonian rain forest. Journal of Geophysical Research, 130 (D24), 31593-31612.

Mammarella, I., P. W. Werle, M. Pihlatie, W. Eugster, S. Haapanala, R. Kiese, T. Markkanen, U. Rannik, and T. Vesala, 2010. A case study of eddy covariance flux of N2O measured within forest ecosystems: quality control and flux error analysis, Biogeosciences, 7, 427-440, doi:10.5194/bg-7-427-2010.

Marchesini L. B., A. Bombelli, T. Chiti, C. Consalvo, A. Forgione, E. Grieco, F. Mazzenga, D. Papale, P. Stefani, E. Vittorini, R. Zompanti, R. Valentini, 2011. Ankasa flux tower: a new research facility for the study of the carbon cycle in a primary tropical forest in Africa. World Soil Resources Reports, 105, 13-22.

Matson, A., D. Pennock, and A. Bedard-Haughn, 2009. Methane and nitrous oxide emissions from mature forest stands in the boreal forest, Saskatchewan, Canada, Forest Ecol. Manag., 258 (7), 1073-1083, doi: 10.1016/j.foreco.2009.05.034.

McBain, M.C., J. S. Warland, R.A. McBride, and C. Wagner-Riddle, 2004. Laboratory-scale measurements of N2O and CH4 emissions from hybrid poplars (Populus deltoides x Populus nigra), Waste Manage. Res., 22 (6), 454-465.

McDermitt D., Burba G., Xu L., Anderson T., Komissarov A., Riensche B., Schedlbauer J., Starr G., Zona D., Oechel W., Oberbauer S., Hastings S., 2011. A new low-power, open-path instrument for measuring methane flux by eddy covariance. Appl Phys B, 102: 391–405. DOI 10.1007/s00340-010-4307-0.

Miyata, A., R. Leuning, O. Denmead, J. Kim, and Y. Harazono, 2000. Carbon dioxide and methane fluxes from an intermittently flooded paddy field, Agric. For. Meteorol., 102 (4), 287-303, doi: 10.1016/S0168-1923(00)00092-7.

Moncrieff J. B., Malhi Y., Leuning R., 1996. The propagation of errors in long-term measurements of land-atmosphere fluxes of carbon and water. Global Change Biology, 2, 231-240.

Moncrieff, J., J. Massheder, H. de Bruin, J. Elbers, T. Friborg, B. Heusinkveld, P. Kabat, S. Scott, H. Soegaard, and A. Verhoef, 1997a. A system to measure surface fluxes of momentum, sensible heat, water vapour and carbon dioxide, J. Hydrol., 188-189, 586-611, doi: 10.1016/S0022-1694(96)03194-0.

Moncrieff, J., R. Valentini, S. Greco, and S. Guenther, 1997b. Trace gas exchange over terrestrial ecosystems: methods and perspectives in micrometeorology, J. Exp. Bot., 48 (310), 1133-1142, doi: 10.1093/jxb/48.5.1133.

Moncrieff, J., P. G. Jarvis, and R. Valentini, 2000. Canopy fluxes, in Methods in Ecosystem Science, edited by O.E Sala et al., pp. 171-180, Springer-Verlag New York.

Moncrieff J. B., R. Clement, J. Finnigan, and T. Meyers. 2004. Averaging, detrending and filtering of eddy covariance time series, in Handbook of micrometeorology: a guide for surface flux measurements, eds. Lee, X., W. J. Massman and B. E. Law. Dordrecht: Kluwer Academic, 7-31.

Monin, A. S., and A. M. Obukhov, 1954: Basic laws of turbulent mixing in the groundlayer of the atmosphere. Trans. Geophys. Inst. Akad. Nauk USSR, 151, 163-187.

Montgomery, R. B., 1948. Vertical eddy flux of heat in the atmosphere. J. Meteor., 5, 265–274.

Montzka, S. A., E. J. Dlugokencky, and J. H. Butler, 2011. Non-CO2 greenhouse gases and climate change, Nature, 476, 43-50.

Moore C. J., 1986. Frequency response corrections for eddy correlation systems. Boundary-Layer Meteorology, 37, 17–35.

Mosier, A., J. M. Duxbury, J. R. Freney, O. Heinemeyer, and K. Minami, 1998. Assessing and mitigating N2O emissions from agricultural soils, Clim. Change, 40, 7-38, doi: 10.1023/A:1005386614431.

Mukhopadhyay, S., H. Biswas, T. De, B. Sen, S. Sen, and T. Janaa, 2002. Impact of Sundarban mangrove biosphere on the carbon dioxide and methane mixing ratios at the NE Coast of Bay of Bengal, India, Atmos. Environ., 36, 629-638, doi: 10.1016/S1352-2310(01)00521-0.

Nakai T., van der Molen M. K., Gash J. H. C., and Kodama Y., 2006. Correction of sonic anemometer angle of attack errors. Agricultural and Forest Meteorology, 136, 19-30.

Neftel, A, C. Flechard, C. Ammann, F. Conen, L. Emmenegger, and K. Zeyer, 2007. Experimental assessment of N2O background fluxes in grassland systems, Tellus Ser. B, 59 (3), 470-482, doi: 10.1111/j.1600-0889.2007.00273.x.

Neftel, A., C. Ammann, C. Fischer, C. Spirig, F. Conen, L. Emmenegger, B. Tuzson, and S. Wahlen, 2010. N2O exchange over managed grassland: Application of a quantum cascade laser spectrometer for micrometeorological flux measurement, Agric. For. Meteorol., 150 (6), 775-785, doi: 10.1016/j.agrformet.2009.07.013.

Nelson, D.D., B. McManus, S. Urbanski, S. Herndon, and M. Zahniser, 2004. High precision measurements of atmospheric nitrous oxide and methane using thermoelectrically cooled mid-infrared quantum cascade lasers and detectors, Spectrochim. Acta, Part A, 60 (14), 3325-3335.

Papale D. and Valentin R. 2003. A new assesment of European forest carbon exchanges by eddy fluxes and artificial neural network spazialization. Global Change Biology, 9, 525-535.

Papale D., M. Reichstein, M. Aubinet, E. Canfora, C. Bernhofer, W. Kutsch, B. Longdoz, S. Rambal, R. Valentini, T. Vesala, and D. Yakir, 2006. Towards a standardized processing of Net Ecosystem Exchange measured with eddy covariance technique: algorithms and uncertainty estimation. Biogeosciences, 3, 571–583.

Park, K., C. Wagner-Riddle, and R. J. Gordon, 2010. Comparing methane ?uxes from stored liquid manure using micrometeorological mass balance and floating chamber methods, Agric. For. Meteorol., 150, 175-181, doi: 10.1016/j.agrformet.2009.09.013.

Pattey, E., G. Edwards, R. Desjardins, D. Pennock, W. Smith, B. Grant, and J. MacPherson, 2007. Tools for quantifying N2O emissions from agroecosystems, Agric. For. Meteorol., 142, 103–119, doi: 10.1016/j.agrformet.2006.05.013.

Pattey, E., I. Strachan, R. Desjardins, G. Edwards, D. Dow, and J. MacPherson, 2006. Application of a tunable diode laser to the measurement of CH4 and N2O fluxes from field to landscape scale using several micrometeorological techniques, Agric. For. Meteorol., 136 (3-4), 222-236, doi: 10.1016/j.agrformet.2004.12.009.

Paw U K., Baldocchi D., Meyers T. P., Wilson K. B., 2000. Correction Of Eddy-Covariance Measurements Incorporating Both Advective Effects And Density Fluxes. Boundary-Layer Meteorology, 97 (3), 487-511.

Phillips, F., R. Leuning, R. Baigent, K. Kelly, and O. Denmead, 2007. Nitrous oxide flux measurements from an intensively managed irrigated pasture using micrometeorological techniques, Agric. For. Meteorol., 143 (1-2), 92-105, doi: 10.1016/j.agrformet.2006.11.011.

Phillips, O. L., Malhi Y., Higuchi N., Laurance W. F., Núñez P. V., Vásquez R. M., Laurance S. G., Ferreira L. V., Stern M., Brown S., Grace J., 1998. Changes in the Carbon Balance of Tropical Forests: Evidence from Long-Term Plots. Science, 282 (5388) 439-442. DOI: 10.1126/science.282.5388.439.

Pihlatie, M., P. Ambus, J. Rinne, K. Pilegaard, and T. Vesala, 2005a. Plant-mediated nitrous oxide emissions from beech (Fagus sylvatica) leaves, New Phytol., 168, 93-98, doi: 10.1111/j.1469-8137.2005.01542.x.

Pihlatie M. , Rinne J. , Ambus P. , Pilegaard K. , Dorsey J. R. , Rannik U., Markkanen T. , Launiainen S. , and Vesala T. ., 2005b. Nitrous oxide emissions from a beech forest floor measured by eddy covariance and soil enclosure techniques. Biogeosciences Discussions, 2, 581–607.

Pihlatie M. K., Kiese R., Bruggemann N., Butterbach-Bahl K., Kieloaho A.-J., Laurila T., Lohila A., Mammarella I., Minkkinen K., Penttila T., Schonborn J., and Vesala T., 2010. Greenhouse gas fluxes in a drained peatland forest during springfrost-thaw event. Biogeosciences, 7, 1715–1727.

Priemé A. and Christensen S., 1999. Methane uptake by a selection of soils in Ghana with different land use. Journal of Geophysical Research, 104 (D19), 23617–23622.

Querino C. A. S. , Smeets C. J. P. P., Vigano I., Holzinger R., Moura V., GattiL. V., Martinewski A., Manzi A. O., de Araujo A. C., and Rockmann T., 2011. Methane flux, vertical gradient and mixing ratio measurements in a tropical forest. Atmos. Chem. Phys. Discuss., 11, 5313–5350.

Ramaswamy, V., et al., 2001. Radiative forcing of climate change. In: Climate Change 2001: The Scientific Basis. Contribution of Working Group I to the Third Assessment Report of the

Intergovernmental Panel on Climate Change [Houghton, J.T., et al. (eds.)]. Cambridge University Press, Cambridge, United Kingdom and New York, NY, USA, pp. 349–416.

Reichstein M., Falge E., Baldocchi D., Papale D., Aubinet M., Berbigier P., Bernhofer C., Buchmann C., Gilmanov T., Granier A., Grunwald T., Havrankova K., Ilvesniemi H., Janous D., Knohl A., Laurila T., Lohila A., Loustau D., Matteucci G., Meyers T., Miglietta M., Ourcival J.M, Pumpanen J., Rambal S., Rotenberg E., Sanz M., Tenhunen J., Seufert G., Vaccari F., Vesala T., Yakir D., Valentini R., 2005. On the separation of net ecosystem exchange into assimilation and ecosystem respiration: review and improved algorithm. Global Change Biology, 11, 1–16, doi: 10.1111/j.1365-2486.2005.001002.x

Rinne, J., M. Pihlatie, A. Lohila, T. Thum, M. Aurela, J. Tuovinen, T. Laurila, and T. Vesala, 2005. Nitrous Oxide Emissions from a Municipal Landfill, Environ. Sci. Technol., 39, 7790-7793, doi: 10.1021/es048416q.

Rinne, J., T. Riutta, M. Pihlatie, M. Aurela, S. Haapanala, J. Tuovinen, E. Tuittila, and T. Vesala, 2007. Annual cycle of methane emission from a boreal fen measured by the eddy covariance technique, Tellus Ser B, 59 (3), 449-457, doi: 10.1111/j.1600-0889.2007.00261.x.

Roulet, N. T., P. M. Crill, N. T. Comer, A. Dove, and R. A. Boubonniere, 1997. CO2 and CH4 flux between a boreal beaver pond and the atmosphere, J Geophys. Res., 102, D4, 29313-29319, doi: 10.1029/97JD01237.

Rowe, M. D., C. W. Fairall, and J. A. Perlinger, 2010. Chemical sensor resolution requirements for near-surface measurements of turbulent ?uxes, Atmos. Chem. Phys. Discuss., 10, 24409-24433, doi: 10.5194/acp-11-5263-2011.

Rusch, H. and H. Rennenberg, 1998. Black alder (Alnus Glutinosa (L.) Gaertn.) trees mediate methane and nitrous oxide emission from the soil to the atmosphere, Plant Soil, 201, 1-7, doi: 10.1023/A:1004331521059.

Sachs, T., C. Wille, J. Boike, and L. Kutzbach, 2008. Environmental controls on ecosystem-scale CH4 emission from polygonal tundra in the Lena River Delta, Siberia, J. Geophys. Res., 113, G00A03, doi:10.1029/2007JG000505.

Scanlon, T.M. and G. Kiely, 2003. Ecosystem-scale measurements of nitrous oxide fluxes for an intensely grazed, fertilized grassland, Geophys. Res. Lett., 30 (16), 1852, doi:10.1029/2003GL017454.

Schrier-Uijl, A., P. S. Kroon, A. Hensen, P. A. Leffelaar, F. Berendse, and E. Veenendaal, 2010. Comparison of chamber and eddy covariance-based CO2 and CH4 emission estimates in a heterogeneous grass ecosystem on peat, Agric. For. Meteorol., 150 (6), 825-831, doi: 10.1016/j.agrformet.2009.11.007.

Shurpali, N. and S. Verma, 1998. Micrometeorological measurements of methane flux in a Minnesota peatland during two growing seasons, Biogeochemistry, 40 (1), 1-15.

Simon L., Lopez-Gonzalez G. , Sonké B., Affum-Baffoe K., Baker T. R., Ojo L. O., Phillips O. L., Reitsma J. M., White L., Comiskey J. A., et al., 2009. Increasing carbon storage in intact African tropical forests. Nature, 457, 1003-1006, doi:10.1038/nature07771.

Simpson, I. J., G. C. Edwards, G. W. Thurtell, G. den Hartog, H. H. Neumann, and R. M. Staebler, 1997. Micrometeorological measurements of methane and nitrous oxide exchange above a boreal aspen forest, J. Geophys. Res. 102 (D24), 29331-29341, doi: 10.1029/97JD03181.

Singh J.S., Singh S., Raghubanshi A.S., Saranath S., Kashyap A.K. and Reddy V.S., 1997. Effects of soil nitrogen, carbon and moisture on methane uptake by dry tropical forest soils. Plant and Soil, 196, 115–121

Sinha, V., J. Williams, P. J. Crutzen, and J. Lelieveld, 2007. Methane emissions from boreal and tropical forest ecosystems derived from in-situ measurements, Atmos. Chem. Phys. Discuss., 7, 14011–14039, doi: 10.5194/acpd-7-14011-2007.

Smeets C.J.P.P., Holzinger R., Vigano I., Goldstein A. H., and Rockmann T., 2009. Eddy covariance methane measurements at a Ponderosa pine plantation in California. Atmos. Chem. Phys., 9, 8365–8375.

Smeets, C., R. Holzinger, I. Vigano, A. Goldstein, and T. Röckmann, 2009. Eddy covariance methane measurements at a Ponderosa pine plantation in California, Atmos. Chem. Phys. Discuss., 9, 5201-5229, doi: 10.5194/acp-9-8365-2009.

Smith, K. A., H. Clayton, J. R. M. Arah, S. Christensen, P. Ambus, D. Fowler, K. J. Hargreaves, U. Skiba, G. W. Harris, F. G. Wienhold, L. Klemedtsson, and B. Galle, 1994. Micrometeorological and chamber methods for measurement of nitrous oxide fluxes between soils and the tmosphere: Overview and conclusions. J. Geophys. Res., 99 (D8), 16541-16548, doi: 10.1029/94JD00619.

Snyder, C., T. Bruulsema, T. Jensen, and P. Fixen, 2009. Review of greenhouse gas emissions from crop production systems and fertilizer management effects, Agric. Ecosyst. Environ., 133 (3-4), 247-266, doi: 10.1016/j.agee.2009.04.021.

Stull, R. B., 1988: An introduction to Boundary Layer Meteorology. Kluwer Academic Publishers.

Subke J. and Tenhunen J. D., 2004. Direct measurements of CO2 flux below a spruce forest canopy. Agricultural and Forest Meteorology, 126, 157–168.

Swinbank W. C., 1950. The Measurement of Vertical Transfer of Heat and Water Vapor by Eddies in the Lower Atmosphere. Journal of Atmospheric Sciences, 8 (3), 135-145.

Symonds P., 2000. Ankasa Conservation Area Management Plan. Wildlife Division Forestry Commission, Ghana.

Tan Z., Zhang Y., Yu., Sha L., Tang J., Deng X., Song Q., 2010. Carbon balance of a primary tropical seasonal rain forest. Journal of Geophysical Research 115, D00H26, doi:10.1029/2009JD012913.

Teh Y. A., Silver W. L., Conrad M. E., 2005. Oxygen effects on methane production and oxidation in humid tropical forest soils. Global Change Biology 11, 1–15.

Teh, Y. A., W. L. Silver, O. Sonnentag, M. Detto, M. Kelly, and D. D. Baldocchi, 2011. Large Greenhouse Gas Emissions from a Temperate Peatland Pasture, Ecosystems, 14, 311–325, doi: 10.1007/s10021-011-9411-4.

Tseng, K., J. Tsai, A. Alagesan, B. Tsuang, M. Yao, and P. Kuo, 2010. Determination of methane and carbon dioxide fluxes during the rice maturity period in Taiwan by combining profile and eddy covariance measurements, Agric. For. Meteorol., 150 (6), 852-859, doi: 10.1016/j.agrformet.2010.04.007.

Tuzson B., Hiller R. V., Zeyer K., Eugster W., Neftel A., Ammann C., and Emmenegger L., 2010. Field intercomparison of two optical analyzers for CH4 eddy covariance flux measurements. Atmos. Meas. Tech. Discuss., 3, 2961–2993.

Valentini R., Scarascia-Mugnozza G., De Angelis P., Bimbi R., 1991. An experimental test of the eddy correlation technique over a Mediterranean macchia canopy. Plant, Cell & Environment, 14 (9), 987–994, DOI: 10.1111/j.1365-3040.1991.tb00969.x.

van Beek, C. L, B. Meerburg, R. L. Schils, J. Verhagen, and P. J. Kuikman, 2010. Feeding the world's increasing population while limiting climate change impacts: linking N2O and CH4 emissions from agriculture to population growth, Environ. Sci. Policy,13 (2), 89-96, doi: 10.1016/j.envsci.2009.11.001.

van der Laan, S., R. E. M. Neubert, and H. A. J. Meijer, 2009. A single gas chromatograph for accurate atmospheric mixing ratio measurements of CO2, CH4, N2O, SF6 and CO, Atmos. Meas. Tech. Discuss., 2, 1321-1349, doi: 10.5194/amt-2-549-2009.

van Gorsel E., Leuning R., Cleugh H. A., Keith H., Suni T., 2007. Nocturnal carbon efflux: reconciliation of eddy covariance and chamber measurements using an alternative to the u*-threshold filtering technique. Tellus B, 59 (5), 397-403.

van Gorsel E., Delpierre N., Leuning R., Black A., Munger W., Wofsy S, et al., 2009. Estimating nocturnal ecosystem respiration from the vertical turbulent flux and change in storage of CO2. Agricultural and Forest Meteorology, 149, 1919–1930.

van Hulzen, J. B., R. Segers, P. M. van Bodegom, and P. A. Leffelaar, 1999. Temperature effects on soil methane production: an explanation for observed variability, Soil Biol. Biochem., 31, 1919-1929, doi: 10.1016/S0038-0717(99)00109-1.

Verma, S., F. Ullman, D. Billesbach, R. Clement, J. Kim, and E. Verry, 1992. Eddy correlation measurements of methane flux in a northern peatland ecosystem, Boundary Layer Meteorol., 58 (3), 289-304, doi: 10.1007/BF02033829.

Vickers D., and Mahrt L., 1997. Quality control and flux sampling problems for tower and aircraft data. Journal of Atmospheric and Oceanic Technology, 14, 512-526.

Vigano I., van Weelden H., Holzinger R., Keppler F., McLeod A., and Rckmann, T., 2008. Effect of UV radiation and temperature on the emission of methane from plant biomass and structural components. Biogeosciences, 5, 937–947.

Wagner-Riddle, C., G. Thurtell, G. Kidd, G. Edwards, and I. Simpson, 1996. Micrometeorological measurements of trace gas fluxes from agricultural and natural ecosystems, Infrared Phys. Technol., 37 (1), 51-58.

Wagner-Riddle, C. and G. W. Thurtell, 1998. Nitrous oxide emissions from agricultural fields during winter and spring thaw as affected by management practices, Nutr. Cycling Agroecosyst., 52, 151-163, doi: 10.1023/A:1009788411566.

Wagner-Riddle, C., G. W. Thurtell, G. K. Kidd, E. G. Beauchamp, and R. Sweetman, 1997. Estimates of nitrous oxide emissions from agricultural fields over 28 months, Can. J. Soil Sci., 77, 135–144, doi: 10.4141/S96-103.

Wagner-Riddle, C., K. Park, and G. Thurtell, 2006. A micrometeorological mass balance approach for greenhouse gas flux measurements from stored animal manure, Agric. For. Meteor., 136 (3-4), 175-187, doi: 10.1016/j.agrformet.2004.11.014.

Wang, Z., X. Han, G. Wang, Y. Song, and J. Gulledge, 2008. Aerobic methane emission from plants in the Inner Mongolia steppe, Environ. Sci. Technol., 42 (1), 62-68, doi: 10.1021/es071224l.

Webb E. K., Pearman G. I., Leuning R., 1980. Correction of flux measurements for density effects due to heat and water vapour transfer. Quart. J. Met. Soc., 106, 85-100. doi: 10.1002/qj.49710644707.

Werle, P., 1999. Eddy correlation measurements of methane fluxes from Italian rice-paddy fields, Proc. SPIE, 3758 (41), doi: 10.1117/12.366467.

Werle, P. and R. Kormann, 2001. Fast chemical sensor for eddy-correlation measurements of methane emissions from rice paddy fields, Appl. Opt., 40 (6), 846-858.

Wesely M. L. , Cook D. R., Hart R. L., 1983. Fluxes of gases and particles above a deciduous forest in wintertime. Boundary-Layer Meteorology, 27 (3), 237-255, DOI: 10.1007/BF00125000

Wienhold, F. G., H. Frahm, and G. W. Harris, 1994. Measurements of N2O fluxes from fertilized grassland using a fast response tunable diode laser spectrometer, J. Geophys. Res. 99 (D8), 16557-16567, doi: 10.1029/93JD03279.

Wienhold, F. G., M. Welling, and G. W. Harris, 1995. Micrometeorological measurement and source region analysis of nitrous oxide fluxes from an agricultural soil, Atmos. Environ. 29 (17), 2219-2227, doi: 10.1016/1352-2310(95)00165-U.

Wilczak J. M., Oncley S. P., and Stage S. A., 2001. Sonic anemometer tilt correction algorithms. Boundary Layer Meteorology, 99, 127-150.

Wille, C., I. Forbrich, and L. Kutzbach, 2008a. Intercomparison of measurement performance - Campbell Sci. TGA 100A and Los Gatos RMT 200, Poster presented at the Workshop on Eddy Covariance Flux Measurements of CH4 and N2O Exchanges, Hyytiälä, Finland.

Wille, C., L. Kutzbach, T. Sachs, D. Wagner, and E. M. Pfeifer, 2008b. Methane emission from Siberian arctic polygonal tundra: eddy covariance measurements and modeling, Global Change Biol., 14, 1395-1408, doi: 10.1111/j.1365-2486.2008.01586.x. Aubinet M. , Chermanneb B., Vandenhaute M., Longdoz B., Yernaux M., Laitat E., 2001. Long term carbon dioxide exchange above a mixed forest in the Belgian Ardennes. Agricultural and Forest Meteorology, 108, 293–315.

Appendix A

Tables reporting the scientific papers cited and analysed in Chap. 2.

Table A1. Geographical localization and climatic characteristics of reported works.

	reference	ref. ID	region	site name	coordinates			climate parameters	
					lat	long	alt (m)	Air T (°C)	P (mm)
Forests	Bowling et al., 2009	1	Colorado	Niwot Ridge	43°18' N	105°33' W	3050	1.5_{AM}	800_{AM}
	Mammarella et al., 2010 - 1 [α]	2 [α]	Finland	Kalevansuo	60° 39' N	24° 22' E	---	4.3_{AM}	606_{PT}
	Philatie, et al., 2010 [α]	3 [α]							
	Smeets et al., 2009	4	California	Berkeley's Blodgett Forest	38°90' N	120°63'W	1315	$0/27_{AM}$	1290_{AM}
	Pattey et al., 2006 - 1	5 - 1	Canada	Whiteswan lake	53°59'16.8''N	105°07'4.8'' W	---	---	---
	Sinha et al., 2007 - 1	6 - 1	Finland	Hyytiäla	61°51' N	24°17' E	170	$-5/11_{PM}$	---
	Mammarella et al., 2010 - 2 [β]	7 [β]	Denmark	Lille Bøgeskov, Sorø	55° 29' N	11° 38' E	---	8_{AM}	650_{PT}
	Pihlatie et al., 2005 [β]	8 [β]							
	Simpson et al., 1997	9	Canada	Pr. Albert N.P., Saskatchewan	53°37' N	106°12' W	---	-0.2_{AM}	462.2_{AM}
	Eugster et al., 2007a,b	10	Switzerland	Lägeren	47°28'40.8''N	8°21'55.2'' E	682	---	18.3_{PM}
	Carmo et al., 2006 - 1	11 - 1	Brazil	Caxiuanã Nat. Forest, Melgaço	01°43'05'' S	51°27'36'' W	---	---	2060_{AM}
	Carmo et al., 2006 - 2	11 - 2	Brazil	Manaus, Cuieiras Res.	02°36'32'' S	60°01'16'' W	---	---	2250_{AM}
	Carmo et al., 2006 - 3	11 - 3	Brazil	Sinop	11°24'47'' S	55°19'30'' W	---	---	2037_{AM}
	Querino et al., 2011	12	Brazil	Manaus	2°36′ 32.7″ S	60°12′ 33.5″W	130	---	2400_{AM}
	Sinha et al., 2007 - 2	6 - 2	Suriname	Brownsberg	04°56' N	55°10' W	512	$20/32_{PM}$	---
Wetlands	Haapanala et al., 2006	13	Finland	Siikaneva	61°48' N	24°09' E	160	$-8/16_{AM}$	700_{AM}
	Rinne et al., 2007	14	Finland	Siikaneva, Ruovesi	61°50'	24°12' E	---	3.3_{AM}	713_{AM}
	Kormann et al., 2001	15	Germany	Murnauer Moos	47°39' N	11°11' E	622	5.3_{AM}	1096_{AT}
	Mukhophadhya et al., 2002 - 1	16 - 1	India	Sagar Island, Sundarban	21°32' N	88°05' E	---	29.4_{AM}	---
	Mukhophadhya et al., 2002 - 2	16 - 2	India	Lothian Island, Sundarban	21°32' N	88°05' E	---	29.4_{AM}	---
	Beswick et al., 1998	17	Finland	Jänkäjärvi, Kaamanen	---	---	---	---	---
	Edwards et al., 2001 - 1,2	18 - 1,2	Canada	Lake 979, Exp. Area, Ontario	49°40' N	93°44' W	---	---	---
	Friborg et al., 1997	19	Sweden	Stordalen Mire, Abisko	68° 21' N	19° 02' E	360	---	---
	Hargreaves et al., 2001	20	Finland	Kaamanen, Finnish Lapland	69°08' N	27°16' E	155	---	---
	Hendriks et al., 2008	21	Netherlands	Horstermeer	52°11'44'' N	05°44'33'' E	-2	9.8_{AM}	779_{AM}
	Beverland et al., 1996a - 1	22 - 1	Scotland	Strathy Bog, Sutherland	---	---	---	---	---
	Beverland et al., 1996a - 2	22 - 2	Scotland	Loch More, Caithness	---	---	---	---	---
	Beverland et al., 1996b - 1	23 - 1	Scotland	Loch More, Caithness	---	---	---	---	---
	Edwards et al., 1994	24	Canada	Kinosheo Lake, Ontario	51°33' N	81°49.5' W	---	17.2_{PM}	30.4_{PT}
	Friborg et al., 2003	25	Siberia	Bakchar Bog, Plotnikovo	56° 51' N	82° 58' E	---	$4.5/26.7_{PM}$	105_{PT}
	Hargreaves and Fowler, 1998	26	Scotland	Loch More, Caithness	58°30' N	---	---	$7/11_{PM}$	---
	Roulet et al., 1997	27	Canada	Thompson, Manitoba	55°55' N	98°01' W	---	---	---

Table A1. Continue.

	reference	ref. ID	region	site name	coordinates			climate parameters	
					lat	long	alt (m)	Air T (°C)	P (mm)
Wetlands	Shurpali and Verma, 1998 - 1,2	28 - 1,2	Minnesota	Bog Lake, Chippewa Nat. For.	47°32' N	92° 28' W	---	13.6_{PM}	553_{PM}
	Verma et al., 1992	29	Minnesota	Bog Lake, Chippewa Nat. For.	47°32' N	93° 28' W	416	3_{AM}	770_{AM}
	Detto et al., 2011 - 1,2	30 - 1,2	California	Sherman Island	38°3' N	121°43' W	---	---	---
	Teh et al., 2011	83	California	Sherman Island	38°3' N	121°43' W	---	15.6_{AM}	325_{AM}
	Kim et al., 1998a	31	Nebraska	Ballards Marsh, Valentine	42° 52' N	100° 33' W	788	$2/26_{AM}$	270
	Kim et al., 1998b	32	Nebraska	Ballards Marsh, Valentine	42° 52' N	100° 33' W	788	$2/26_{AM}$	270
	Fan et al., 1992	33	Alaska	Yukon-Kuskokwim River	61°05.41'N	162°00.92' W	---	---	---
	Sachs et al., 2008	34	Siberia	Lena River Delta, Samoylov Is.	72°22' N	126°30' E	2	-14.7_{AM}	137_{AM}
	Wille et al., 2008	35	Siberia	Lena River Delta, Samoylov Is.	72°22' N	126°30' E	---	-14.7_{AM}	137_{AM}
	Detto et al., 2011 - 3,4	30 - 3,4	California	Twitchell Island	38°6' N	121°38' W	---	---	---
	Miyata et al., 2000	36	Japan	Hachihama farm, Okayama	34°32' N	133°56' E	2	$23/32_{PM}$	---
	Werle, 1999 [γ]	37 [γ]	Italy	Ist. Sup. Risicoltura, Vercelli	---	---	---	---	---
	Werle and Kormann, 2001 [γ]	38 [γ]							
	Tseng et al., 2010	39	Taiwan	Caotun	23°58'13.3"N	120°39'27.2"E	100	---	---
	Detto et al., 2011 - 5,6	30 - 5,6	California	Twitchell Island	38°6' N	121°38' W	---	---	---
	Herbst et al., 2011	40	Denmark	Skjern Meadows	55°54'46'' N	8°24'17" E	2	7.5_{AM}	781_{AM}
Managed lands	Christensen et al., 1996 [δ]	41 [δ]	Denmark	Lammefjorden, Sealand Is.	---	---	2	---	---
	Griffith & Galle, 2000 [δ]	42 [δ]							
	Hargreaves et al., 1996 [δ]	43 [δ]							
	Wienhold et al., 1995 [δ]	44 [δ]							
	Beverland et al., 1996b - 2	23 - 2	Scotland	Howmuir Farm	---	---	---	---	---
	Denmead et al., 2010	45	Australia	New South Wales	---	---	---	28.8_{PM}	1879_{PT}
	Desjardins et al., 2010 - 1	46 - 1	Canada	Greenbelt, Ottawa	---	---	---	---	---
	Desjardins et al., 2010 - 2	46 - 2	Canada	Casselman/Morewood, Ontario	---	---	---	---	---
	Grant and Pattey, 1999	47	Canada	Greenbelt, Ottawa	45°18' N	75°44' W	---	---	---
	Grant and Pattey, 2003 [ε]	48 [ε]	Canada	Greenbelt, Ottawa	45°18' N	75°44' W	---	---	155_{PT}
	Pattey et al., 2006 - 2 [ε]	5 - 2 [ε]							
	Laville et al., 1999	49	France	Bordeaux	45°45' N	0°45' W	60	20.0_{PM}	---
	Li et al., 2008 - 1	50 - 1	China	Luancheng Agro-ecosystem	37°53' N	114°41' E	50	---	---
	Li et al., 2008 - 2	50 - 2	China	Luancheng Agro-ecosystem	37°53' N	114°41' E	50	---	---
	Maggiotto & Wagner-Riddle, 2001 - 1-4	51 -1-4	Canada	Guelph Turfgrass Institute	43° N	80° W	346	---	---
	Pattey et al., 2007 - 1	52 - 1	Canada	Ottawa, Ontario	45°18' N	75°44' W	---	---	---

Table A1. Continue.

	reference	ref. ID	region	site name	coordinates			climate parameters	
					lat	long	alt (m)	Air T (°C)	P (mm)
	Pattey et al., 2007 - 2	52 - 2	Canada	Laird & Melfort, Saskatchewan	52°43' N	106°30' W	---	-2.0_{PM}	---
	Wagner-Riddle et al., 1997	53	Canada	Elora Res. St.	43°49' N	80°35' W	---	$-8.2/19_{AM}$	---
Managed lands	Wagner-Riddle & Thurtell, 1998 - 1	54 - 1	Canada	Elora Res. St.	43°49' N	80°35' W	---	---	---
	Wagner-Riddle & Thurtell, 1998 - 2	54 - 2	Canada	Arkell Res. St.	43°30' N	80°15' W	---	---	---
	Arah, et al., 1994 $^{\zeta}$	55 $^{\zeta}$	Scotland	Stirling	---	---	---	---	3.6_{PT}
	Galle et al., 1994 $^{\zeta}$	56 $^{\zeta}$							
	Hargreaves, et al., 1994 $^{\zeta}$	57 $^{\zeta}$							
	Smith et al.,1994 $^{\zeta}$	58 $^{\zeta}$							
	Wienhold et al., 1994 $^{\zeta}$	59 $^{\zeta}$							
	Di Marco et al., 2004 $^{\eta}$	60 $^{\eta}$	Scotland	Easter Bush	55°52' N	03°02' W	190	8.8_{AM}	638_{AM}
	Flechard et al., 2007 $^{\eta}$	61 $^{\eta}$							
	Kroon et al., 2007 $^{\theta}$	62 $^{\theta}$	Netherlands	Oukoop, Reeuwijk	52°01'15'' N	4°01'17'' W	-2	17_{PM}	870_{AM}
	Schrier-Uijl et al., 2010 $^{\theta}$	63 $^{\theta}$							
	Leahy et al., 2004	64	Ireland	Co. Cork	52°08'24'' N	8°39'36" W	180	$5.5/14.3_{AM}$	1210_{AT}
	Neftel et al., 2007	65	Switzerland	Oensingen	47°17' N	07°44' E	450	9_{AM}	1200_{AM}
	Neftel et al., 2010	66	Switzerland	Oensingen	47°17' N	07°44' E	450	9_{AM}	1200_{AM}
	Scanlon and Kiely, 2003	67	Ireland	Donoughmore, Co. Cork	---	---	---	---	1470_{AM}
	Wagner-Riddle et al., 1996 - 1	68 - 1	Canada	Elora Res. St.	43°49' N	80°35' W	---	---	---
	Wagner-Riddle et al., 1996 - 2	68 - 2	Canada	Elora Res. St.	43°49' N	80°35' W	---	---	---
	Dengel et al., 2011	69	UK	Easter Bush	55°51'55.2''N	3°12'22.4'' W	190	---	---
	Denmead et al., 2000	70	Australia	Wagga Wagga	35°03" S	147°22' E	---	$9.5/21.6_{AM}$	538_{AM}
	Griffith et al., 2002	71	Australia	Wagga Wagga	35°04' S	147°21' E	219	---	434
	Judd et al., 1999	72	NewZealand	Aorangi Farm	40°21' S	175°29' E	15	16.4PM	6_{PM}
	Kelliher et al., 2002	73	NewZealand	Hollymount Farm, Springston	43°24' S	172°18' E	112	---	---
	Phillips et al., 2007 - 1,2	74 - 1,2	Australia	Kyabram	36°20' S	145°04' E	---	$3/30_{AM}$	350500_{AM}
Anthr env.	Park et al., 2009	75	Canada	Arkell Univ. Guelph, Ontario	43°33' N	80°25' W		---	---
	Wagner-Riddle et al., 2006 - 1	76 - 1	Canada	Jarvis, Ontario	42°58' N	80°04' W		---	---
	Wagner-Riddle et al., 2006 - 2	76 - 2	Canada	Arkell Univ. Guelph, Ontario	43°33' N	80°25' W		---	---
	Eugster and Pluss, 2010	77	Switzerland	Lindestock, Liestal	47°29'41'' N	07°45'04'' E		570	---
	Hovde et al., 1995	78	Tennessee	Oak Ridge	---	---		---	---
	Laurila et al., 2005	79	Finland	Ämmässuo, Helsinki	60°13' N	24°36' E		---	---

Table A1. Continue.

	reference	ref ID.	region	site name	coordinates			climate parameters	
					lat	long	alt (m)	Air T (°C)	P (mm)
Anthr	Lohila et al., 2007	80	Finland	Ämmässuo, Helsinki	60°13' N	24°36' E		---	---
	Rinne et al., 2005	81	Finland	Ämmässuo, Helsinki	60°13' N	24°36' E		---	---
	Famulari et al., 2010	82	Scotland	Edinburgh	55°57'17'' N	3°10'52" W	102	---	800_{AM}

References with the same Greek letter refer to the same work. Climate acronyms are AM: annual mean; AT: annual total; PM: period mean; PT: period total.

Table A2. Main ecological sites characteristics.

	ref. ID	soil characteristics				manag.[1]	fertilization[2]	main species
		type or typology	pH	C/N	SWC		(kgN ha^{-1})	
Forests	1	---	---	---	---	---	---	*Pinus contorta, Picea engelmannii, Abies lasiocarpa*
	2 [α]	ombrotrophic	5	41-45	flooded			*Pinus sylvestris L., Sphagnum, Betula pubescens*
	3 [α]							
	4	60% sand, 29% loam	5.5	4	---	3	---	*Pinus ponderosa*
	5 - 1	---	---	---	---	---	---	*Picea mariana*
	6 - 1	---	---	---	---	---	---	*Picea abies, Pinus sylvestris, Populus* sp.
	7 [β]	Alfisol/Mollisol	4-5	10-20	---	---	---	*Fagus sylvatica*
	8 [β]							
	9	Orthic Gray Aluvisol	---	---	---	---	---	*Populus tremuloides, Populus balsamifera*
	10	---	---	---	---	---	---	*Fagus sylvatica*
	11 - 1	---	---	---	---	---	---	---
	11 - 2	---	---	---	---	---	---	---
	11 - 3	---	---	---	---	---	---	---
	12	---	---	---	---	---	---	---
	6 - 2	---	---	---	---	---	---	Rainforest, lowland mixed spp.
Wetlands	13	minerotrophic	---	---	---	---	---	*Sphagnum* spp., *Andromeda polifolia*
	14	oligotrophic	---	---	---	---	---	*Sphagnum* spp., *Carex* spp.
	15	gravel and limestone	5.5	---	56-67	---	---	*Primula arinose, Schoenus ferrugineus*
	16 - 1,2	---	---	---	---	---	---	*Avicenia* spp.
	17	pools and hummoks	---	---	---	---	---	Mosses, lichens and sedges
	18 - 1,2	---	---	---	---	---	---	*Sphagnum spp., Picea mariana*
	19	ombrotrophic/minerotrophic	4	---	---	---	---	*Betula* sp., *Dicranum* spp., *Eriophorum* sp.
	20	pools and carpets	---	---	---	---	---	*Carex* spp., *Eriophorum angustifolium, Betula nana*
	21	Eutric Histosol	6.9	15.5	---	0	---	*Phragmites australis, Holcus lanatus, Agrostis* sp.
	22 - 1	ombrotrophic bog	---	---	---	---	---	*Calluna vulgaris, Sphagnum* spp. *Erica* spp.
	22 - 2	ombrotrophic bog	---	---	---	---	---	*Calluna vulgaris, Sphagnum* spp. *Erica* spp.
	23 - 1	ombrotrophic bog	---	---	---	---	---	*Calluna vulgaris, Sphagnum* spp. *Erica* spp.
	24	bog	---	---	---	---	---	*Picea mariana, Scripus caspitosus, Carex limosa*
	25	---	---	---	---	---	---	*Menynantes* sp., *Eriphorum* sp., *Sphagnum* spp.
	26	---	---	---	---	---	---	---
	27	pond area	---	---	---	---	---	*Carex aquatilis, Utricularia* spp.
	28 - 1,2	Dysic Typic Borohemist	4.6	---	---	---	---	*Sphagnum papillosum, Scheuchzeria* sp.

Table A2. Continue.

	ref. ID	soil characteristics				manag.[1]	fertilization[2]	main species
		type or typology	pH	C/N	SWC		(kgN ha^{-1})	
Wetlands	29	oligotrophic organic soil	4.6	---	---	---	---	*Sphagnum* spp., *Scheuchzeria* sp., *Carex* spp.
	30 - 1,2	oxidized peat (20–40 cm)	---	---	---	2	---	*Lepidium latifolium L.*
	83	Cumulic Endoaquolls	---	---	---	2	---	*Lepidium latifolium, Hordenum murinum*
	31, 32	---	7.2	---	---	---	---	*Phragmites australis, Scirpus acutus, Zizania* sp.
	33	---	---	---	---	---	---	---
	34	Historthels, Aquiturbels	---	---	<100	---	---	*Carex spp., Drepanocladus revolvens, Dryas* sp.
	35	Historthels, Aquiturbels	---	---	<100	---	---	*Carex spp., Limprichtia revolvens, Dryas octopetala*
	30 - 3,4	---	---	---	---	---	---	*Oryza* sp.
	36	>60% clay	---	---	---	2	77	*Oryza sativa*
	37 [γ]	---	---	---	---	2	---	*Oryza sativa*
	38 [γ]							
	39	---	---	---	---	2	---	*Oryza sativa*
	30 - 5,6	---	---	---	flooded	---	---	*Schoenoplectus acutus*
	40	Fluvisols	---	---	flooded	2	---	*Juncus effusus, Phalaris arundinacea*
Managed lands	41 [δ]	Aquepts, silty clay organic	7.7	---	---	3	---	*Triticum* sp., *Daucus* sp., *Allium* sp., *Solanum* sp.
	42 [δ]							---
	43 [δ]							---
	44 [δ]							---
	23 - 2	sandy clay loam	---	---	---	---	43_{AN}	*Triticum* sp.
	45	Sulfaquets/Humaquets □	4-5	---	---	---	160_{U}	*Saccharum officinarum*
	46 - 1	clay loam	---	---	---	3	170,155,78,112	*Zea mais, Glycine max, Triticum sp., Brassica sp.*
	46 - 2	---	---	---	---	3	---	*Zea mais, Glycine max*
	47	clay loam	7	12	22	---	---	---
	48 [ε]	clay loam	6.7	1.2	21	3	127_{U}	*Zea mais*
	5 - 2 [ε]							---
	49	Podzosoil, acid humic	6	---	15	3	200_{AA}	*Zea mais*
	50 -1	brown humic soil	---	16	---	3	320.5_{U}	*Triticum* sp.
	50 - 2	brown humic soil	---	16	---	3	247_{U}	*Zea mais*
	51 - 1	Alfisol	6.97	---	---	3	50,50U	*Lolium perenne L.*

Table A2. Continue.

	ref. ID	soil characteristics				manag.[1]	fertilization[2]	main species
		type or typology	pH	C/N	SWC		(kgN ha^{-1})	
Managed lands	51 - 2	Alfisol	6.97	---	---	3	50,50SRU	*Lolium perenne L.*
	51 - 3	Alfisol	6.97	---	---	3	50,50AN	*Lolium perenne L.*
	51 - 4	Alfisol	6.97	---	---	3	0	*Lolium perenne L.*
	52 - 1	---	6.6	---	---	---	---	*Zea mais*
	52 - 2	---	---	---	---	---	---	*Brassica napus, Pisum sativum, Triticum aestivum*
	53	gleyed melanic brunisol	7.3	12.3	---	3	325_{NA}, 210_{AM}	*Medicago* sp., *Poa* sp., *Hordeum* sp., other spp.
	54 - 1	32% sandy, 52% silt, 16% clay	7	12.3	---	3	850_{AN}, 150_{AM}	*Hordeum* sp., *Glycine* sp., *Medicago* sp., other spp.
	54 - 2	38% sand, 47% silt, 16% clay	7.4	15.5	---	1	75_{AM}	*Triticum aestivum, Avena* sp., *Trifloium pratense*
	55 $^{\zeta}$	fluvisol	---	---	---	3	185_{AN}	*Phleum pratense*
	56 $^{\zeta}$							
	57 $^{\zeta}$							
	58 $^{\zeta}$							
	59 $^{\zeta}$							
	60 $^{\eta}$	Gleyic cambisol	5.1	13.7	---	3	200_{AN}	*Lolium perenne*
	61 $^{\eta}$							
	62 $^{\theta}$	peaty clay,eutrophic peat	---	---	---	3	253_{M}, 84	*Lolium perenne, Poa trivialis*
	63 $^{\theta}$							---
	64	peaty podzols, brown	---	---	---	3	345.6	*Lolium perenne*
	65	Cambisol (eutric)	7.3	8	---	3	$200_{AN,AM}$	*Trifolium* sp.
	66	Cambisol (eutric)	7.3	9	---	3	$60A_{N}$, 35_{AM}	*Trifolium* spp.
	67	peaty podzols, brown	---	---	---	3	---	*Lolium* sp.
	68 - 1	---	---	---	---	3	---	*Medicago sativa, Poa pratensis*
	68 - 2	---	---	---	---	3	---	bare soil
	69	---	---	---	---	3	180_{AN}	*Lolium perenne L.*
	70	red clay loam	4	---	40	---	---	*Trifolium subterranean, Lolium sp.*
	71	---	---	---	---	---	---	*Medicaco sativa*
	72	---	---	---	---	2	---	---
	73	Lismore silt loam	---	---	---	3	---	*Lolium perenne*
	74 - 1,2	Sodosol	---	---	65-95	3	$45\text{-}50_{U}$, $35A_{P}$	*Triofolium repens, Lolium perenne*
Anthr. env.	75	---	---	---	---	---	---	---
	76 - 1	---	---	---	---	---	---	---
	76 - 2	---	---	---	---	---	---	---
	77	---	---	---	---	---	---	---
	78	soil-clay	---	---	---	---	---	---

Table A2. Continue.

	ref. ID	soil characteristics				manag.[1]	fertilization[2]	main species
		type or typology	pH	C/N	SWC		(kgN ha^{-1})	
Anthr. env.	79	---	---	---	---	---	---	---
	80	compost soil, diamict clay	---	---	---	---	---	---
	81	mixture organic/mineral	---	---	---	---	---	---
	82	---	---	---	---	---	---	---

[1] degree of managements, 0: low - 3: intensive

[2] AA: anhydrous ammonia; AM: animal manure; AN: ammonium nitrate; AP: ammonium phosphate; U: urea; SRU: slow-release urea

Table A3. Overview of CH_4 and N_2O mean fluxes.

	ecosystems	ref. ID	measurement campaign		N_2O (mg m^{-2} h^{-1})			CH_4 (mg m^{-2} h^{-1})		
			tech.	period[1]	mean	range[2]	SD	mean	range[2]	SD
Forests	conifer forest	1	FG	07,JUN-AUG,43	---	---	---	-0.071	---	---
		2 [α]	EC	07,APR-JUN	0.005		---	---	---	---
		3 [α]								
		4	EC	07,AUG,9	---	---	---	-0.126	$-0.360\|0.072_{HM}$	0.144
		5 - 1	FG	94,AUG,6	---	---	---	0.729	---	0.25
		5 - 1	EC	94,JUL,8	---	---	---	2.188	---	1.104
		5 - 1	REA	02,APR,2	---	---	---	1.167	---	0.625
		6 - 1	NBL	05,APR-MAY,17	---	---	---	0.347	---	---
	deciduous forest	7 [β]	EC	03,MAY-JUN,35	0.008	$-0.001\|0.032_{DA}$	0.001	---	---	---
		8 [β]								---
		9	FG	94,APR-SEP	0.005	---	0.003	0.058	---	0.01
	mixed forest	10	EC	05,OCT-NOV,28	0.035	$-0.968\|3.653_{HM}$	0.018	---	---	---
	tropical forest	11 - 1	FG	05,MAY,4	---	---	---	0.858	---	---
		11 - 1	FG	04,NOV,4	---	---	---	0.228	---	---
		11 - 2	FG	04,JAN,5	---	---	---	0.15	---	---
		11 - 2	FG	04,AUG,4	---	---	---	0.154	---	---
		11 - 3	FG	04,APR,4	---	---	---	0.083	---	---
		11 - 3	FG	04,JUL,4	---	---	---	0.213	---	---
		12	EC	08,NOV-09,JUL	---	---	---	0.116	$0.029\|0.578_{DA}$	---
		6 - 2	NBL	05,OCT,10	---	---	---	0.352	---	---
Wetands	boreal fen	13	REA	04,JUL-OCT	---	---	---	4.3	$0.000\|10.000_{DA}$	---
				05,APR-JUL,14						
		14	EC	05,MAR-06,MAR,365	---	---	---	1.438	$-2.000\|8.500_{HM,G}$	---
	fen	15	EC	96,JUN,6	---	---	---	5.4	$1.700\|8.900_{DA}$	1.8
	flooded forest	16 - 1	FG	98-00	---	---	---	---	$-20.988\|31.968_{DA}$	---
		16 - 2	FG	98-00	---	---	---	---	$-16.308\|16.056_{DA}$	
	mire	17	FG	95,AUG,4	---	---	---	3.172	$0.294\|10.556_{HM}$	---
		17	NBL		---	---	---	3.85	$0.738\|7.877_{HM}$	---
		17	EC		---	---	---	0.921	$0.420\|1.301_{HM}$	---
		18 - 1	FG	92,JUN-JUL,35	---	---	---	0.298	$0.008\|15.375_{DA}$	0.015
				93,JUN-JUL,32						

Table A3. Continue.

	ecosystems	ref. ID	measurement campaign		N_2O (mg m^{-2} h^{-1})			CH_4 (mg m^{-2} h^{-1})		
			tech.	period[1]	mean	range[2]	SD	mean	range[2]	SD
Wetlands		18 - 2	FG	92,JUN-JUL,35 93,JUN-JUL,31	---	---	---	0.032	$-0.004\|5.833_{DA}$	0.005
		19	EC	96,MAY,6 JUN-JUL,3	---	---	---	---	$0.108\|4.250_{DA}$	---
		20	EC	95,AUG,19	---	---	---	1.591	$0.000\|3.960_{HM}$	---
		20	EC	97,MAY-JUN,29	---	---	---	1.44	$0.000\|4.320_{HM}$	---
		20	EC	98,SEP-OCT,19	---	---	---	0.45	$0.000\|1.800_{HM}$	---
	peat meadow	21	EC	06,JUN,14	---	---	---	1.175	$0.000\|4.620_{HM}$	0.673
		21	REA*		---	---	---	1.488	---	0.828
		21	DEC*		---	---	---	1.518	---	0.733
	peatland	22 - 1	REA	92,JUL-AUG,5	---	---	---	5.102	$1.604\|9.626_{HM}$	---
		22 - 2	REA	93,MAY-JUN,9	---	---	---	0.364	$-1.123\|1.765_{HM}$	---
		23 - 1	REA	93,MAY-JUN	---	---	---	0.364	---	0.565
		23 - 1	EC		---	---	---	0.236	---	0.236
		24	EC	90,JUN-JUL,35	---	---	---	0.648	---	0.936
		25	EC	99,MAY-SEP,42	---	---	---	5.667	$3.125\|9.250_{DA}$	---
		26	EC	94,MAY-JUN,15	---	---	---	0.626	$0.000\|2.272_{HM}$	---
		27	FG	94,JUN-SEP	---	---	---	4.536	$-2.898\|135.000_{HM}$	6.732
		28 - 1	EC	91,MAY-OCT	---	---	---	3.9	$1.000\|6.500_{HM}$	---
		28 - 2	EC	92,MAY-OCT	---	---	---	4.1	$1.500\|8.000_{HM}$	---
		29	EC	90,AUG,6	---	---	---	7.375	$5.000\|11.250_{DA}$	1.458
	peatland pasture	30 - 1,2	EC	10,MAY-AUG	---	---	---	0.289	---	0.751
		83	EC	07,APR-08,MAY,420	---	---	---	0.312	---	0.017
	prairie marsh	31	EC	94,APR-OCT,178	---	---	---	7.7	$2.200\|27.000_{DA}$	---
		32	EC	93,JUL-SEP,65	---	---	---	16	$17.000\|47.000_{DA}$	---
	tundra	33	EC	88,JUL-AUG,35	---	---	---	1.042	$0.458\|1.208_{DA}$	0.042
		34	EC	06,JUN-SEP,103	---	---	---	0.779	$0.238\|3.542_{DA}$	---
		35	EC	03,JUL-OCT,96	---	---	---	---	$0.292\|1.250_{DA}$	---
		35	EC	04,JUN-JUL,51	---	---	---	---	$0.167\|1.250_{DA}$	---
	rice field	30 - 3,4	EC	10,MAY-AUG	---	---	---	1.733	---	3.176
		36	FG	96,AUG,7	---	---	---	2.654	$0.720\|7.560_{HM}$	---

Table A3. Continue.

	ecosystems	ref. ID	measurement campaign		N_2O (mg m^{-2} h^{-1})			CH_4 (mg m^{-2} h^{-1})		
			tech.	period[1]	mean	range[2]	SD	mean	range[2]	SD
Wet-lands		37 [γ]	EC	98,JUL,8	---	---	---	14.5	$6.000\|24.000_{HM,G}$	---
		38 [γ]								
		39	FG	06,OCT-NOV,30	---	---	---	0.982	---	---
	restored wetland	30 - 5,6	EC	10,MAY-AUG	---	---	---	10.973	---	3.465
		40	EC	08,AUG-09,OCT	---	---	---	1.258	$0.833\|7.500_{DA}$	---
Managed lands	crop on drained fjord	41 [δ]	EC	93,AUG,10	0.422	$0.266\|0.647_{DA}$	---	---	---	---
		42 [δ]	REA	93,AUG,5	0.69	$0.253\|0.850_{DA}$	---	---	---	---
		43 [δ]	FG	93,AUG,9	0.355	$0.182\|0.765_{DA}$	0.113	---	---	---
		44 [δ]								
	cropland	23 - 2	REA	94,APR,10	0.34	$0.167\|0.646_{DA}$	0.195	---	---	---
		23 - 2	EC		0.7	$0.215\|1.080_{DA}$	---	---	---	---
		45	FG	05,OCT-06,SEP,342	0.879	$0.000\|4.167_{DA,G}$	---	0.283	---	---
		46 - 1	FG	00-01	---	$-0.164\|2.357_{DA,G}$	---	---	---	---
				03-04,MAR-JUN						
		46 - 2	REA	00-01	---	$-0.033\|1.178_{DA,G}$	---	---	---	---
				03-04,MAR-JUN						
		47	FG	96,FEB-APR,19	0.393	$0.000\|1.571_{HM}$	---	---	---	---
		48 [ε]	FG	98,MAY-JUL,38	0.445	$0.108\|1.980_{DA}$	0.022	---	---	---
		5 - 2 [ε]								
		49	EC	96,JUN,7	0.352	$0.096\|0.741_{DA}$	0.271	---	---	---
		49	FG	96,JUN,7	0.928	$0.074\|2.240_{DA}$	1.045	---	---	---
		50 - 1	FG	95,JUL-AUG,10	0.514	$-4.410\|4.840_{HM}$	0.316	---	---	---
		50 - 1	BR	95,JUL-AUG,10	0.452	$-4.410\|4.840_{HM}$	0.288	---	---	---
				97,AUG,4						
		50 - 2	FG	96,MAY,7	0.293	$-2.820\|3.590_{HM}$	0.14	---	---	---
		50 - 2	BR	95,OCT,6	0.405	$-2.820\|3.591_{HM}$	0.265	---	---	---
				96,MAY,7						
				97,OTT-NOV,8						
		51 - 1	FG	97,NOV-98,APR	0.052	---	0.080	---	---	---
		51 - 2	FG	97,NOV-98,APR	0.084	---	0.016	---	---	---
		51 - 3	FG	97,NOV-98,APR	0.006	---	0.003	---	---	---
		51 - 4	FG	97,NOV-98,APR	-0.0003	---	0.001	---	---	---
		52 - 1	FG	97,FEB-MAR,15	0.065	$-0.033\|0.720_{DA}$	---	---	---	---
				APR-MAY,45						

Table A3. Continue.

	ecosystems	ref. ID	measurement campaign		N_2O (mg m^{-2} h^{-1})			CH_4 (mg m^{-2} h^{-1})		
			tech.	period[1]	mean	range[2]	SD	mean	range[2]	SD
Managed lands	managed grassland	52 - 2	REA	02,APR,14	0.03	$-0.002\|0.094_{DA}$	---	---	---	---
		53	FG	92,JUL-NOV 93,MAR-95,FEB	---	$-0.017\|0.705_{DA}$	---	---	---	---
		54 - 1	FG	93,MAR-96,APR	0.085	$-0.027\|0.957_{HM}$	---	---	---	---
		54 - 2	FG	95,OCT-96,APR	0.153	$0.004\|0.562_{HM}$	---	---	---	---
		55 [ζ]	EC	92,APR	0.362	$0.215\|0.639_{HM}$	---	---	---	---
		56 [ζ]	FG - 1	92,APR	0.317	$0.017\|0.594_{HM}$	0.369	---	---	---
		57 [ζ]	FG - 2	92,APR	0.283	$0.000\|0.735_{HM}$	---	---	---	---
		58 [ζ]	FG - 3	92,APR	0.288	$0.113\|0.396_{HM}$	---	---	---	---
		59 [ζ]								
		60 [η]	EC	02,184	0.054	$-1.674\|4.938_{DA}$	---	---	---	---
		61 [η]	EC	03,141	0.032	$-0.633\|1.765_{DA}$	---	---	---	---
		62 [θ]	EC	06,AUG-NOV,74	0.29	$-1.131\|2.545_{HM}$	0.59	2.464	$-4.812\|4.812_{HM}$	1.85
		63 [θ]								
		64	EC	03,FEB-APR	0.183	---	---	---	---	---
		64	EC	03,MAR-JUL	0.5	---	---	---	---	---
		64	EC	03,AUG-OCT	0.117	---	---	---	---	---
		64	EC	03,NOV-JAN	0.05	---	---	---	---	---
		65	EC	05,AUG-SEP	0.05	$0.036\|0.064_{DA}$	0.097	---	---	---
		66	EC	08,JUN-SEP	0.089	$-0.230\|3.169_{HM}$	---	---	---	---
		67	EC	02,JUL-03,MAR	0.17	$-0.200\|2.500_{DA,G}$	---	---	---	---
		68 - 1	FG	93,MAR-DEC	---	$-0.100\|3.400_{DA,G}$	---	---	---	---
		68 - 2	FG	93,MAR-DEC 94,JAN-APR	---	$-0.050\|2.400_{DA,G}$	---	---	---	---
	pasture	69	EC	10,MAR-OCT,167	---	---	---	1.040	$0\|5.775_{HM}$	---
		70	MB	97,OCT-NOV,8	3.535	---	1.113	---	---	---
		70	FG	95,OCT,15	0.039	---	0.021	---	---	---
		71	FG	95,OCT,19	0.079	---	0.244	0.09	---	1.641
		71	NBL		0.011	$-0.006\|0.062_{DA}$	0.018	0.392	$0.000\|2.160_{DA}$	0.248
		72	FG	97,APR,5	---	---	---	---	$0.360\|3.600_{HM}$	---
		73	FG	95,MAR,5	0.136	---	0.028	---	---	---
		74 - 1	FG	03,JUL-04,JUN,306	0.065	$0.026\|1.061_{DA}$	0.032	---	---	---
		74 - 2	FG	04,JUL-05,JUN,323	0.052	$0.026\|0.524_{DA,G}$	0.026	---	---	---

Table A3.Continue.

	ecosystems	ref. ID	measurement campaign		N_2O (mg m^{-2} h^{-1})			CH_4 (mg m^{-2} h^{-1})		
			tech.	period[1]	mean	range[2]	SD	mean	range[2]	SD
Anthropic environments	manure storage	75	MB	06,JUN	---	---	---	5940	1116.000|16632.000$_{HM}$	---
		76 - 1	MB	01,MAY-JUL 01,NOV	---	---	---	1329.5	563.400|2141.640$_{HM}$	64.755
		76 - 2	MB	01,JUL-AUG 01,OCT 03,JAN-APR	---	---	---	1566.5	75.600|3937.320$_{HM}$	93.93
	landfill	77	EC	08,JUL,5	---	---	---	---	5.760|39.600$_{DA}$	---
		78	EC	91,NOV,1	---	---	---	272.72	---	---
		79	EC	03,AUG,8	---	---	---	1600	0.000|9326.200$_{HM,G}$	---
		80	EC	03,JUN-DEC	---	---	---	1908	0.000|10800.00$_{HM}$	---
		81	EC	03,AUG,10	4.242	0.786|7.856$_{HM}$	---	---	---	---
	urban area	82	EC	05,NOV-DEC,41	0.515	0.000|3.015$_{HM}$	---	---	---	---

[1] Measurement campaign period is: year, month(s), number of days.

[2] DA: daily average; HM: hourly, half hourly or 15' mean; G: graphical extrapolation.

* Simulated results.

Table A4. Overview of gas sensors, measurements accuracy, precision and flux detection limits. Values in brackets are in percent of measured value.

					N_2O			CH_4		
	ref.ID	tech.	sensor[1]	instr.ID[2]	accuracy[3]	precision[3]	FDL[3] (mg m^{-2} h^{-1})	accuracy[3]	precision[3]	FDL[3] (mg m^{-2} h^{-1})
Forests	1	FG	CRDS	12	---	---	---	0.200_C	0.350_C	---
	2 [α]	EC	TDLAS	6	---	---	---	---	---	---
	3 [α]									
	4	EC	CRDS	12	---	---	---	---	1.0-5.0C	0.079
	5 - 1	FG	TDLAS	6	---	---	---	---	---	---
	5 - 1	EC	TDLAS	6	---	2.0C	0.018-0.036	---	8.0C	0.025-0.042
	5 - 1	REA	TDLAS	6	---	---	---	---	0.1C	0.125
	6 - 1	NBL	GC	16	---	---	---	$(2.0)_C$	$(0.6)_C$	---
	7 [β]	EC	TDLAS	6	---	1.0_C	0.007	---	---	---
	8 [β]									
	9	FG	TDLAS	6	---	---	---	---	---	---
	10	EC	QCLAS	2-3	---	0.3_C	---	---	---	---
	11 - 1	FG	GC	---	---	---	20.0_C	5.0_C	---	---
	12	EC	CRDS	12	---	---	---	---	---	---
	6 - 2	NBL	GC	16	---	---	---	$(2.0)_C$	$(0.6)_C$	---
Wetlands	13	REA	GC	8	---	---	---	---	---	---
	14	EC	TDLAS	6	---	---	---	---	---	---
	15	EC	TDLAS	---	---	---	---	---	---	---
	16	FG	GC	14	---	---	---	---	$(2.0\text{-}3.2)_C$	---
	17	FG	TDLAS	---	---	---	---	---	---	---
	17	NBL	TDLAS	---	---	---	---	---	---	---
	17	EC	TDLAS	---	---	---	---	---	---	---
	18 - 1,2	FG	TDLAS	---	---	---	---	---	---	0.001
	19	EC	TDLAS	2	---	---	---	---	$<0.30_F$	0.11
	20	EC	TDLAS	2	---	---	---	---	---	---
	21	EC	CRDS	12	---	---	---	$(0.3)_C$	0.008_C	---
	21	REA	CRDS	12	---	---	---	---	---	---
	21	DEC	CRDS	12	---	---	---	---	---	---
	22 - 1,2	REA	GC	8	---	---	---	---	$0.109\text{-}0.299_F$	0.204-0.689
	23 - 1	REA	GC	8	---	---	---	---	---	---
	23 - 1	EC	TDLAS	2	---	---	---	---	---	---
	24	EC	TDLAS	18	---	---	---	0.1_C	5.0_C	0.36

Table A4. Continue.

	ref.ID	. tech.	sensor[1]	instr.ID[2]	N_2O accuracy[3]	N_2O precision[3]	N_2O FDL[3] (mg m^{-2} h^{-1})	CH_4 accuracy[3]	CH_4 precision[3]	CH_4 FDL[3] (mg m^{-2} h^{-1})
Wetlands	25	EC	TDLAS	2	---	---	---	---	---	---
	26	EC	TDLAS	2	---	---	---	---	---	---
	27	FG	GC	13	---	---	---	---	4.0_C	---
	28 - 1,2	EC	TDLAS	17	---	---	---	---	---	0.4
	29	EC	TDLAS	17	---	---	---	---	---	---
	30 - 1	EC	CRDS	12	---	---	---	---	4	0.218
	30 - 2	EC	WMS	11	---	---	---	---	3	0.197
	83	EC	CRDS	12	---	---	---	---	---	---
	31	EC	TDLAS	6	---	---	---	---	---	0.4
	32	EC	TDLAS	6	---	---	---	---	---	0.4
	33	EC	GC IR-HeNe	15 2	---	---	---	$20\text{-}30_C$	---	---
	34	EC	TDLAS	6	---	---	---	$(10.0\text{-}20.0)_F$	0.071_F	---
	35	EC	TDLAS	6	---	---	---	---	0.113_F	---
	30 - 3	EC	CRDS	12	---	---	---	---	4	---
	30 - 4	EC	WMS	11	---	---	---	---	3	---
	36	FG	IRGA	9	---	---	---	---	$1.00\text{-}2.25_C$	---
	37 [γ]	EC	TDLAS	---	---	---	---	---	0.01_C	---
	38 [γ]									
	39	FG	GC	7	---	---	---	10_C	10_C	---
	30 - 5	EC	CRDS	12	---	---	---	---	4	---
	30 - 6	EC	WMS	11	---	---	---	---	3	---
	40	EC	CRDS	12	---	---	---	---	---	---
Managed lands	41 [δ]	EC	TDLAS	2	---	0.1_C	0.027	---	---	---
	42 [δ]	REA	TDLAS	---	---	---	---	---	---	---
	43 [δ]	FG	FTIR	4	---	$0.5(0.2)_C$	0.113	---	---	---
	44 [δ]									
	23 - 2	REA	TDLAS	2	---	---	---	---	---	---
	23 - 2	EC	TDLAS	2	---	---	---	---	---	---
	45	FG	FTIR	5	---	$1.0(0.1)_C$	---	---	$6.0(0.1)_C$	---
	46 - 1	FG	TDLAS	6	---	---	---	---	---	---
	46 - 2	REA	TDLAS	6	---	0.011_C	0.029	---	---	---
	47	FG	TDLAS	6	---	---	---	---	---	---

Table A4. Continue.

		.			N_2O			CH_4			
	ref.ID	tech.	sensor[1]	instr.ID[2]	accuracy[3]	precision[3]	FDL[3] (mg m^{-2} h^{-1})	accuracy[3]	precision[3]		FDL[3] (mg m^{-2} h^{-1})
Managed lands	48 [ε]	FG	TDLAS	6	---	0.022_F	---	---	---		---
	5 – 2 [ε]										
	49	EC	TDLAS	2	---	$1.2(0.1\text{-}1.0)_C$	---	---	---		---
	49	FG	TDLAS	2	---	$0.2(0.1\text{-}1)_C$	---	---	---		---
	50 – 1,2	FG	GC	8	---	$0.270\text{-}0.460_C$	---	---	---		---
		BR	GC	8	---	$0.270\text{-}0.460_C$	---	---	---		---
	51 – 1-4	FG	TDLAS	6	---	---	---	---	---		---
	52 – 1	FG	TDLAS	6	---	0.019_F	---	---	---		---
	52 – 2	REA	TDLAS	6	0.01_C	0.018_F	0.018	---	---		---
	53	FG	TDLAS	---	---	0.007_F	---	---	---		---
	54 – 1,2	FG	TDLAS	---	---	0.007_F	---	---	---		---
	55 [ζ]	EC	TDLAS	---	---	1.0_C	0.034	---	---		---
	56 [ζ]	FG – 1	GC	---	---	$1.0(0.5)_C$	---	---	$0.5(0.1)_C$		---
	57 [ζ]	FG – 2	FTIR	---	---	$(0.1\text{-}0.5)_C$	---	---	---		---
	58 [ζ]	FG – 3	TDLAS	---	---	1.0_C	---	---	---		---
	59 [ζ]										
	60 [η]	EC	TDLAS	2	---	$(1.0)_C$	---	---	---		---
	61 [η]										
	62 [θ]	EC	QCLAS	1	---	0.5_C	0.034	---	2.9_C		0.197
	63 [θ]										
	64	EC	TDLAS	6	---	---	---	---	---		---
	65	EC	QCLAS	2	---	$0.3\text{-}0.6_C$	0.016	---	---		---
	66	EC	QCLAS	2	---	0.7_C	0.027	---	---		---
	67	EC	TDLAS	6	---	---	---	---	---		---
	68 – 1	FG	TDLAS	---	---	---	---	---	---		---
	68 – 2	FG	TDLAS	---	---	0.2_C	---	---	---		---
	69	EC	WMS	11	---	---	---	---	---		---
	70	MB	FTIR	5	---	0.2_C	---	---	---		---
	70	FG	FTIR	5	---	0.7_C	0.027	---	---		---
	71	FG	FTIR	5	---	$0.19(0.10.2)_C$	0.057-0.113	---	$1.60(0.1\text{-}0.2)_C$		0.216-0.432
	71	NBL	FTIR	5	---	$0.19(0.1\text{-}0.2)_C$	0.057-0.113	---	$1.60(0.1\text{-}0.2)_C$		0.216-0.432
	72	FG	GC	8	---	---	---	---		1.5	---
	73	FG	FTIR	4	---	$(0.6\text{-}1.0)_C$	0.113	---	---		---
	74 – 1,2	FG	TDLAS	6	---	$0.006\text{-}0.007_C$	---	---	---		---

Table A4. Continue.

		.			N_2O			CH_4		
	ref.ID	tech.	sensor[1]	instr.ID[2]	accuracy[3]	precision[3]	FDL[3] (mg m^{-2} h^{-1})	accuracy[3]	precision[3]	FDL[3] (mg m^{-2} h^{-1})
Anthropic environments	75	MB	TDLAS	6	---	---	---	---	---	---
	76 - 1,2	MB	TDLAS	6	---	0.130-0.260$_C$	---	---	4.0-6.5$_C$	---
	77	EC	CRDS	12	---	---	---	---	1.5(0.08)$_C$	---
	78	EC	TDLAS	10	---	---	---	(1.0)$_C$	65.0$_C$	0.833
	79	EC	GC/	8	---	---	---	---	---	---
			TDLAS	6						
	80	EC	GC	8	---	---	---	---	---	---
	81	EC	TDLAS	6	---	---	---	---	---	---
	82	EC	TDLAS	2	---	---	---	---	---	---

[1] Gas sensors: CRDS, Cavity Ring-down Spectroscopy. FTIR, Fourier Transform Infrared Spectroscopy. GC, Gas Chromatography. IR-HeNe, Zeeman-split He-Ne Laser Absorption Spectroscopy (prototype). IRGA, Infra-Red Gas Analyzer. QCLAS, Quantum Cascade Laser Absorption Spectroscopy. TDLAS, Tunable Diode Laser Absorption Spectroscopy. WMS, Wavelength Modulation Spectroscopy.

[2] Instrument manufacturer: 1: Aerodyne QCL-TILDAS-76. Aerodyne Research Inc., Billerica MA, USA. 2: Prototype. Aerodyne TDLAS. Aerodyne Research Inc., Billerica, MA, USA. 3: Alpes QCLAS. Alpes Laser Neuchatel, Switzerland. 4: Bomem MB-100. ABB-Bomem, Quebec, Canada. 5: Bomem MB104. ABB-Bomem, Quebec, Canada. 6: Cambpell TGA-100. Campbell Scientific Inc., Logan, Utah USA. 7: Dani TNMH 451. Dani S.p.A., Milan, Italy. 8: Hewlett Packard HP 5890/5890. Hewlett Packard, Bracknell, Berks., UK. 9: Horiba GA-360E. Horiba Co. Ltd., Kyoto, Japan. 10: InGaAsP, Near-infrared diode laser. 11: Licor LI-7700. LI-COR Bioscience, Lincoln, Nebraska, USA. 12: Los Gatos DLT-100, Fast Methane Analyzer. Los Gatos Research, Mountain View, CA. 13: Shimadzu GC Mini II. Shimadzu Scientific Instruments Inc.. 14: Shimadzu GC-14B Series. Shimadzu Scientific Instruments Inc.. 15: Shimadzu GC-6A. Shimadzu Scientific Instruments Inc.. 16: Thermo 55C Hydrocarbon Analyzer. Thermo Electron Corporation, Massachusetts, USA. 17: Unisearch TDLAS. Unisearch Associates, Inc., Ontario, Canada. 18: University of Guelph TDLAS.

[3] Flux Detection Limit is reported in C: concentration (ppb); F: flux.